T149

50502

Tezpur University
Acc 50502
Date 26/12/11

CENTRAL LIB
TEZPUR UNIV
Accession No. T149
Date 27/02/13

A STUDY OF LOW FREQUENCY DRIFT MODE AND COULOMB SOLID FORMATION IN COMPLEX PLASMA

A thesis submitted in partial fulfillment of the
requirements for the degree of

Doctor of Philosophy

Swati Baruah

Registration No. 008 of 2009

School of Science and Technology

Department of Physics

Tezpur University

Napaam, Tezpur - 784 028

Assam, India

January, 2011

I would like to dedicate this thesis

to

my beloved parents

And

all those

who waited for it, eagerly

Abstract

In this thesis, a detailed analysis has been done on low-frequency dissipative drift instability in dusty plasma. Besides that, Coulomb crystal formation in strongly coupled dusty plasma has been elaborately studied in presence of different interacting potentials among the grains, using Molecular Dynamics (MD) simulation.

Ionized gases containing small particles of solid matter are called dusty (complex) plasmas. In the last decades there has been a growing interest in this field. The presence of static charged dust in a plasma can modify the standard plasma modes, whereas the inclusion of the dust inertia in the analysis provides the possibility of some completely new modes. Recent experiments have shown that under appropriate conditions dust grains crystallize. This is significant because it provides an easily observable model for studying the dynamics and structure of crystal lattice, solid-liquid phase transitions and to investigate basic plasma interactions.

In the 1st Chapter of the thesis, a general introduction of dusty plasma has been presented. A short overview of the most common dusty plasma systems both in space and in the laboratory is given. Then different forces acting on dust particles, the basic dust waves, instabilities and dust crystal formation are briefly introduced and reviewed.

In Chapter 2, dissipative drift instability is investigated in collisional dusty plasma, in the low frequency regime. The presence of dust density inhomogeneity perpendicular to the direction of magnetic field produces the drift wave. In developing the theory, dust charge fluctuation is taken into consideration. The dispersion relation for low-frequency drift wave is obtained by normal mode analysis. The effect of dust density

inhomogeneity and the ion neutral collision on the growth rate of the instability are investigated.

In Chapter 3, discussion has been made on crystal formation in complex plasma. A molecular dynamics (MD) code is developed for this purpose and is used to study the crystal formation of the system. The interaction potential among the dust grains is taken as Yukawa type. The structure of the complex plasma system is investigated by calculating Pair correlation function ($g(r)$) for different values of temperature, density and size of dust grains. Next, the presence of the lattice structure is verified by the study of long range order. The triple point of phase transition between solid (FCC) to solid (BCC) and solid to fluid phase is found out. These results may help to identify accurately the parameters suitable for the formation of Coulomb crystal in a Yukawa dusty plasma system.

In Chapter 4, the role of attractive force on Coulomb crystal formation has been investigated in a 3D dusty plasma system. For this study the interaction potential is considered to be consist of repulsive Yukawa potential and attractive Shadowing potential. In such a system, the grains arrange themselves in crystalline pattern due to the Yukawa potential. However, it is seen that the presence of Shadowing potential modifies this arrangement. Pair correlation function $g(r)$ has been calculated for this purpose. The effects of combined Yukawa-Shadowing potential on phase transition of dust crystal has been compared with that of the purely repulsive Yukawa potential.

In Chapter 5, a comparative study between the effect of coupled Yukawa-Shadowing potential and coupled Yukawa-Overlapping Debye Sphere (ODS) potential on 2D dust crystal formation have been made by using MD simulation. Here, by calculating Radial Distribution Function ($g(r)$) for different values of κ, Γ and dust number densities, the structure of the system is investigated. It is seen from our study that the Coulomb coupling parameter does not have significant effect on both ODS and Shadowing force. The attractive Shadowing force is more dominant for grains with large screening parameter. The results for Yukawa-Shadowing and ODS potential are compared with experimental results and a close agreement is obtained for attractive

Shadowing force.

In Chapter 6, an effort has been made to study the importance of external magnetic field on the formation of dust crystal and phase transition of a three-dimensional dusty plasma system. The interaction potential among the dust grains gets modified and becomes anisotropic in presence of magnetic field. The pair correlation function has been calculated to characterize the structural properties of the dusty plasma for different values of magnetic field strength. The shifting of the triple point towards the lower value of screening constant, but to higher value of Coulomb coupling parameter as compared to pure Yukawa interaction is observed from the study of the phase diagram plot for the system for different values of magnetic field strength. The phase diagrams also show the existence of solid (FCC-like), solid (BCC-like) and fluid phases for the system.

In Chapter 7, a critical magnetic field for phase transition from crystalline state to liquid state of dusty plasma is found. Modified Yukawa potential is used as the interaction potential among the grains. The direct effect on dust grains due to the magnetic field has been taken into account by incorporating the term $Q_d\left(\overrightarrow{v} \times \overrightarrow{B}\right)$ in the equation of motion for strong magnetic field. Our study reveals that low magnetic field may facilitate formation of Coulomb crystal.

Finally, in Chapter 8, the results obtained in the present thesis are summarized and future scopes of the present investigation are included. The bibliography can be found at the end.

DECLEARATION

I hereby declare that the thesis entitled **'A Study of Low Frequency Drift Mode and Coulomb Solid Formation in Complex Plasma'** being submitted to Tezpur University, Tezpur, Assam in partial fulfillment of the requirements for the award of the degree of Doctor of Philosophy, has previously not formed the basis for the award of any degree, diploma, associate ship, fellowship or any other similar title or recognition.

Swati Baruah

Date: 1.1.2011

(Swati Baruah)

Place: Napaam, Tezpur

Department of Physics
Tezpur University
Tezpur-784 028 (Assam)

CERTIFICATE OF SUPERVISOR

This is to certify that the thesis entitled **A Study of Low Frequency Drift Mode and Coulomb Solid Formation in Complex Plasma** submitted to Tezpur University in the Department of **Physics** under the School of **Science and Technology** in partial fulfillment for the award of the degree of Doctor of Philosophy in **Physics** is a record of research work carried out by **Ms. Swati Baruah** under my personal supervision and guidance.

All helps received by her from various sources have been duly acknowledged.

No part of this thesis has been reproduced elsewhere for award of any other degree.

1.1.2011

Date:

Place: Napaam, Tezpur

(Dr. Nilakshi Das)
Supervisor
Associate Professor
School of Science and Technology
Department of Physics
Tezpur University

CERTIFICATE OF THE EXTERNAL EXAMINER AND ODEC

This is to certify that the thesis entitled **A Study of Low Frequency Drift Mode and Coulomb Solid Formation in Complex Plasma** submitted by **Ms. Swati Baruah** to Tezpur University in the Department of **Physics** under the School of **Science and Technology** in partial fulfillment of the requirement for the award of the degree of Doctor of Philosophy in **Physics** has been examined by us on ____________and found to be satisfactory.

The committee recommends for the award of the degree of Doctor of Philosophy.

Signature of:

Principal Supervisor External examiner

Associate Supervisor

Co Supervisor

Date______________

Acknowledgements

It is a great pleasure to me for taking this opportunity to convey my thanks and gratitude to my respected teacher and supervisor, Dr. Nilakshi Das for her valuable guidance and immense help during the course of my Ph. D. work. It would have not been possible for me to bring out this thesis without her help and constant encouragement.

During my tenure as research scholar I got an opportunity to work with Dr. Manoj Warrier of Computational Analysis Division, Bhabha Atomic Research Center, Visahkapatnam, Andhra Pradesh, during my stay at Institute of Plasma Research (IPR), Ahmedabad. It was a privilege to learn Molecular Dynamics (MD) Simulation from him. I am really grateful to him for sparing so much time from his busy schedule to guide me during the development of our own MD code and in offering his useful suggestions from time to time.

I am grateful to Prof. K. S. Goswami, Center of Plasma Physics, Sonapur, for his concern about my work and for giving me the opportunity to search literature in their institute relating to my research. I sincerely thank to Dr. Utpal Kr. Das, for his help during the implementation of C-programming and fruitful discussions. I am greatly benefited by the idea given by him. I would like to specially thanks to Dr. Gazi A. Ahmed for helping me in different ways at different point of time whenever required. I convey my gratitude and thank to the honorable faculty members and staff of Department of Physics, staff of computer center, library and administration of Tezpur University, for extending their help to me.

I am deeply indebted to my parents and well-wishers for their moral support and encouragement throughout my Ph. D. work. I also express my thank to all of my colleagues and friends for offering co-operative assistance in various manners during my stay in Tezpur University.

I further acknowledge my indebtedness to the authorities of Tezpur University, Plasma Science Society of India (PSSI) and University Grants Commission (UGC) for the research fellowships, under which this work has been performed.

Looking back at all the hurdles, twists and turns that I have crossed at various stages in my life, I honestly agree it is not only me who did everything to reach this stage. At each difficult moment there has been someone who rescued me.

Date: 1.1.2011
Place: Tezpur

Swati Baruah
(Swati Baruah)

Table of Contents

Table of Contents 1

Abstract ii

Acknowledgements vii

1 Introduction 1
- 1.1 A review of dusty plasma 1
- 1.2 Theory of charging of dust grains 9
  - 1.2.1 Charging equation for isolated grains in plasma: 13
  - 1.2.2 Physical effects manifested by charged dust: 20
  - 1.2.3 Forces acting on the dust grains : 23
  - 1.2.4 Waves in dusty plasma: 27
  - 1.2.5 Instabilities in dusty plasma: 38
  - 1.2.6 Dust plasma crystal: 47

2 Dissipative Drift Instability in Dusty Plasma 62
- 2.1 Introduction: 62
- 2.2 Theoretical model and equations: 66
- 2.3 Dispersion Relation: 69
- 2.4 Analysis of the Results and Discussions: 70
- 2.5 Conclusions: 75

3 Molecular Dynamics Simulation of Dust Crystal Formation 76
- 3.1 Brief introduction to Molecular Dynamics simulation: 76
- 3.2 Development of code for the study of crystal formation: 79
  - 3.2.1 Equations of motion: 79
- 3.3 MD code for Yukawa crystal in dusty plasma: 82
  - 3.3.1 Theoretical Model: 83

3.3.2 Results and Discussions: 88
3.3.3 Conclusions: 95

4 Role of Shadowing force in formation of 3D dust crystal 97
4.1 Introduction: 97
4.2 Formulation: 101
4.3 Results and Discussions: 103
4.4 Conclusion: 108

5 Study of effects of attractive potentials on Coulomb crystal formation 109
5.1 Introduction: 109
5.2 Theoretical modelling and simulation 113
5.3 Results and Discussions: 115
5.4 Conclusion: 125

6 The effect of magnetic field on the structure of dust crystal in magnetized plasma 127
6.1 Introduction: 127
6.2 Theoretical Model: 130
6.3 Results and Discussions: 133
6.4 Conclusions: 141

7 Determination of Critical Magnetic field for phase transition of Coulomb crystal 142
7.1 Introduction: 142
7.2 Theoretical Model and development of MD code: 145
7.3 Results and Discussions: 147
7.4 Conclusions: 158

8 Summary and Conclusions 160

Bibliography 166

A Appendix 185

List of Tables

5.1 Summary of simulational data. 125

6.1 Values of f for different values of magnetic fields 131
6.2 Variation of P.E. with magnetic field 136
6.3 Values of κ and Γ at which triple points appear with magnetic field strength 141

7.1 Values of Γ_m, κ_m, and B_c for different values of r_d 156

List of Figures

1.1 Dynamic spokes in Saturn's B ring[8] observed by Voyager 2 in 1981. . 4

1.2 Charging of dust grain. 11

1.3 Spontaneously exited dust acoustic waves. 30

1.4 (a) shows Crystalline phase, (b) and (c) show 'flow and floe' state[118] . 48

1.5 Phase diagram of Yukawa system. 49

1.6 Existing diagram of Wigner crystal. 50

1.7 Micrographs and sketches of different crystal structures (a) Hexagonal; (b) bcc; (c) fcc[120]. 52

1.8 Experimental set-up for dusty plasma crystal[118]. 54

1.9 Rotation of dust particles in the azimuthal direction on the horizontal plane in presence of magnetic field applied in the vertical direction[138]. 57

1.10 Repulsion and attraction for particles with a dipole moment; the + and - sign denote the charge imbalance between upper and lower side of the particle. 59

1.11 The ion weak potential in an ion flow. Downstream of the particle an oscillating potential is formed with alternating attractive ($\phi_c > 0$) and repulsive ($\phi_c < 0$) regions. 60

2.1 Schematic diagram showing the direction of magnetic field and density gradients in dusty plasma. 67

2.2 $\frac{\omega_r}{\omega_{pd}}$ vs. $k_y\lambda_{Dd}$, for $K\lambda_{D\imath} = 2.0$. 71

2.3 $\frac{\gamma}{\omega_{pd}}$ vs. $k_y\lambda_{Dd}$, for $K = 1.7/\lambda_{D\imath}$, $2.0/\lambda_{D\imath}$, $2.3/\lambda_{D\imath}$ respectively 72

2.4 $\frac{\gamma}{\omega_{pd}}$ vs. $k_y\lambda_{Dd}$, for $\nu_{in} = 4.19 \times 10^{10}, 6.29 \times 10^{10}, 8.38 \times 10^{10}$ Hz. respectively 73
2.5 $\frac{\gamma}{\omega_{pd}}$ vs. $k_y\lambda_{Dd}$, for T_i/T_e = 0.0125, 0.0145, 0.0175 respectively. 74

3.1 Basic MD Algorithm. 84
3.2 Plot of $g(r)$ vs. r for dust temperatures $T_d = 5K, 10K, 50K$ respectively. 89
3.3 Plot of $g(r)$ vs. r for dust temperatures $T_d = 5K, 500K, 7000K$ respectively. 90
3.4 Plot of $g(r)$ vs. r for different values of dust number densities at T_d=5K. 91
3.5 Plot of $g(r)$ vs. r for different dust sizes. 92
3.6 Time dependence of long-range order for different dust number densities. 93
3.7 Phase diagram of Yukawa system in the (κ, Γ) plane. 94

4.1 Shadow interaction between two dust grains. The ions with velocities lying within the shadow region do not reach the grains. 99
4.2 Plot of $g(r)$ vs. r/λ_D for κ=1.6 and Γ=130, 300, 444, 1389 respectively. 104
4.3 Plot of $g(r)$ vs. r/λ_D for Γ=2025 and κ=1.5, 2.0, 2.5, 3.0 respectively. 105
4.4 Plot of $g(r)$ vs. r/λ_D for grain radius r_d=0.7, 1.3, 2.0, 3.0 μm respectively. 107

5.1 Plot of $g(r)$ vs. r/λ_D for Shadowing force and ODS for different values of Γ, taking κ=1.6 116
5.2 Plot of $g(r)$ vs. r/λ_D for Shadowing force and ODS for different values of κ with $\Gamma = 6.40924 \times 10^3$ 117
5.3 Plot of $g(r)$ vs. r/λ_D for Shadowing force and ODS for different values of dust number density 119
5.4 Experimental and Simulational $g(r)$ vs. r/λ_D for Γ=121, κ=1.79, $n_d = 14300cm^{-3}$, $n_e = 2.69 \times 10^{10}cm^{-3}$, $Z_d = 2.1 \times 10^4$ 121
5.5 Experimental and Simulational $g(r)$ vs. r/λ_D for Γ=239, κ=2.67, $n_d = 3940cm^{-3}$, $n_e = 2.1 \times 10^{10}cm^{-3}$, $Z_d = 2.1 \times 10^4$ 122
5.6 Experimental and Simulational $g(r)$ vs. r/λ_D for Γ=68.50, κ=1.68, $n_d = 10712cm^{-3}$, $n_e = 2.4 \times 10^{10}cm^{-3}$, $Z_d = 2.1 \times 10^4$ 123

5.7 Experimental and Simulational $g(r)$ vs. r/λ_D for Γ=40.68, κ=1.48, $n_d = 20995 cm^{-3}$, $n_e = 2.4 \times 10^{10} cm^{-3}$, $Z_d = 2.1 \times 10^4$ 124

6.1 Plot of $g(r)$ vs. r for external magnetic field strength of $B_0 = 1.0, 2.0$ and $3.0T$ respectively. 134
6.2 Plot of time dependence of long-range order for external magnetic field strength of $B_0 = 1.0, 2.0$ and $3.0T$ respectively. 135
6.3 Phase diagram of modified Yukawa system in (Γ, κ) plane using magnetic field $B_0 = 0.5T$. 137
6.4 Phase diagram of modified Yukawa system in (Γ, κ) plane using magnetic field $B_0 = 1.0T$. 138
6.5 Phase diagram of modified Yukawa system in (Γ, κ) plane using magnetic field $B_0 = 1.5T$. 139
6.6 Plot of shifting of the triple point towards lower value of κ, higher value of Γ with increase in B_0. 140

7.1 Plot of $g(r)$ vs. r/λ_d, for grain radius of 2 μm with magnetic field of 0.7 T. 148
7.2 Plot of $g(r)$ vs. r/λ_d, for grain radius of 2 μm with magnetic field of 2.0 T. 149
7.3 Plot of $g(r)$ vs. r/λ_d, for grain radius of 2 μm with magnetic field of 3.0 T. 150
7.4 Plot of $g(r)$ vs. r/λ_d, for B = 0.2, 0.5, 0.7, 1.0, 2.0 and 3.0 T respectively, taking grain radius r_d = 2.0 μm. 151
7.5 Plot of $g(r)$ vs. r/λ_d, for B = 0.2, 0.5, 0.7, 1.0, 2.0 and 3.0 T respectively, taking grain radius r_d = 2.5 μm. 153
7.6 Plot of $g(r)$ vs. r/λ_d, for B = 0.2, 0.5, 0.7, 1.0, 2.0 and 3.0 T respectively, taking grain radius r_d = 3.0 μm. 154

7.7 Phase diagrams in (κ_m, Γ_m) plane for grain size of (a) = 1.5 μm, (b) = 2.0 μm, (c) = 2.5 μm, (d) = 3.0 μm, (e) = 3.5 μm, (f) = 4.0 μm, and (g) = 4.7 μm respectively. 155

7.8 Plot of fitting of curve between critical magnetic field and grain radius. 157

Chapter 1

Introduction

1.1 A review of dusty plasma

The study of dusty plasmas is a relatively new research area in the field of plasma physics. A dusty (or complex) plasma is a normal electron-ion plasma with an additional highly charged ($Q_d \sim 10^3e - 10^4e$) component of small micron-sized particulates. This extra component, which increases the complexity of the system, can be anything from simple ice particulates to metallic particulates (magnetite, graphite, silicate etc.). Dusty plasmas are ubiquitous in different parts of our environments, namely, in planetary rings, in circumsolar dust rings, in interplanetary medium, in cometary comae and tails, in interstellar molecular cloud, etc. Cometary dust generally has a size distribution of about 0.1 μm diameter. In interstellar clouds, dielectric or metallic dust particles of 0.01 to 10 μm are found. Dusty plasma also occurs in noctilucent clouds in the arctic troposphere and mesosphere, lightning in thunderstorms, in the flame of candle, as well as in microelectronic processing devices, in laboratory discharges, and in tokamak etc. Since a dusty plasma system involves the charging and dynamics of massive charged dust grains, it can be can be characterized as a complex plasma system[1].

Plasma with dust particles can be treated as either "dust in a plasma" or "a dusty plasma" depending on the ordering of a number of characteristic lengths. These are the dust grain radius (r_d), the average inter-grain distance ($a \approx n_d^{-1/3}$), where n_d is the dust number density, the plasma Debye radius (λ_D) and the dimension of the dusty plasma.

1. Dust in Plasma ($r_d << \lambda_D < a$): The dust grains in the plasma do not interact electrostatically and do not affect significantly the properties of neighboring dust grains. The number density is very low. These dust grains can not be treated as a collection of isolated screened grains in the plasma.
2. Dusty Plasma ($r_d << a < \lambda_D$): The dust grains in the plasma interact electrostatically with each other. Thus they significantly affect the properties of neighboring dust grains and the collective effects take place. Their number density is relatively dense compared to dust in plasma.

The dust grains become charged through collection of plasma electrons or through photo-ionization or both. If their density is sufficiently high, they begin to act collectively. *The physics of collective processes has grown many folds following the great* discovery of the low frequency dust related waves (e. g. dust acoustic waves (DAW), dust ion-acoustic waves (DIAW) etc.) and associated instabilities and the dusty plasma crystal. The dust-plasma crystals are made of highly (negatively) charged dust particulates of micrometer size levitated in the sheath region above a horizontal negatively biased electrode. Complex plasma plays a key role in understanding process of phase transition. The importance of complex plasma research is growing in surface and boundary physics and in paving the way towards certain areas of nano-technology.

Dusty Plasma in Various Environment:

"If the claim is made that more than 99 percent of the observable universe is in

the plasma state then it could be jokingly asserted that the remainder is dust" [2]

Dusty plasmas are common in various natural plasmas and laboratory devices. In his 1954 monograph *On the Origin of the Solar system*, Professor Hannes Alfven considered how the coagulation of dust particles in the solar nebula could have led to planetesimals and subsequently to comets and planets. He was one of the very first scientists to suggest how the electromagnetic forces acting on small dust particles played an important role in the evolution of entire solar system. He recognized planetary rings, for example, as an important laboratory for studying processes that not only act today, but also shaped the evolution of the entire solar system billions of years ago [3].

Dusty plasmas in space physics received considerable attention when Jupiter's ring was discovered and active volcanism on Io[4] with its ejection of fine "ash" in to Jovian magnetosphere, was first seen by the detector aboard the Voyager spacecraft. The Galileo and Ulysses missions made measurements of dust streams from Jupiter, and rocket flights collected data through noctilucent clouds high in Earths atmosphere. Horanyi et al.[5] found that the Lorentz force on these charged grains with radius $\leq 0.1\mu m$ is sufficient to overcome Io's gravity and inject the Jovian magnetosphere. This observation was followed by new discoveries in Saturn's rings in particular the "spokes"[6], the structure of the F-ring and the E-ring, and an unusual electromagnetic angular transport in the B-ring[7]. In all these observations the dust particles were highly charged but assumed not to be strongly interacting. In the early 1980s, the images of Saturn's rings taken by Voyager 2 revealed certain features in the B ring that were probably mysterious to modern planetary scientists. They were first discovered by Galileo in 1610 using his first telescope. The Voyager images revealed a pattern of nearly radial "spokes" rotating around the outer portion of Saturn's dense B ring[8]. They appear dark in backscattered light and bright in forward-scattering.

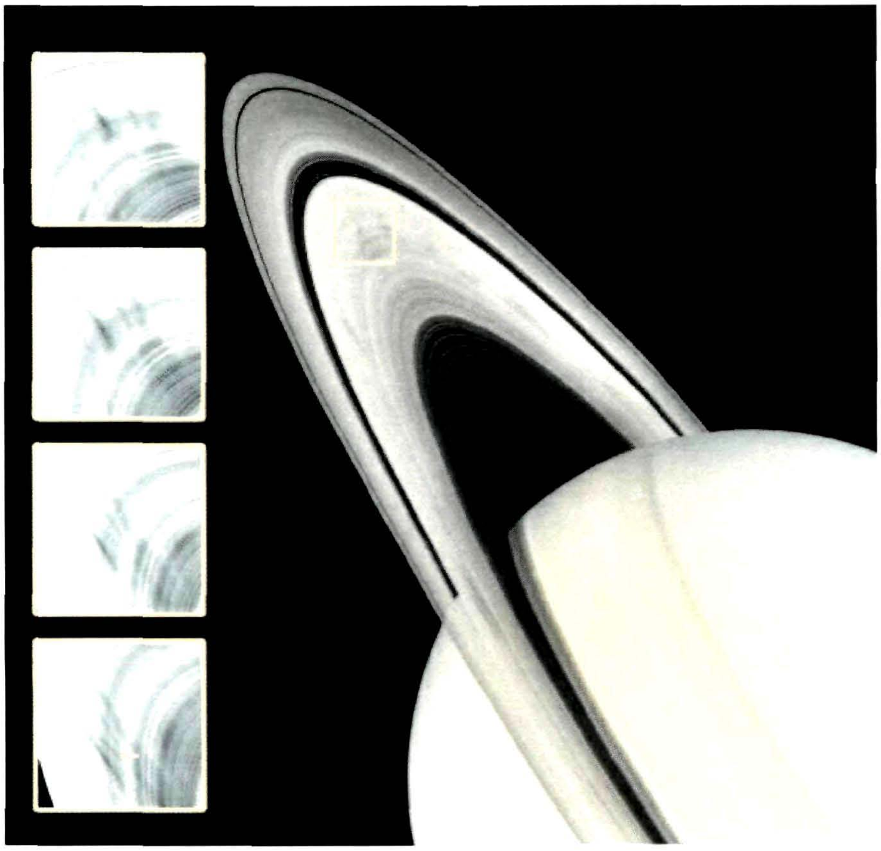

Figure 1.1: Dynamic spokes in Saturn's B ring[8] observed by Voyager 2 in 1981.

Hill and Mendis[9] gave proposal for the first time that the spokes might be consist of negatively charged dust particles. Goertz and Morfill[10] showed that the charged dust particles were electrostatically levitated about 80 km above the ring plane. One of the most unexpected findings of the Voyager mission was that the spokes are not stationary structures. They develop fast, with new spokes forming in as little as five minutes. The apex of the spokes is at synchronous orbit. This would tend to corroborate the idea that the dust grains essentially follow Keplerian orbits around the planet, whereas the plasma rigidly co-rotates with the planet, being trapped in the planetary magnetosphere. These structures cannot be explained by gravitational forces. Successful models for the formation of spokes recognized the importance of the electromagnetic forces acting on small charged dust grains. The filamentation of a ring disc finds a natural explanation in terms of the tearing instability of the dust-ring current. The Voyager 1 polarimeter shows images of several strands within F-rings which are braided. This ring also contains bright clumps, knots and kinks in several places. Avinash and Sen[11] showed the braids to be a consequence of the electromagnetic equilibrium of moving charged grains, involving collective effects. The electrostatic pressure on the grains is balanced by the electromagnetic Bennett-like pinch produced by the dust ring current. Helical current filaments, with three strands as observed, are easily produced. The formation of braids and filaments is shown to be a dynamic process, critically dependent upon local plasma conditions, which could explain why braids and kinks are not seen in all rings all the time.

Outer space is divided into many levels and the one that separates the stars is called interstellar space. Presence of dust grains in interstellar clouds has been known for a long time. Reddening of the light from stars and the wavelength dependence of interstellar excitation in the visible and near ultraviolet provided the first clue of the size of the interstellar dust particles, but provide little insight into their composition. In diffuse interstellar clouds, the dust component contains about one percent of the total mass[12]. The space is filled with tiny particles called cosmic dust and elements like hydrogen and helium. The actual density of hydrogen as it exist in interstellar space is on the average of about 1 atom per cubic centimeter. In the extremes, as low as 0.1 atom per cubic centimeter has been found in the space between the spiral arms and as high as 1000 atoms per cubic centimeter are known to exist near the galactic core. It is estimated that cosmic dust is 1000 times less common than hydrogen atoms in the interstellar medium. The dust grains in interstellar clouds are dielectric (ice, silicate etc.) and metallic (graphite, magnetite, amorphous carbons etc.) with a size distribution $n_d = A_a exp[-5(r_d/r_{di})^3]$ where n_d is the number density of grains of radius "r_d" and the constant "r_{di}" depends on the nature of the grain ($r_{di} = 0.5$ μm for ice, 0.25 μm for silicates etc.)[13]. Interstellar dust grains streaming into the solar system have recently been identified first by the Ulysses spacecraft in the heliocentric distance range from 2.2 to 5.4 AU[14] and subsequently by the Hiten spacecraft at 1 AU from the Sun. In the case of dust grains, it depends on the charge-to-mass ratio, whether they are sufficiently neutral to enter the solar system[15].

Our solar system is also believed to contain a large amount of dust grains and the origins of these dust grains in the solar system could possibly be, for example, micrometeoroids, space debris, man-made pollution and lunar ejecta, etc. Interplanetary space contains electromagnetic radiation, hot plasma, the solar wind, cosmic rays, microscopic interplanetary dust particles, and magnetic fields (primarily the Suns). The existence of interplanetary dust was known from the zodiacal light, with extremely small (0.001cm in diameter) grains or particles and are among the most primitive materials in the solar system. This dust is thought to be derived from collisions of asteroidal material and from comets[16].

The dusty cometary environment is an ideal cosmic laboratory for the study of physical and dynamical consequences of dust-plasma interaction. Comets are composed of admixture of non-volatile grains and frozen gases. The cometary dust particles, which are entrained by the gas sublimating from the nucleus, are immersed in a plasma and radiative environment, and are thus, electrically charged[17]. Comets possess separate ion and dust tails. It is quite possible that the space between the two tails are filled with some dusty plasmas which are invisible [18]. The data from the Vega and Giotto spacecrafts have provided much information about the cometary dust particles. A detailed analysis of this data showed that a significant amount of small grains were found to exist in cometary environment obeying a size distribution fitted by a power law given by the relation $n(r_d) \simeq r_d^{-s}$, with s being equal to 3.3 for Vega and 4.1 for Giotto[19]

In the Earths troposphere, dust is present at different altitudes. The dust can ascend to the stratosphere and ionosphere in the course of violent volcanic eruptions[20], rocket launchings and high-altitude flights and also as a result of convective and synoptic processes in the atmosphere. In the lower parts of the Earth's ionosphere dust particles can be seen as illuminated clouds long after sunset in the summer months, the so-called noctilucent clouds. These were for the first time observed in 1885, a few years after the explosion of the Krakatoa volcano in 1883. The presence of these clouds often coincides with strong radar backscatters, which have been shown to be associated with charged dust layers, and consist of ice particles which are charged by the plasma of the ionosphere. Dust particles can also become contaminated with Earths ionosphere as a result of bombardment by meteor showers. Ablation of the meteors at altitudes of 80 to 120 *km* in the lower ionosphere produces supersaturated vapors of metals, such as sodium, calcium, magnesium, etc.[21], which then condense into small grains with characteristic sizes of several nanometers to a few tenths of a micrometer. Dusty plasma in the ionosphere can also be formed[22] during active geophysical rocket experiments, which, e.g. can use the scheme of the experiments

'Fluxus' and 'North Star'[23] involve the release of some gaseous substance in near-Earth space. The formation of an artificial dusty plasma in the ionosphere was also revealed during the Spacelab 2 mission when the space shuttle orbital maneuver system engines were fired[24]. Recently, the presence of charged dust in the mesosphere has been detected by direct rocket probe measurements[25].

On Earth, the most common occurrence of plasmas are artificial ones, whether it be in lighting technology, fusion reactors or plasma processing techniques used for etching, thin film deposition, etc. In many of these systems, dust can seriously disturb the system or even destroy the product.

In the eighties, contamination of semiconductor surfaces caused by dust particles was recognized as a very serious problem for the semiconductor industry. This contamination influenced device topography, performance, reliability, and as a result manufacturing yield was reduced. Therefore, all fabrication steps were moved to clean rooms in which the particle contamination levels could be controlled and monitored. Furthermore, several other polluting processes like wafer handling and material flaking of the chamber walls were identified and corrected by improved procedures for chamber cleaning and maintenance. However, in spite of all these and several other precautions, chemical sources of particulate contamination remained present in the processing environment: the semiconductor processing plasmas themselves appeared to be a serious source of dust particulate production[19].

Dust can play an important role in fusion devices. In fusion reactors, dust can either grow inside the plasma or be evaporated or sputtered from the walls. This is not a problem for the current fusion experiments, but might prove a serious hinderance for the experimental reactor ITER, which is currently under construction in France. There, on the one hand, the dust is a safety concern due to radioactive activation of the grains, incorporation of tritium and beryllium, chemical reactivity and possible migration to and blockage of gaps or direct damage of the reactor blanket. Dust in fusion devices spans a wide size distribution from a size scale of mm down to $< 100nm$[19]. Part of the dust is ferromagnetic although no magnetic bulk materials are used for the in-vessel components. The presence of particles of size $< 100nm$ requires adequate measures to prevent incorporation and health damage for the people working inside the fusion devices. Redeposited layers contain significant amount of hydrogen isotopes. In future machines, this may lead to high T inventory in a form that can be liberated during a vacuum accident or opening. The large surface area and chemical activation by the nuclear decay will make the dust chemically highly reactive and reactions incase of water and air ingress have to be considered. On the other hand, dust could pose a threat to the operation of the fusion reactor. Flaking of dust from the walls could disrupt the plasma, increases the plasma resistivity, leading to increased voltages needed for start-up.

1.2 Theory of charging of dust grains

Dust particles in plasmas are usual charge carriers. They are many orders of magnitude heavier ($\sim 10^8$ times) than any other plasma particles and they can have many orders of magnitude larger (negative or positive) time-dependent charges. Such heavily charged objects will be strongly affected by electric fields. They can be suspended against gravity by the electric fields in wall sheaths. Their presence can influence the collective plasma behavior, for example, by alternating the wave modes and by triggering new instabilities. When dust grains are embedded in plasma they get charged by several mechanisms, e.g., by collecting electrons and ions, or through photo-electron or secondary electron emission. The charge on a dust particle is of fundamental interest, for it allows for the coupling between the fields and particles environment to the dynamics of the dust grains.

The evaluation of the electrical charge Q_d of a dust grain in a plasma is described by the current balance equation:

$$\frac{dQ_d}{dt} = \sum I_k = I$$

where I is the total charging current to the grain. Contributions to I come from various ways:

(a) electron and ion collection
(b) photoelectric emission
(c) secondary electron emission due to energetic electron impact
(d) secondary electron emission due to energetic ion impact
(e) electron field emission
(f) thermoionic emission
(g) triboelectric emission
(h) radioactive emission of electrons and α particles.

Out of these, electron and ion collection, photo emission and secondary electron emission due to energetic electron impact are very important for cosmic environment, while electron field emission is important for very small grains. In the charging of dust in volcanic plumes, friction mediated (triboelectric) emission is known to be very important, and may also have played some role in the early protoplanetary nebulae.

The currents to the grains depend on a number of properties of both the grains and the ambient medium. For instance, the electron and ion collection currents depend not only on the size and shape of the grains, but also on the electron and ion velocity distributions and densities, motion of the grain relative to the plasma, and the potential difference between the grain surface and the ambient dusty plasma, $(\Phi_s - \bar{\Phi})$. The photo-electron current depends on the electric properties of the grain, the grain surface potential and on the photo ionizing (ultra-violet) flux of radiation. The secondary electron emission current due to the energetic electron impact depends

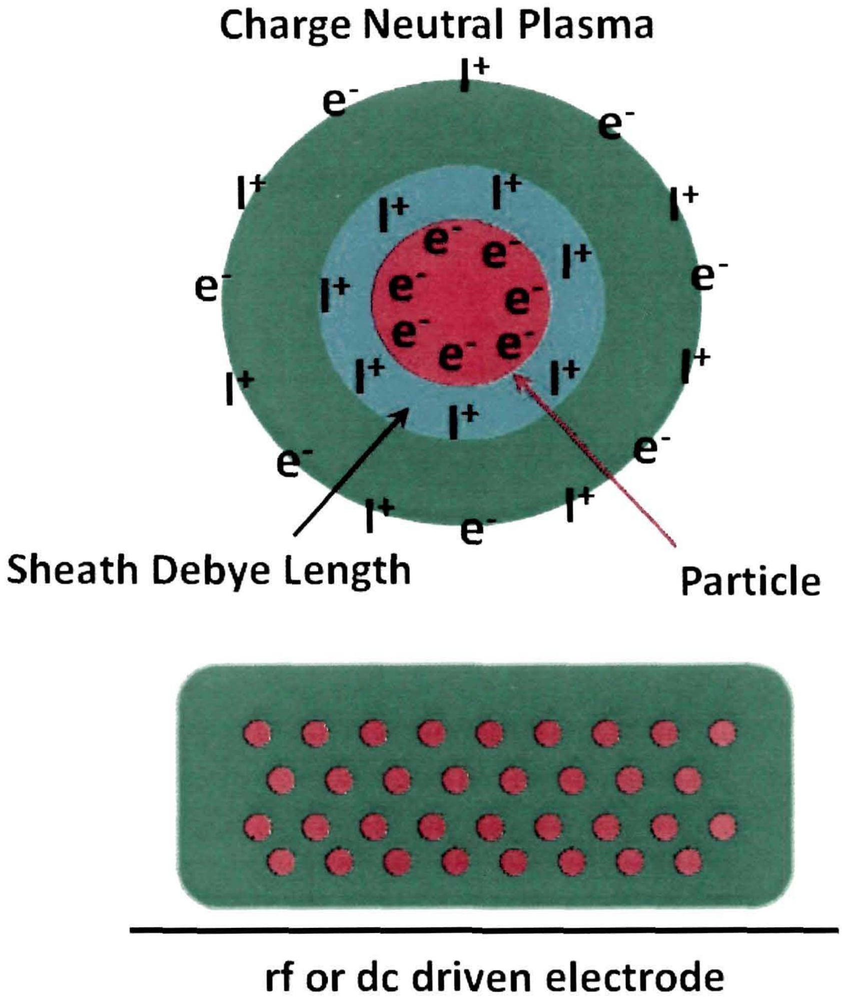
Charge Neutral Plasma
I+
e-
Sheath Debye Length
Particle
rf or dc driven electrode

Figure 1.2: Charging of dust grain.

on the secondary emission yield, which is dependent on the grain size. The electric field emission current, which is caused by large surface electric fields, is negligible for the large grains, but could become the dominant one when the grains become very small.

As a dust grain collects charges it changes the electrostatic potential distribution in its environment. If a grain initially collects more electrons than ions, the developing negative potential well around it will increase the ion flux and lower the electron flux. The electrostatic charge on the grain that balances these fluxes is the equilibrium charge. At equilibrium, the net current at the grain surface is zero, i.e.

$$\frac{dQ_d}{dt} = 0 \tag{1.2.1}$$

and

$$Q_d = C\left(\Phi_s - \bar{\Phi}\right)$$

here $(\Phi_s - \bar{\Phi})$ is the potential difference between the grain surface and the ambient dusty plasma and 'C' is the grain capacitance. For a spherical particle of radius r_d, the capacitance is

$$C = 4\pi\varepsilon_0 r_d.$$

Here, λ_D is the plasma Debye length. The values of both 'C' and $\bar{\Phi}$ depend on how closely the grains are packed together. The potential difference between the grain and the ambient plasma depends not only on the intrinsic electrical and physical properties of the grain but also on the relative motion between the grain and the plasma and on whether the grain can be regarded as being 'isolated' (i.e. $a >> \lambda_D$) or not $(a << \lambda_D)$. Here 'a' is the average inter-grain distance. For isolated grain of radius r_d, $C_{iso} = r_d(1 + 1/\lambda_D)$ and $\bar{\Phi} \longrightarrow 0$ and $Q_d = C\Phi$. On the otherhand, when $a << \lambda_D$, Φ_s approaches $\bar{\Phi}$ and Q_d can become very small despite the fact that C increases slightly above that of a isolated grain [17].

50502

1.2.1 Charging equation for isolated grains in plasma:

An important feature of a dusty plasma is the grain charge fluctuation. Charge and potential of a body immersed in plasma are determined by a balance between various electron and ion currents to the body. Charging of micron-sized grains can amount to *several thousand electron charges. The electric charge on the dust particles is a time-*dependent quantity and has to be considered as a dynamical variable. Calculation of charge on a particle is the starting point of every theory of dusty plasma, and it is important to study the charging of particles, because it is necessary in determining or predicting most of the plasma properties.

Electron and ion currents:

Orbit Motion Limited Theory

Most of the charging theories for dust grains are based on the theories of the electrostatic probes in a plasma. The probe theories predict the electron and ion currents to the probe. The currents are termed "orbit-limited" when the condition $r_d << \lambda_{Di} << \lambda_{mfp}$ applies, where r_d is the particle radius, λ_{Di} is the ion Debye length, and λ_{mfp} is a collision mean free path between neutral gas atoms and either electrons and ions ^{26}. This theory describes the way how the study of the currents collected by a small probe leads to information on the plasma parameters. Dust particles in a plasma behave as a microscopic probe. Therefore the general aspects of probe theory are relevant to dusty plasmas. According to the OML approximation the plasma currents can be calculated assuming that the electrons and ions are collected if their collisionless orbits intersects the probe surface.

For a Maxwellian ion distribution in the plasma, the ion current to the dust

CENTRAL LIBRARY, T. U.
ACC. NO. T149

particle in the OML regime has a form

$$I_i = +\pi r_d^2 e \sqrt{\frac{8T_i}{\pi m_i}} n_i \left[1 - \frac{e(\Phi_s - \Phi)}{K_B T_i}\right] \tag{1.2.2}$$

For Boltzmann distribution of the electron density, the electron current at the grain surface is given by

$$I_e = -\pi r_d^2 e \sqrt{\frac{8T_e}{\pi m_e}} n_e exp\left(\frac{e(\Phi_s - \Phi)}{K_B T_e}\right) \tag{1.2.3}$$

Here, $T_{i,e}$, $m_{i,e}$, and $n_{i,e}$ are the temperatures, masses and number densities of the ions and electrons respectively and K_B is the Boltzmann constant.

Equilibrium potential of a grain:

When the electron and ion thermal currents are the only charging currents, at equilibrium the net current at the grain surface is zero, i.e. $I_{0i} = I_{0e} = 0$ (where I_{0i}, I_{0e} are the equilibrium ion and electron currents collected by the grains respectively) and the grain surface potential (Φ_s) reaches an equilibrium potential called the equilibrium floating potential Φ_{f0}. The equilibrium potential of a negatively charged grain in a plasma with $T_e = T_i = T$ is,

$$\Phi_{f0} = -\beta \frac{K_B T}{e} \tag{1.2.4}$$

where β is a coefficient depending on the plasma parameters. e.g., $\beta = 2.5$, 3.6, 3.9 for H^+, O^+ and S^+ plasma, respectively.

Limitation of orbital motion limited theory:

OML theory of charging of dust grains has been derived under the condition that $r_d << \lambda_{Di} << \lambda_{mfp}$, where λ_{mfp} is the collisional mean free path between neutral gas atoms and either electrons and ions. The currents are calculated by assuming that the electrons and ions are collected if their collisionless orbits intersect the probe's surface. An absorption radius exist, outside the probe, such that particles which cross it are able to hit the probe. The collisional effect has been completely neglected. OML theory fails if

$$\lambda_{mfp} < r_d \left(-\frac{e\Phi_s}{K_B T_i} \right)^{1/2} \tag{1.2.5}$$

This provides a limitation to the use of OML theory in cases where collisional effect is not negligible [27]. The equation (1.2.5) is applicable for negatively charged grains.

Some effects, like, reduction in charge due to high dust density, positive charging by electron emission, reduction in electric forces due to ion trapping and charge fluctuations are often neglected in the OML model, but may have a significant impact on the particle transport.

Charge Fluctuation :

The OML model neglects that the electron and ion currents collected by the particle actually consist of individual electrons and ions. The charge on the particle is an integer multiple of the electron charge, $Q_d = Ne$ where N changes by -1 when an electron is collected and by z_i when an ion is absorbed. Electrons and ions arrive at the particle's surface at random times and the charge on a particle will fluctuate in discrete steps (and at random times) about the steady state value $< Q_d >$ [26]. The dust charge fluctuations can lead to resonance, diffusion, and drift phenomena, which would not be present if their charges were constant.

Ion trapping :

Ion trapping has been ignored in OML theory. A particle's negative charge creates Debye sheath for positive ions. An ion can be trapped in this region when it suffers a collision within the particle's Debye sphere, simultaneously losing energy and changing its orbital angular momentum. It remains trapped there, in an orbit bound to the particle, until it is detrapped by another collision. Trapped ions shield the charged particle from external electric fields. The effectiveness will vary with the number of trapped ions [26].

Secondary electron current:

The effect of electrons or ions bombarding grains with high energies can lead to an ionization of the grain material and ejection of electrons from the grain surface. This process is called secondary electron emission. The emission of secondary electrons can be caused by both electrons and ions. The secondary electrons emission yield δ depends on the energy of the plasma electrons/ions and on the material properties of the dust grains. The yield is generally much larger for the electron impact than for the ion impact.

Electron impact:

In case of electrons, secondary electron emission is a phenomenon that occurs when electrons impact on a dust grain surface with sufficient energy to 'knock' additional electrons from the surface of that grain. Generally, one electron gives rise to several secondary electrons. When the electron strikes the dust grain surface, several things can happen: An electron may be scattered or reflected by the dust grain surface without penetration. It may be stopped and stick to the grain surface. If the electron penetrates the dust grain surface, it may excite other electrons which may then be emitted at the surface. Some electrons may pass through the grain and leave with a little loss of energy.

Ion impact:

When the low energy ions (less than 1 KeV) are incident on a dust grain surface, these ions may become neutralized by the electrons tunnelling from within the grain across the potential barrier. The energy released can then excite other electrons leading to surface emission.

Generally secondary emission yield exhibits a maximum, δ_M, at an optimum energy E_M, which indicates that low energy primary electrons will not produce secondaries. Assuming a Maxwellian distribution of ambient plasma the secondary current for negatively charged grains ($\Phi_s < 0$) becomes,

$$I_{sec} = 3.7\delta_M I_e exp\left(\frac{e\Phi_s}{K_BT_e}\right) F_5\left(E_M/4K_BT_e\right) \tag{1.2.6}$$

where

$$F_5(x) = x^2 \int_0^\infty u^5 e^{-(xu^2+u)}du.$$

For positively charged grains ($\Phi_s > 0$),

$$I_{sec} = 3.7\delta_M I_e \left(1 - \frac{e\Phi_s}{K_BT_e}\right) exp\left(\frac{e(\Phi_s - \Phi)}{K_BT_e}\right) F_{5,B}\left(\frac{E_M}{4K_BT_e}\right) \tag{1.2.7}$$

The function $F_{5,B}\left(\frac{E_M}{4K_BT_e}\right)$ is defined as

$$F_{5,B}(x) = x^2 \int_B^\infty u^5 exp\left[-(xu^2+u)\right] du$$

here

$$x = \frac{E_M}{4K_BT_e}$$

and $B = \left(-\frac{x_e}{E_M/4K_BT_e}\right)^{1/2}$
where $x_e = -\frac{e\Phi_s}{K_BT_e}$.
Here B is not an imaginary value.

Photoelectric emission:

Absorption of UV-radiation releases photoelectrons and hence causes a positive charging current. Photoelectrons can be emitted from the surface of a dust grain when a flux of photons with energy larger than the photoelectric work function of the dust grain incidents on the grain surface. The magnitude of the current depends on the frequency of the incident photons, the surface area of dust grain, photoemission efficiency μ and particle's surface potential, which may, if positive, recapture a fraction of its photoelectrons. In many cases the released photoelectrons can be described by the Maxwellian distribution with a temperature T_P. The photoemission current is given as

$$I_{ph} = \pi r_d^2 K \mu \qquad \Phi_s \leq 0 \tag{1.2.8}$$

$$I_{ph} = \pi r_d^2 K \mu exp\left(-\frac{e\Phi_s}{K_B T_P}\right) \qquad \Phi_s \geq 0 \tag{1.2.9}$$

Here K is the UV flux,

$K_B T_P (\approx 1 - 3eV)$ is the average energy of the photoelectrons

$$\mu = \begin{cases} 1 & \text{for conducting materials} \\ 0.1 & \text{for dielectric materials} \end{cases}$$

Astrophysical and space plasmas are typically much less dense than laboratory plasmas. They are subjected to much more UV light. Consequently, the dominant process for charging dust particles in astrophysical plasmas is often photoelectron emission rather than the collection of electrons and ions. Apollo astronauts in 1960s and 70s reported about a "wired glow" on the horizon of the Moon. This turned out to be the reflection of sunlight from Moon dust particles photoelectrically charged and electrostatically levitated above the lunar surface[28].

Charging of grain ensembles: Reduction of charge

Until now we are dealing with a single grain in a plasma. This assumption is often unsuitable for modelling dusty laboratory plasmas, since they can have high particle concentrations. When dust number density becomes very large and intergrain distance is small, the grains may interact with each other via electrostatic

Coulomb forces, and collective effects may occur. Then dust particles may not move independently of each other but in a coherent way. In addition, in presence of grain ensembles, the floating potential and grain charge get reduced[29]. There exist two mechanisms of reduction of grain charges due to the presence of other dust grains:

1) the depletion of the electron density, and

2) the change of the electron and ion distributions due to charging processes on many grains[30].

This electron depletion modifies the plasma potential. There are two competing effects that lead to this result. One is that the capacitance of the grain increases, which tends to increase the charge and the other is that the magnitude of the grain surface potential relative to plasma potential decreases, which decreases the charge. The more important effect at high density arises from electron depletion, when the dust grains carry a significant fraction of charge density in the plasma, so that much of the electron charge resides on the grain surfaces. In this case, the surface potential of the grain does not have to be as negative with respect to the plasma potential as in the isolated grain case to balance the electron and ion currents to the grain. This leads to decrease in the magnitude of the grain charge, since the charge is proportional to $(\Phi_s - \Phi)$.

Xu et al.[31] has demonstrated experimentally the reduction of the magnitude of the grain charge when the dust density is high.

The depletion in grain charge can be investigated using "Havnes parameter" P_H, which is basically the ratio of the charge density of the particles to that of the electrons. When $P_H > 1$, the charge and floating potential are significantly diminished, while for $P_H << 1$, the charge and floating potentials approach the values for an isolated particle. In practical units P_H is given by

$$P_H = 695 T_d(eV) r_d(\mu m) n_d(cm^{-3}) / n_i(cm^{-3}) \quad (1.2.10)$$

where n_d, n_e are number densities of dust and electrons respectively In most cases it is more convenient to use the parameter P_H which does not depend explicitly on the value of the grain charge Z_d However, the dust charge is itself the function of the dust size and vice-versa and this independence of P_H on the grain charge is illusive[26]

1.2.2 Physical effects manifested by charged dust:

Coagulation

Coagulation is a randomly growth process whereby particles can stick together via mutual collisions forming larger grains This process can take place in the presolar nebula, circumsolar, circumplanetary, cometary, etc environments For most cases the coagulating particles are immersed in a radiative and plasma environment, and they will collect electrostatic charges The charge collected on a submicron sized grain is sufficient to prohibit collisions if the relative velocity of the coagulating particles is of the order of few cms^{-1} In this case, grains may not be energetic enough to overcome the Coulomb repulsion

Horanyi and Goertz[32] have run numerical simulations of the coagulation processes in a plasma, with a model in which the grain charge is determined by plasma charging currents and secondary emission They assume a constant source of small grains from condensation and these then coagulate to larger ones Safranov[33] has also studied the coagulation of uncharged grains Birmingham and Northrop[34] are including all electrostatic forces between two grains as well as plasma shielding Coulomb force between the positively charged larger grains and negatively charged smaller grains enhance the coagulation rate

When grains with different compositions coexist in a given environment, photoemission might lead to oppositely charged grains In that case a significantly increased coagulation rate is expected due to the Coulomb attraction between oppositely charged grains Photoemission is of little significant in dark molecular clouds or in the optically thick presolar nebula where grain growth may occur When the plasma temperature varies in time one can get opposite charges between grains identical in composition

Chow et al [35] have shown that dust grains of different sizes can acquire opposite charges in warm plasmas even in the absence of charges in plasma environment They have calculated the equilibrium potential for conducting and insulating grains immersed in both Maxwellian and generalized Lorentzian plasmas Due to the effect of size of grains on secondary emission, they have found that insulating grains with diameter $0\ 01\mu m$ and $1\mu m$ have opposite polarity (the smaller one being positive) when the plasma temperature is in the range of $25 - 48eV$ in Maxwellian plasma Existence of different sized grains of opposite polarity-negatively charged large grains and positively charged small grains is possible in the interplanetary medium, local inter-stellar medium, supernova remnants etc Both secondary emission and photo-emission may cause dust grains to acquire opposite charges in the same plasma and radiative environment, even if they have the same size, if their secondary emission and photo-emission yield vary widely This leads to enhanced dust coagulation in certain region of the interstellar space

Disruption

Disruption is an opposite physical effect of coagulation It occurs if the grains acquire numerically very high potentials This is a consequence of the electrostatic repulsion of like surface charges which produces an electrostatic tension in the body If this electrostatic tension exceeds the tensile strength of the body across any section, the body will break up across that section

According to Opik[36], electrostatic disruption occurs across a section if the electrostatic energy density $\Phi^2/8\pi r_d^2$ exceeds the tensile strength F_t, i e

$$F_t < \frac{\Phi^2}{8\pi r_d^2} \qquad (1\ 2\ 11)$$

or we can say that disruption will occur if the grain radius is less than a critical value r_d^c, i.e.

$$r_d < r_d^c \qquad (1.2.12)$$

where $r_d^c = 6.65 F_t^{-1/2} |\Phi|$, Φ is in volts, F_t is in $dyncm^{-2}$ and r_d^c (or r_d) is in microns. From equation (1.2.11) it is clear that, the value of F_t required to prevent grain disruption increases rapidly as the size of the dust grains r_d decreases. It means that as the dust grain begins to disrupt electrostatically, the process continues until smaller fragments for which $r_d > r_d^c$ appear. In that case, it can provide an obstacle for grain growth in plasma. However, the electric field emission of the electrons from small grains may truncate this runway disruption. The reason behind is that, as the grain radius decreases, the surface electric field increases to reach such a value ($\geq 10^7 V/cm$) that rapid electron emission occurs from negatively charged dust grains and the value of the grain potential decreases to a value that is no longer given by the plasma environment but rather by the size alone. Consequently, materials such as iron ($F_t \simeq 2 \times 10^{10} dyncm^{-2}$) and tektites ($F_t \simeq 7 \times 10^{10} dyncm^{-2}$) are stabilized by this process against electrostatic disruption of grains regardless of their size. Very fragile grains such as cometary grains ($F_t \simeq 10^6 dyncm^{-2}$) of very small radii ($\approx 10A^0$) will be stable only if $|\Phi| \leq 0.15eV$.

The electric field emission effect will enable the grain growth to take place in the above environments only if the grains are negatively charged, which means that if there is sufficient UV radiation to make the grain charge positive due to the photoemission, the growth of the dust grain will not proceed even in a low-temperature plasma.

Leviation

Electrostatic charging of the dust grains can also lead to the levitation of the fine dust lying on large surfaces. In this case, the charge Q_d acquired by the dust grain is proportional to its projected surface area[37] and so,

Q_d = surface area × surface charge density = $(1/4)\,(r_d/\lambda_D)\,(r_d\Phi_s)$

Typically, $r_d/\lambda_D << 1$, hence the dust grain charge in a plasma medium is much smaller than that in free space. Mendis et al [38] considered the charging of the bare cometary nucleus by the solar wind plasma and the solar UV radiation at large heliocentric distances. They showed that while the subsolar point of the cometary surface acquires a positive potential of $\sim +5V$ due to dominance of photoemission, the nightside could acquire a negative potential. Therefore, submicron-sized grains could overcome the gravitational attraction of the nucleolus and levitate on the nightside of the comet, even when they had a deficit of just one electron charge.

1.2.3 Forces acting on the dust grains :

There are a number of forces that act on charged dust grains, and may control their dynamics in the plasma. These are

(a) force due to gravity
(b) self-gravitational force
(c) thermophoretic force
(d) electrostatic and electromagnetic forces
(e) radiation pressure force
(f) neutral drag force
(g) ion drag force

Force of gravity :

A dust particle in the plasma is subject to gravity and the exerted force is proportional to the dust particle mass density $\rho_d = n_d m_d$. For a spherical dust particle, the gravity force can be expressed as

$$F_g = \frac{4\pi r_d^3}{3}\rho_d g \tag{1.2.13}$$

where g is the gravitational acceleration. The gravitational force is important in radio-frequency discharges, where the dust particle is pulled downward toward the lower electrode.

In a self-gravitating system, the force acting on a dust grain is

$$F_g = -\frac{G\rho_d M r}{r^3} \tag{1.2.14}$$

where $G = 6.672\times 10^{-8}$ dyn cm^2 g^{-2} is the gravitational constant and r is the distance to the dust grain from the central body of mass M. The central body may be a nearby planet, a star, or a satellite. For a distribution of masses, the force is

$$F_g = -\rho_d \nabla\psi \tag{1.2.15}$$

where the potential ψ is obtained from the gravitational Poisson equation $\nabla^2\psi = 4\pi G\rho_d$. The self-gravitational force may be important for molecular clouds[2] and dust elevated above Saturns rings[39].

Thermophoretic force :

In the presence of the neutral gas temperature gradient ∇T_n, the dust particles feel thermophoretic force. When the mean free path of the neutral particles is larger than the dust particle radius r_d, the thermophoretic force acting on a spherical dust particle in a monatomic gas becomes[40]

$$F_T = -\frac{8\sqrt{2\pi}r_d^2}{15v_{tn}}\left[1 + \frac{5\pi}{32}(1-\alpha)\right] k_T \nabla T_n \tag{1.2.16}$$

where $v_{tn} = (T_n/m_n)^{1/2}$ is the average thermal speed of the neutral atoms, k_T is the translational part of the thermal conductivity and the accommodation coefficient α is of order unity for surface and gas temperatures between 300 and 500 K.

The thermophoretic force plays an important role in the formation of different shapes of plasma-dust structures[41] It has been proposed that the thermophoretic force may also play a decisive role in production of semiconductors[42], as well as in fabrication of amorphous solar cell[43]

Electrostatic force :

In the presence of an electric field E in the plasma, the force acting on a conducting dust particle is referred to as electrostatic force This force can ce expressed as

$$F_e = Q_d E_{eff} \tag{1 2 17}$$

where the effective electric field in the plasma is[44]

$$E_{eff} = E\left[1 + \frac{r_d/\lambda_D}{3(1+r_d/\lambda_D)}\right]$$

An increase in E_{eff} compared to E is associated with the plasma polarization in the vicinity of the dust particle, which is induced by the external electric field However, the plasma polarization effect is small for $r_d/\lambda_D << 1$

Radiation pressure force :

In the presence of the electromagnetic radiation, dust grains are subject to the radiation pressure force

$$F_r = \frac{\pi r_d^2 I_0}{c}\hat{e_r} \tag{1 2 18}$$

where I_0 is the photon energy flux along the direction $\hat{e_r}$ The radiation pressure force is important for submicron particles that are generated close to the Sun and are driven out of the solar system on hyperbolic orbits Such particles (β meteorids) have been observed by the Pioneer 8, 9 and Ulysses spacecrafts in the solar wind[45]

Neutral drag force :

A neutral drag force results from collisions with neutral gas molecules and causes momentum transfer from the neutral gas to the dust particles. The neutral drag force F_{dn} for a Maxwellian distribution of neutral gas molecules is approximated by[19,46]

$$F_{dn} = -\frac{8}{3}\sqrt{2\pi} r_d^2 \rho_n v_{tn} \left(v_d - v_n\right) \tag{1.2.19}$$

where $\rho_n = n_n m_n$ is the mass density of the neutral molecules, v_n is the velocity of the neutral molecules and $v_{tn} = \left(\frac{K_B T_n}{m_n}\right)^{1/2}$ is the thermal speed of neutral particles. Where T_n is the neutral temperature.

Ion-drag force :

The ion-drag force F_{ion} in plasmas arises due to collisions between drifting ions and charged dust grains. The force basically describes the momentum transfer from the drifting ions to the dust particles on account of (i) direct collection of momentum for ions that collide with the negatively charged grain and (ii) deflection of the ions in the electrostatic field of the negatively charged dust grain. Thus, the ion-drag force is the sum of the collection and Coulomb forces, i. e. $F_{ion} = F_{coll} + F_{Coul}$. Assuming that the dust particles are at rest, the collection force is given by

$$F_{coll} = \pi b_c^2 \rho_i v_s v_i \tag{1.2.20}$$

where $\rho_i = n_i m_i$ is the ion mass density, v_i is the ion streaming velocity, $v_s = \left(v_i^2 + 8T_i/\pi m_i\right)^{1/2}$ is the mean speed of ions approaching the dust particle, and $b_c = R(1 - 2Z_i e\phi_s/m_i v_s^2)^{1/2}$ is the maximum impact parameter for dust-ion collision from the orbital motion limited probe theory. Here ϕ_{f0} is the floating potential of the dust particle. The orbital motion limited treatment is justified if the potential can be treated as spherically symmetric and $r_d < \lambda_D$.

The Coulomb force can be written as

$$F_{Coul} = 4\pi b_{\pi/2}^2 (1/2) ln \left[\left(\lambda_D^2 + b_{\pi/2}^2\right) / (b_c^2 + b_{\pi/2}^2)\right] \rho_i v_s v_i \tag{1.2.21}$$

where $b_{\pi/2} = Q_d e/m_i v_s^2$ is the impact parameter for 90^0 deflection.

1.2.4 Waves in dusty plasma:

Dusty plasmas known to support new kinds of very low-frequency modes that are more specifically 'dust-mode' since they involve the dynamics of the dust grains themselves.

When $r_d << a << \lambda_D$, the charged dust grain may be considered as point particles, similar to multiply charged positive or negative ions[47]. However plasma consisting of electrons, ions and dust grains is quite different from negative ion plasma in several aspects. Typical dust grains have charge to mass ratios, which are generally orders of magnitude smaller than those of ions. For example, a dust grain of mass density $0.5 gm/cm^2$ and radius $r_d \sim 1$ micron has a mass of about 10^{12} proton masses. The charge on such a grain in a thermal $10eV$ oxygen plasma, when only plasma collection is considered, is of the order of 2.5×10^4 elementary electron charges. The plasma frequency of species α is

$$\omega_{p\alpha} = \left(4\pi n_\alpha q_\alpha^2/m_\alpha\right)^{1/2}$$

and gyrofrequency of species α is

$$\Omega_\alpha = |q_\alpha B/m_\alpha|$$

The typical frequencies associated with the dynamics of dust grains are very low compared with typical ion frequencies in standard electron-ion plasmas. Moreover, the grain charge depend on both the properties of the dust particles and the ambient plasma and radiative properties. Hence, the charge to mass ratio can differ in different environments even for a grain of fixed size and electrical properties. It is also observed that dust grains are generally poly disperse, i.e. they have a size distribution. Since the dust mass $m_d \propto r_d^3$ and dust charge $Q_d \propto r_d$, the frequencies associated with dust grains may be continuous variable[17].

The presence of charged dust not only modifies the usual linear modes, but also gives rise to new modes in the low frequency and low velocity regimes[48]. New low frequency modes associated with the dust grain dynamics are included via the momentum and continuity equations for the dust species as given by,

$$n_\alpha m_\alpha \left(\frac{\partial}{\partial t} + \vec{v_\alpha}\,\nabla\right)\vec{v_\alpha} = -\nabla P_\alpha + Q_\alpha n_\alpha \left(\vec{E} + \frac{\vec{v_\alpha} \times \vec{B}}{c}\right) \tag{1.2.22}$$

$$\frac{\partial n_\alpha}{\partial t} = -\nabla\,(n_\alpha \vec{v_\alpha}) \tag{1.2.23}$$

The balance of charge is altered by the presence of the dust, so that the condition for charge neutrality in a plasma becomes

$$n_e = Z_i n_i + \epsilon_d Z_d n_d \tag{1.2.24}$$

where $\epsilon_d = 1$, -1 for positively and negatively charged grains respectively. When one consider frequencies well below the typical frequencies of an electron/ion plasma, new dust mode appears in the dispersion relations for plasma consisting of ions, electrons, and charged dust grains.

In particular, three wave modes arising due to dust dynamics have been extensively studied, both theoretically as well as experimentally. The existence of electrostatic acoustic like mode called the 'Dust-Acoustic Wave" (DAW) was theoretically predicted by Rao et al.[49] by using a collision less fluid model applicable in the weak coupling regime. This mode is a long wave length, low-frequency collective oscillation in an unmagnetized dusty plasma in which the dust mass provides the inertia, while the restoring force comes from the pressure of the intertialess electrons and ions. The dispersion relation for the dust-acoustic wave is

$$\omega^2 = 3k^2 v_{th\,d}^2 + \frac{k^2 C_{DA}^2}{1 + k^2 \lambda_D^2}$$

where $C_{DA} = \omega_{pd}\lambda_d$ is the dust acoustic (DA) speed. This DAW mode exists for constant grain charge. The frequency range for this mode is given by $k v_{th\,d} <<$

$\omega << kv_{th\,i}$, where ω and k are the wave angular frequency and wave number and $v_{th\,d}$ and $v_{th\,i}$ are the thermal speeds of the dust and ions[50]. The phase velocity of linear waves is approximately given by $(n_{d0}ZT_e/n_{i0}m_d)^{1/2}$; where, n_{d0}, Z and m_d are number density, charge and mass of the dust particle. T_e is the electron temperature and n_{i0} is the ion density.

In the strong coupling regime ($\Gamma >> 1$), Dust lattice (DL) waves are produced by the oscillations of regularly spaced charged micrometer sized particles suspended in a plasma i.e., in so-called plasma crystals, which are formed as a result of strong mutual Coulomb interaction. The simplest model of one dimensional longitudinal dust lattice wave (DLW) was theoretically described by Melandsø[51] , taking into account only small vibrations in the dust lattice and the electrostatic interaction between the nearest dust grains. In a dusty plasma crystal, the microscopic potential from the individual dust particles will be efficiently shielded by the plasma. This allows to consider only interactions between neighbor particles, when the average dust particle separation 'a' is of the order of or larger than the plasma shielding length (λ_D). Melandsø considered as a simple model a one-dimensional Bravais lattice for dust lattice wave (DLW) propagation. A quasi-particle approach, where, the dust particles are modelled as discrete particles, while the plasma is described as a continuous medium, has been used. In the linear approximation, the dispersion relation of DLW can be expressed as

$$\omega^3(k) = \pm 2\left(\frac{\beta(a)}{m_d} sin^2\left(\frac{1}{2}ka\right) + \frac{\beta(2a)}{m_d} sin^2(ka)\right)^{\frac{1}{2}} \tag{1.2.25}$$

where m_d is the mass of the dust particle, $a = r_{j+1,0} - r_{j,0}$, $r_{j,0}$ is the equilibrium positions. The dust particles are assumed to be sufficiently strongly coupled so that they only obtain small oscillations $r_j = r_{j,0} + \eta_j$. For $a/\lambda_D > 1$ only interactions between nearest neighbor particles may be sufficient to include, which gives

$$\omega^3(k) = \pm 2\left(\frac{\beta(a)}{m_d}\right)^{\frac{1}{2}} sin\left(\frac{1}{2}ka\right) \tag{1.2.26}$$

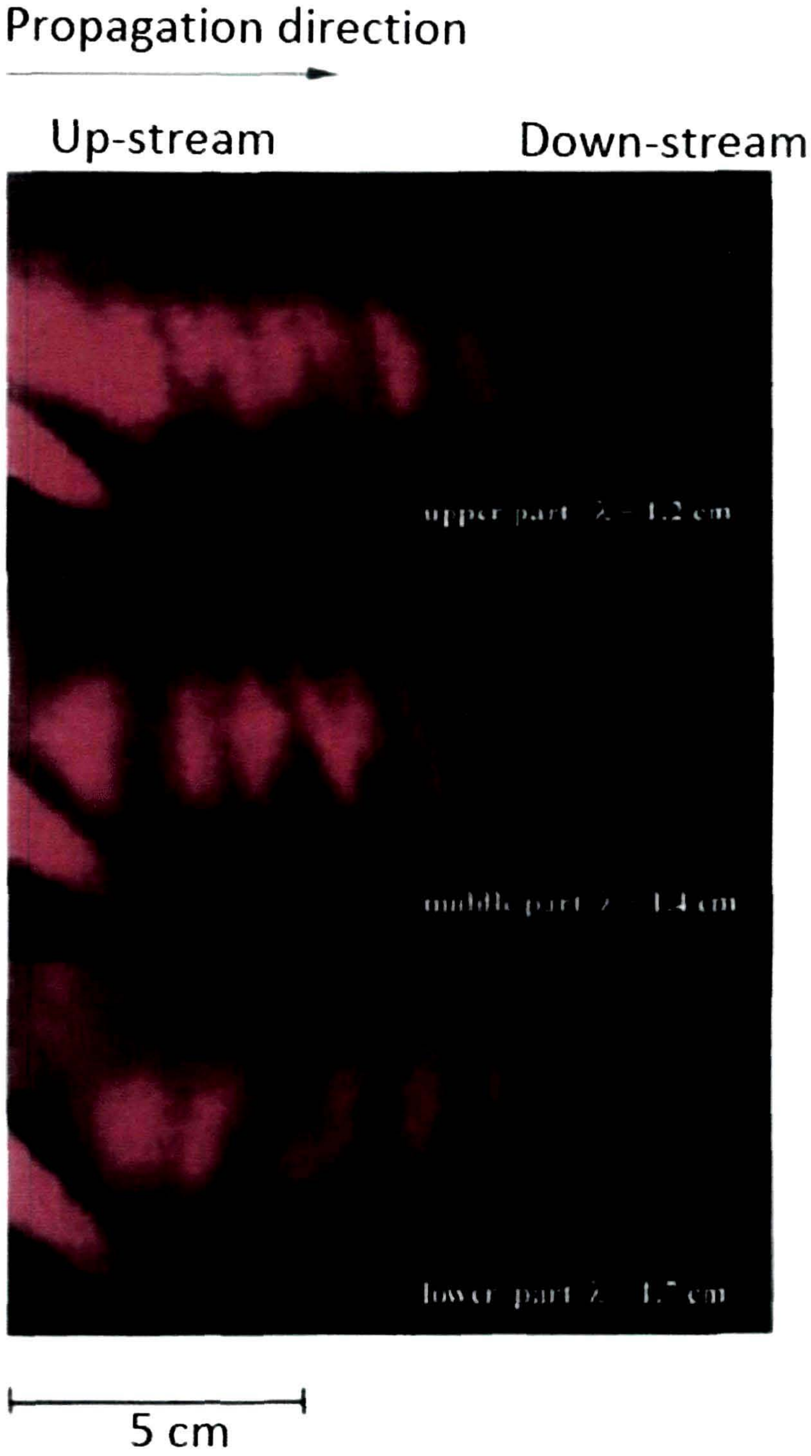
Propagation direction
Up-stream
Down-stream
upper part λ = 1.2 cm
middle part λ = 1.4 cm
lower part λ = 1.7 cm
5 cm

Figure 1.3: Spontaneously exited dust acoustic waves.

where

$$\beta(x) = \frac{Q_d^2}{2\pi\varepsilon_0 x^3} exp\left[-xk_D\right]\left(1 + k_D x + \frac{k_D^2 x^2}{2}\right)$$

while

$$k_D = \lambda_D^{-1},\ \eta_j \sim exp\left[i(\omega t - r_{j,0}k)\right]$$

However, in physical system with periodic boundary conditions, the wave numbers are obtained by satisfying

$$exp[ikNa] = 1$$

or

$$kNa = 2\pi m$$

.

This relation gives the N (total number of dust grains) possible wave frequencies

$$\omega^3(m) = \pm 2\left(\frac{\beta(a)}{m_d}\right)^{\frac{1}{2}} sin\left(\frac{\pi}{n}m\right) \quad (1.2.27)$$

or the first Brillouin zone for the harmonic numbers $m = 1, 2, ..., N/2$.

Non-linear waves can be described by including terms of the order $(\eta_{j+1} - \eta_j)^2$ or larger. This results in the well known Korteweg-de Vries equation[51].

DL waves have been experimentally observed by Morfill et al.[52] and Homann et al.[53]. The analytical results of Melandø have been tested numerically and very good agreement has been found between theory and experiment.

On the otherhand, Shukla and Silin[54] showed that in dusty plasma an ion-acoustic wave exists even when electron and ion temperatures are equal, called "Dust ion-acoustic wave" (DIAW). The DIA wave occurs in the frequency range $kv_{th\,i} <<$

$\omega << kv_{th.e}$. In the phase velocity regime where electron inertia is negligible and in the limit of very large dust mass, the dispersion relation for dust-ion-acoustic waves in a plasma with electrons, singly charged ions and charged dust is

$$\omega^2 = \frac{k^2 C_S^2}{1 + k^2 \lambda_{De}^2}$$

where $C_S = \omega_{pi}\lambda_{De} = (n_{i0}/n_{e0})^{1/2} c_s$ and $c_s = (K_B T_e/m_i)^{1/2}$. In the long wavelength limit (i. e. $k^2\lambda_{De}^2 << 1$) the above equation reduces to

$$\omega = k \left(\frac{n_{i0}}{n_{e0}}\right)^{1/2} c_s \tag{1.2.28}$$

The equation (1.2.28) shows that the phase velocity $V_{ph} = \omega/k$ of the DIA waves in a dusty plasma is larger than c_s, because, $n_{i0} > n_{e0}$ for negatively charged dust grains. The increase in the phase velocity is attributed to the electron density depletion in the background plasma, so that the electron Debye radius becomes larger. As a result, there appears a stronger space charge electric field which is responsible for the enhanced phase velocity of the DIA waves. This DIA wave may have some relevance to low-frequency noise in the F-ring of Saturn. Typical frequencies of this waves for laboratory plasma parameters are tens of kHz.

Rosenberg identified a dimensionless parameter f in dusty plasma, called 'fugacity' which is a measure of grain packing[55]. It is defined by

$$f = 4\pi n_d \lambda_D^2 r_d \sim \frac{N_D r_d}{\lambda_D}$$

where, $N_D = n_d\lambda_D^3$ is the dust plasma parameter[56] and n_d, λ_D and r_d are the dust number density, the Debye length and the grain size respectively. Fugacity is useful in characterizing the different regimes of dusty plasmas for the existence of different types of dust modes. Dusty plasmas are defined to be tenuous (low fugacity), dilute (medium fugacity) or dense (high fugacity) according as $f << 1$, $f \sim 1$ or $f >> 1$ respectively. The usual DAWs and DLWs are applicable for tenuous or dilute dusty plasmas ($f \leq 1$) such as those found in the laboratory experiments [53,57–61] ($f \sim 10^{-2}$), Saturnian E- and G-rings ($f \sim 10^{-4} - 10^{-3}$), and the Jovian ring ($f \sim 1$) [62,63].

During the years 1999 - 2000 Rao proposed the existence of yet another new, very low frequency electrostatic dust plasma wave, called the "Dust-Coulomb wave" (DCW)[56]. The DC waves are the normal modes associated with the grain charge fluctuation, and are derived by an effective pressure called "Coulomb pressure" defined by $P_c = \frac{n_d Q_d^2}{r_d}$. This wave mode occurs in dense dusty plasma regime ($f >> 1$). It was shown that DC wave is accompanied by dust charge as well as number density perturbations, which are proportional to each other. The dispersion relation for DC wave is

$$\frac{\omega^2}{k^2} = \frac{C_{DC}}{\delta(1 + k^2 \lambda_{r_d}^2)} + \gamma_d v_{th.d}^2$$

where $\lambda_{r_d} = a\sqrt{a/3r_d\delta}$ is a new length scale, a is the Wigner-Seitz radius, $C_{DC} = Q_d/\sqrt{m_d r_d}$ is the phase speed, γ_d is the adiabatic index for the dust fluid and $\delta = \frac{\omega_2}{\omega_1}$, while, ω_2, ω_1 are the charging frequencies given by:

$$\omega_1 = \chi + n_{e0} r_d e^2 \left(\frac{2}{\varepsilon_0 T_e m_e}\right)^{1/2} exp\left(\frac{e\phi_{s0}}{T_e}\right) \tag{1.2.29}$$

and

$$\omega_2 = \omega_1 - \frac{e\phi_{s0}}{T_i}\chi$$

$$\chi = \frac{1}{\sqrt{2\pi}} \frac{r_d \omega_{pi}}{\lambda_{Di}} \tag{1.2.30}$$

respectively and $\phi_s = \frac{Q_d}{r_d}$ is the dust grain surface potential relative to the plasma potential. Since $a << \lambda_D$, the Coulomb interaction between the grains plays a dominant role in providing the restoring force for this modes, while the inertia arises from the dust grain mass. For a given wave number, the DC wave frequency is much smaller than the DA wave frequency.

In the dilute regime, the DA wave and DC wave modes merge into a single mode, called the "Dust charge-density wave" (DCDW)[64]. The dispersion relation for DCD wave is given by

$$\frac{\omega^2}{k^2} = \frac{C_{DC}^2 C_{DA}^2}{C_{DC}^2 + C_{DA}^2 \delta} + \gamma_d v_{th\,d}^2$$

where, C_{DA} is the DAW phase speed[49] defined by

$$C_{DA}^2 = \omega_{PD}^2 \lambda_D^2 = \frac{Q_{d0}^2 n_{d0} T_e T_i}{m_d e^2 \left(n_{e0} T_i + n_{i0} T_e\right)}$$

Here,

$$\omega_{PD} = \sqrt{\frac{4\pi n_{d0} Q_{d0}^2}{m_d}}$$

is the dust plasma frequency,

$$C_{DC} = Q_{d0} / \sqrt{m_d r_d}$$

and $v_{th.d} = \sqrt{\frac{2T_d}{m_d}}$ is the dust thermal speed and γ_d the adiabatic index for the dust component.

In a magnetized, homogeneous dusty plasma, the presence of charged dust can similarly affect Electrostatic Ion Cyclotron (EIC) waves and lower hybrid waves. There may exist four modes: two ion-acoustic waves and two EIC waves. One of the EIC modes, the electrostatic dust ion cyclotron (EDIC) mode, corresponds to the usual EIC wave in an electron-ion plasma but is modified by the presence of the negatively charged, but static dust. The other EIC mode is a completely new electrostatic dust cyclotron (EDC) mode which is associated with the gyro-motion of the magnetized dust grains. For negatively charged dust, frequencies of both acoustic waves increase with dust density as does the frequency of the positive ion EIC waves. For positively charged grains, the frequency of the ion-acoustic mode decreases with increasing dust density, while the frequency of ion EIC mode approaches the ion gyrofrequency as n_d increases.

The dispersion relation of the lower hybrid mode in the frequency regime Ω_d, $\Omega_i << \omega << \Omega_e$, is also modified by the presence of charged dust. In the limit

$m_d \longrightarrow \infty$ in a dense plasma with $\omega_{pe}^2/\Omega_e^2 >> 1$, the lower hybrid wave frequency is

$$\omega^2 \approx \delta z_i \Omega_e \Omega_i$$

which increases as the negative dust density increases.

The dispersion properties of a low frequency electromagnetic waves, viz. Alfven waves, magnetosonic waves are also influenced by the presence of dust grains. The Alfven wave spectrum in the cold plasma in very low-frequency regime $\omega << \Omega_d$ becomes

$$\omega^2 = \frac{k^2 v_A^2}{[1 + (v_A/C)^2 + (n_{d0} m_d / n_{i0} m_i)]}$$

where, the Alfven speed is

$$v_A = \left(\frac{B^2}{4\pi n_{i0} m_i} \right)^{1/2}$$

In an inhomogeneous magnetized low β plasma the effect of negatively charged dust grains on electrostatic drift waves was studied by Shukla et al.[65] The dynamics of the dust grains are taken into account by means of a fluid model. A new type of low-frequency waves, the dust-drift waves, is shown to exist in the region $\omega << \Omega_d$. The dust-drift waves may be relevant in astrophysical and cometary plasmas.

We have described different types of waves that are theoretically found to exist in dusty plasmas. Recently, some of these waves have also been observed in laboratory experiments. Chu et al.[66] reported very low-frequency ($\approx 12Hz$) modes with a wavelength of about $0.5cm$. They used a radio-frequency discharge, with a vertical dc electric field that suspended the particles in the sheath region above a horizontal electrode. Based on the apparent phase velocity of 6 cm/s in that experiment, D'Angelo has suggested that the fluctuations were a dust-acoustic mode[67]. In the experimental observation, Barkan et al.[57] used a He-Ne laser beam to illuminate the dust, and a video camera to record planar wave fronts of a polydisperse kaolin dust cloud. The wave was reported to have been excited by ion drift in the system, and had a wavelength of 0.6 cm, a propagation speed of ~ 9 cm/s, and a frequency ~ 15

Hz. Praburam and Goree[68] in their experimental study have tentatively identified low-frequency modes having properties of either an ionization wave or a compressional dust acoustic wave. As the particle size grows, the instability develops in two stages: first a "filamentary mode" of approximately 100 Hz in which the ionization rate and dust number density are both modulated, and then a "great void mode" which is similar, except that there is a single prominent void in the dust cloud which rotates azimuthally with a frequency of about 2 Hz. The filamentary mode appears suddenly when the dust grain diameter exceeds a certain critical value.

Dust lattice wave has been experimentally observed by Homann et al. In their experiment, the screening of dust particles immersed in the sheath of a parallel plate rf discharge in helium is studied by excitation of waves in a linear chain arrangement. The waves are excited by the radiation pressure of a modulated laser beam. The measured dispersion relation is compared with a one-dimensional dust lattice wave to obtain the shielding length[53].

In a dusty plasma laboratory experiment Barkan et al.[69] have observed current driven electrostatic ion cyclotron (EIC) waves for ordinary plasmas. The experimental results verifies the theoretical prediction made by D'Angelo in 1990[70] and Chow et al.[71] in 1995, that EIC waves are possible plasma modes in dusty plasmas.

Recent laboratory observations conclusively reveal that coherent nonlinear waves and structures (viz., solitons, shocks, Mach cones, voids, vortices, etc.) can be produced in a dusty plasma. Bharuthram et al.[72] investigated the formation of large amplitude ion-acoustic solitons in a dusty unmagnetized plasma with negatively charged grains, cold ions and Boltzmann distributed electrons. The presence of dust grains was found to lead to the appearance of rarefactive (negative potential) solitons. DIA solitary waves can have both positive and negative localized potential structures. Solitary waves are formed due to a delicate balance between the wave dispersion and nonlinearity associated with the harmonic generation. Nonlinear ion-acoustic waves may be relevant to the formation of an electrostatic shock inside the ionopause at comet Halley. Shock like structures arise as a result of the balance between nonlinearity (causing wave steepening) and dissipation (e.g., due to wave particle interactions, dust charge fluctuations, anomalous viscosity, etc.). Melandsø and Shukla were the first to predict the formation of the dust acoustic shock due to dust charge fluctuations that produce collisionless dissipation in a dusty plasma[73] Popel et al.[74] and Mamun and Shukla[75] proposed that the DIA shock waves in the experiments of Nakamura and colleagues[76] could be arising due to a balance between the harmonic generation nonlinearity and the dissipation caused by dust charge fluctuations. Rao et al.[49] showed that dust-acoustic waves could also propagate nonlinearly as solitons of either negative or positive potential in a three component plasma with electrons, ion, and negatively charged, cold dust grains. Verheest[77] extended the latter analysis to a multispecies dusty plasma, allowing for both hot and cold electrons and for a number of cold dust grain species, and found also that both refractive and compressive solitons could propagate. Schamel et al.[78] have also shown that a continuum of nonlinear, steady-state, ultra low frequency acoustic mode which propagates near the dust thermal speed, exists in dusty plasma characterized by deficit of dust particles trapped in the trough of wave potential. One of the earliest experimental measurements on the dust acoustic mode in strong coupling regime was made by Pieper and Goree[58] who excited the plasma with a real external frequency and measured the complex wave vector. However in their experiment they were unable to clearly isolate the strong coupling effects from the collisional effects. This is because the background neutral pressure in their experiment was kept quite high in order to cool down the dust component through dust neutral collisions. The damping (as well as the dispersive effects) arising from a large ν_{dn} term then tends to mask out the strong coupling contributions. Numerical simulations have been more successful in tracking the various strong coupling modifications of the longitudinal dust acoustic mode. The transverse shear mode has recently been experimentally seen in a monolayer dusty plasma[79] and also in a three-dimensional dusty plasma that is in the strongly coupled fluid regime[80]. These spontaneous oscillations occur when the ambient neutral pressure is reduced below a threshold value.

1.2.5 Instabilities in dusty plasma:

The stability character of plasma gets modified due to the presence of charged dust particles. Instability is always a motion which decreases the free energy and brings the plasma closure to thermodynamic equilibrium[81]. Instabilities may be classified according to the type of free energy available to drive them. In dusty plasma, there are new classes of instabilities associated with the ion drag force, ionization, dust charge gradient, etc., besides the usual Buneman, Kelvin-Helmholtz, Rayleigh-Taylor, pressure gradient and parametric instabilities. The study of these instabilities are of great importance because they are helpful for understanding the origin of enhanced fluctuations as well as of dust voids and nonlinear dust oscillations in space and laboratory dusty plasmas.

The dust particles experience both electromagnetic forces as well as non-electromagnetic forces such as gravity, friction or radiation pressure. Rosenberg et al.[82] have shown that charged dust can affect the Farley-Buneman instability in the low E-region of Earth's atmosphere at altitude of about $h \sim 90 - 100km$. The presence of negatively charged dust can lower the critical electron drift at $h < 95km$, while it can increase the critical drift at $h > 95km$. This may have implications for meteor echoes from dusty meteor tails in the E-region[83]. On the other hand, the Jeans instability of a self-gravitation system has been well known for a long time. In dusty plasma, it is found that in the presence of particle streaming, both the Jeans and Buneman instability can overlap[84]. Further investigations have examined the influence of particle size distributions on the Jeans-Buneman instability, concluding that the growth rate was enhanced both for discrete particle size distributions as well as continuous size distributions. Farley-Buneman instability is an ion wave instability with frequency $\omega << \nu_{in}$ (ν_{in} is ion neutral collision frequency) that can be excited when the electron $E \times B$ drift is sufficiently larger than the ion sound speed. This instability is applicable to equatorial and auroral electrojet regions. Presence of charged dust grains can affect this instability by reducing it's growth rates at $h \sim 100km$.

The hydrodynamic and kinetic instabilities in dusty plasma have been investigated by various scientists. The two-stream instability has also received attention. Havnes[85] has examined the conditions for the onset of the instability in a plasma model in which two charged dust distributions stream relative to each other. Small grains (below micrometer) are brought to rest with respect to the surrounding gas in very short distances, while larger grains are practically unaffected. This braking mechanism is applied to interstellar gas clouds, for which one observes a large depletion of several elements at low cloud velocities, a depletion which decreases with cloud velocity. Hence, this two-stream instability may be important for grain destruction in high velocity clouds, as it effectively brakes the small grains but leaves the larger ones intact, thereby creating two populations of grains which stream relative to each other with the cloud velocity. Collisions between the grains in the two populations may thus become sufficiently frequent and energetic to ensure the destruction of a large fraction of the total grain content. This could be important when shocks travel through interstellar gas, setting up grain separation and subsequent destruction.

Later, Havnes[86] as studied the instability of an electron-ion-dust plasma in the presence of streams of dust grains. He showed that the free energy stored in the dust grains is coupled to the electrostatic oscillations, which may be relevant for understanding the origin of fluctuations during solar wind plasma flow and cometary dust interactions. Later, Bharuthram et al.[87] and Rosenberg[55] discussed the possibility of dusty plasma wave excitation in the presence of equilibrium ion drifts in a uniform dusty plasma. Specifically, Bharuthram et al. discussed the effect of dust on ion-ion two-stream instabilities, and found that the dust affects both growth rates and ranges of drift speeds for which instability occurs. This may occur in planetary rings. Rosenberg investigated the dust ion-acoustic and dust acoustic instabilities using a standard Vlasov analysis for a dusty unmagnetized plasma with electrons, ions, and dust of uniform mass and charge. When the electrons have a weak drift u in a range $v_{th.i} < u < v_{th.e}$, dust ion-acoustic waves can be excited if $\delta T_e/T_i >> 1$. This ion-acoustic instability is particularly relevant to cosmic plasmas, where generally it is assumed that $T_e \sim T_i$, in environments where dust carries much of the negative charge. Dust-acoustic instability may be excited in planetary rings beyond the corotation radius, where the azimuthal speed of dust grain rolled by gravity and the plasma particle corotate with the planet. Rosenberg and Shukla[88] examined the effect of a strong magnetic field on a DA instability driven by ions streaming along the magnetic field. It is assumed that ions and electrons are strongly magnetized, while the charged dust is unmagnetized. In this case it is found that the growth rate of the instability could be reduced under certain conditions which may have implications for laboratory dusty plasmas such as 'plasma crystals'.

In a pioneering attempt to explore the effect of dust grains on ion-acoustic instabilities, it was shown that this instability can develop in typical gas-discharge dusty plasmas at low or moderate external DC fields. The relative drift between the electrons and ions arising from the large difference in their mobilities can result in the excitation of IAW. The instability becomes lower when the dust grains absorb more electrons and electron-neutral and ion-neutral collisions dominate[89]. Annou included dust-charge fluctuations in the description of this instability[90].

Compared to theoretical progress, experimental progress on instabilities in dusty plasma is not very much. Barkan et al.[69] have observed in a laboratory dusty plasma, the current driven electrostatic ion cyclotron (EIC) instability. D'Angelo[70], Chow and Rosenberg[71] have predicted that presence of negatively charged dust in plasma makes it more unstable to the EIC instability and showed that the critical drift, needed to excite the instability, decreases as the negative dust charge density increases. In the absence of dust measurements at Io, the detection of the electrostatic ion cyclotron instability would signal the presence of negative dust, as without it the mode would be stable under the conditions prevailing near Io. The observations made by Barkan et al. agree with the theoretical predictions of Chow and Rosenberg concerning the enhancement of instability of the dust.

Rosenberg and Krall have discussed drift instabilities[91], when there is a local electron density gradient opposite in sign to a dust density gradient or modified two stream instabilities in dusty space plasmas with electrons or ions drifting across an external magnetic field[92]. They have considered the application of these instabilities to the edges of the ringlets in the F-ring of Saturn are stable against the excitation of this high-frequency mode, whereas the low-frequency two-stream instability could be of importance in the E-ring. Streaming instabilities involving both the longitudinal and transverse waves may also arise in a strongly coupled unmagnetized collisional dusty plasma[93].

Merlino et al.[94] have reported about the theoretical and experimental studies on low frequency electrostatic waves in plasmas containing negatively charged dust grains that they have done. Laboratory experiments on ion-acoustic waves and electrostatic ion-cyclotron waves confirm that these modes are more easily excited in a dusty plasma with negatively charged grains. The dust-acoustic mode was observed in a dusty plasma in which the charged grains were levitated by an electric field. The measured dispersion relation agreed well with the theoretical relation taking into account the effect of dust-neutral collisions.

A current driven electrostatic dust cyclotron instability in a collisional plasma was analyzed by D'Angelo using a four-fluid model[95]. The conditions for excitation of the EDC mode in both laboratory plasmas and in cometary dusty plasma environments were obtained. Very recently, using kinetic theory Rosenberg[96] has studied about EDC instability in a collisional plasma containing dust grains with large thermal speeds. The instability is excited by ions drifting along the magnetic field. The critical ion drift for exciting EDC waves is also compared with that for exciting dust acoustic waves.

Recently,. a resistive ion-dust streaming instability in a collisional dusty plasma, where the ions and electrons are magnetized, and the dust is unmagnetized has been discussed by Rosenberg[97]. The instability is driven by ions streaming along the magnetic field. The emphasis is on the case where the dust has large thermal speed and where the ion drift speed is less than the ion thermal speed.

The most important hydrodynamic instabilities are the Kelvin-Helmholtz (K-H) instability, which occurs, when the character of the equilibrium of a stratified heterogeneous fluid is considered in which the different layers are in relative motion. When two superposed fluids flow one over the other with a relative horizontal velocity, the K-H instability of the plane interface between the two fluids occurs. K-H instabilities can, for instance, be induced when wind is blowing over a water surface. D'Angelo and Song[98] considered the effect of either negatively or positively charged dust on the K-H instability in a magnetized, low β plasma with shear in the ion field-aligned flow, using a multifluid analysis. The dust was assumed to be immobile and of uniform mass and charge. The charged dust alters the critical shear for the onset of instability from that in an electron-ion plasma, where the relative speed between adjacent flows of the order of the ion sound speed is required for instability. The critical shear increases with dust charge density in a plasma with negatively charged grains and decreases with dust charge density in a plasma with positively charged grains. Bharuthram and Shukla[99] have examined the KH instability in magnetized dusty plasmas and found that the nonlinear stationary state of the KH instability in dusty plasmas can be represented as coherent dipolar vortex structures. Rawat and Rao[100] investigated KH instability in a magnetized dusty plasma driven by shear flow in dust fluid. It is found that relative velocity between adjacent layers of the dust fluid should be of the order of the dust-acoustic wave phase speed in order to excite the KH instability. Singh et al.[101] have examined K-H instability by considering the dust charge fluctuations in a dusty plasma. The transverse shear in the flow parallel to the magnetic field is considered. The instability is found to grow for limiting wave numbers for a particular value of shear velocity. The effect of adiabatic dust plasma pressure is to enhance the growth rate of the instability. For dense plasma, growth of the instability is affected by the presence of dust charge fluctuations. Luo et al.[102] have investigated experimentally the effect of negatively charged dust on the KH instability in a magnetized cesium plasma. The dust generally has a stabilizing effect on the instability, although, in some cases, the addition of negatively charged dust into the plasma results in a slight increase in the instability fluctuation amplitude which are in general agreement with theoretical predictions.

A prominent example of the Rayleigh-Taylor (RT) instability is seen in astrophysical dusty plasmas. In particular, they may result in filamentary structures in molecular clouds and in density condensations in accretion disks, where they may influence the planetesimal formation in protostellar dust layers. D'Angelo[103] has studied the influence of very heavy dust grains, that do not participate in the dynamics, on ion RT modes in a situation where the magnetic field acts as the light fluid that supports the plasma. He found that negative dust charges have a stabilizing effect, while the opposite is true for positively charged dust. The influences of dust dynamics and charge fluctuations on RT modes have also been studied quite extensively by Jana et al.[104] and have found that the combined effect of dust dynamics and charge fluctuations significantly reduces the range of unstable wave numbers for the Rayleigh-Taylor mode. A hydrodynamic instability triggered inside the complex plasma cloud has been found by Morfill et al.[105]. In their experiment, microparticles along the surface of a plasma crystal are investigated. If the surface is flat, the flow is stable and laminar and the particle trajectories are almost parallel to the plasma crystal surface, showing almost no deformations. If the surface of the plasma crystal is curved, a mixing layer is formed between the owing region and the crystal. This layer becomes unstable and the particle trajectories are deformed. The cause of this is the centrifugally driven Rayleigh-Taylor instability, arising at the interface between the stable and the owing microparticles.

Another such mixing layer has been observed at the interface of a fluid flow of microparticles around an obstacle and the wake behind this obstacle[106], which has been interpreted as a new type of nonlinear collisional instability.

Recently, Veeresha et al.[107] have studied about low frequency stability of a dusty plasma with a nonuniform mass and charge distribution of the dust component. In their study it is shown that the inverse stratification of the dust mass density in a gravitational field may lead to a Rayleigh Taylor like instability, which can produce an incompressible flow pattern of spontaneously rotating dust plasma fluid in the nonlinear regime. Very recently, Sen et al.[108] have developed a non-local theory to study the Rayleigh Taylor instability in an inhomogeneous dusty plasma in the presence of a uniform magnetic field. Using the fluid equations and the dynamics of charged dust grains, they have derived an eigen-mode equation to study the stability of the mode. In their study, typical space parameters in the vicinity of Saturn are used to investigate the stability of the mode. From their study the growth rate of the Rayleigh Taylor is found to be drastically higher in a dusty plasma than in a pure plasma. This might have a wider consequence in explaining the origin of low frequency modes in various situations in the space atmosphere.

Low frequency drift instability in a dusty magnetized plasma were studied by

Rosenberg and Krall[109] with negatively charged grains in which there is an electron density gradient and dust density gradient opposite to each other. Frequencies less than the ion gyrofrequency but much larger than the dust gyrofrequency are considered. They have analyzed the results of their theory on the basis of data available from the spoke regions in the B-ring of Saturn. The ring edges in spoke region appear to be unstable to this instability. Another possible application may include future artificial dusty plasma experiments in the Earths ionosphere using Space Shuttle exhaust. Rosenberg and Shukla[110] have made further study on low-frequency drift instabilities in a strongly magnetized collisional dusty plasma in the dust acoustic or dust lower hybrid frequency regimes. They assumed that the ions and electrons are magnetized, while the negatively charged dust grains are collisional and non-magnetized. A situation is considered in which the negatively charged dust is spatially localized, creating an electron depletion or electron 'hole', with an electron density gradient in the opposite direction to a dust density gradient at the boundaries. Under such circumstances, drift instabilities in the DA or DLH frequency regimes can be driven by the electron diamagnetic and $E \times B$ cross-field drifts. Using parameters representative of possible laboratory conditions, it is found that the critical drift for such drift instabilities can be lower than that for the excitation of a low-frequency Hall current instability, which is driven primarily by the ion Hall current. Previously, a DA drift instability was considered in a nonuniform collisional dusty magnetoplasma such that the electrons are magnetized, while the ions and dust grains are collisional and non-magnetized, which may be characteristics of dusty plasmas in the E-region of the Earth's ionosphere[111].

Tsytovich et al. have studied about influence of dust drift instability in edge tokamak plasma. They have shown that the new type of drift instability is generated in presence of dust grains. The growth rate of this instability is found to be comparable or much larger than the usual drift instability, even for low dust density. This new instability may be a cause for increase of anomalous diffusion. The phase shift between the charge density on the dust and particle density variation in the drift modes lead to onset of this new type of instability. It has a very low critical value of characteristic dust charge parameter. Whether this critical value is really exceeded in the tokamak SOL plasma is an experimental question.

Ionization instability (IA) in a dusty plasma in which the neutral gas is ionized by a constant flux of energetic electrons with energy slightly above the ionization energy has been examined by D'Angelo[112]. The presence of negatively charged dust increases both the frequency and the growth rate of the IA wave excited through the ionization instability. The DA mode, even in the absence of ion-neutral collisions, ion-viscosity and neutral gas drag on the dust grain, is always damped. Shukla and Morfill[113] have argued that an ionization instability may excite the DA mode. The results of D'Angelo on the DA wave excitation are at variance with results obtained by Shukla and Morfill. Later, as a possible mechanism of excitation of the DA ionization instability the effect of ion drag on negatively charged dust grains is considered[114].

In the magnetic fusion literatures, Ballooning modes are known as driven instability. This mode may be responsible for the plasma depletions observed by Voyager II in the Jovian magnetospheres. Shukla et al.[115] have studied about the linear and non-linear properties of drift-ballooning modes in the presence of an equilibrium electric field and stationary charged dust grains. It is found that the presence of these two contribute to the stability of the ballooning mode. It is shown that the non-linear coupling between finite amplitude drift-ballooning modes give rise to different types of coherent vortex structures, which can affect the transport properties of an inhomogeneous magnetized plasma.

Recently, Piel et al.[116] presented experimental evidence of dust density waves propagating at an arbitrary angle with respect to the ion flow direction in a collisional dusty plasma under microgravity conditions. Here, a dissipative instability driven by an ion beam plays a crucial role in exciting the dust density waves.

1.2.6 Dust plasma crystal:

Plasma crystal is the solid phase of the dusty plasmas. The study of plasma crystal formation provides a tool to understand the physics of crystal in solid state and the properties of strongly coupled plasma. Plasma crystals are regular arrangement of fine dust grains like an atomic crystal, where the "atoms" are represented by the highly negatively charged and highly ordered dust grains and the "electrons" by the mobile plasma ions and electrons. When dust particles interspersed in a plasma have a high enough ratio of interparticle potential energy to average kinetic energy, they form plasma crystal. Plasma crystals were originally theorized in the 1980s and were first observed in laboratory in 1994.

The Coulomb crystals in dusty plasma exist in various systems, such as astroplasma, industrial plasma processing, laboratory discharge, etc. The study of plasma crystal provides a useful tool for investigating lattice defects, dislocations, the thermodynamics of lattices with and without defects, interaction with waves, resonances etc.[117].

Plasma crystal formation is the result of several long-range coulomb interactions that occur in complex plasma. Such interactions include charging of dust particles, Debye screening, ion drag, ionization, thermophoretic force, Coulomb collision, Shadow force and polarization. Coulomb interactions cause particles to become ordered into plasma crystals. Plasma crystals can be described by their thermal energy, inter-particle spacing, Coulomb interaction energy, particle charge, particle density, ion density and particle radius. Plasma crystal structure can be classified as hexagonal close packed (hcp), face centered cubic (fcc) or body centered cubic (bcc) etc. depending on the arrangement of the particles. Like regular matter, plasma crystals can take on "solid", 'liquid" and "gaseous" phases. The four plasma crystal phases

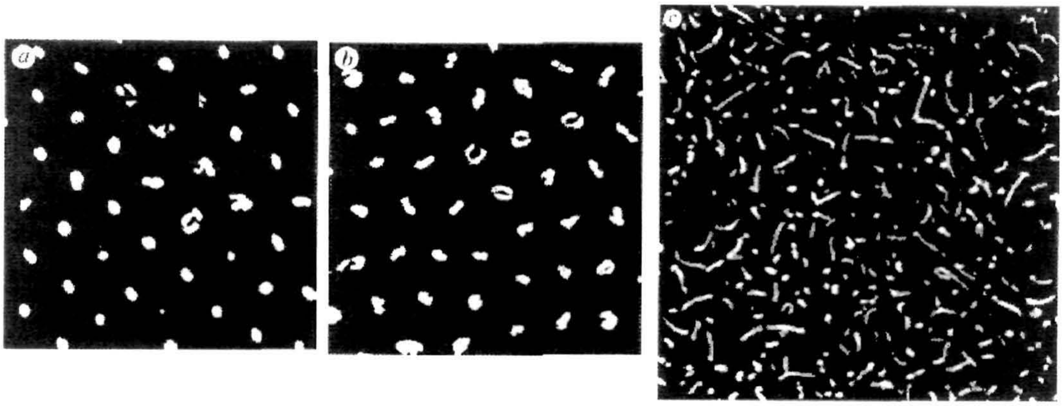

Figure 1.4: (a) shows Crystalline phase, (b) and (c) show 'flow and floe' state[118] .

are labelled as crystalline (solid), flow and floe (melting stage), vibrational (liquid) and gaseous. The crystalline phase is characterized by long-range order. The flow and floe phase is characterized by short-range order. The gaseous phase lacks order.

The Coulomb coupling parameter Γ is the ratio of interparticle potential energy to thermal (or kinetic) energy that determines the degree of order of a plasma crystal:

$$\Gamma = \frac{PE_{interparticle}}{KE} \tag{1.2.31}$$

Depending on the strength of Γ, dusty plasma can be characterized as follows:

- $\Gamma < 1$ Weakly coupled (gaseous state).
- $1 \leq \Gamma < 170$ Strongly coupled (liquid state).
- $\Gamma \geq 170$ Strongly coupled (solid state).

Another controlling parameter of plasma crystal formation is the screening constant, defined as $\kappa = \frac{a}{\lambda_D}$, where, a is the mean-interparticle distance and λ_D is the Debye length of the background plasma.

In Yukawa system the phase diagram (Fig.1.5) shows that the critical value for

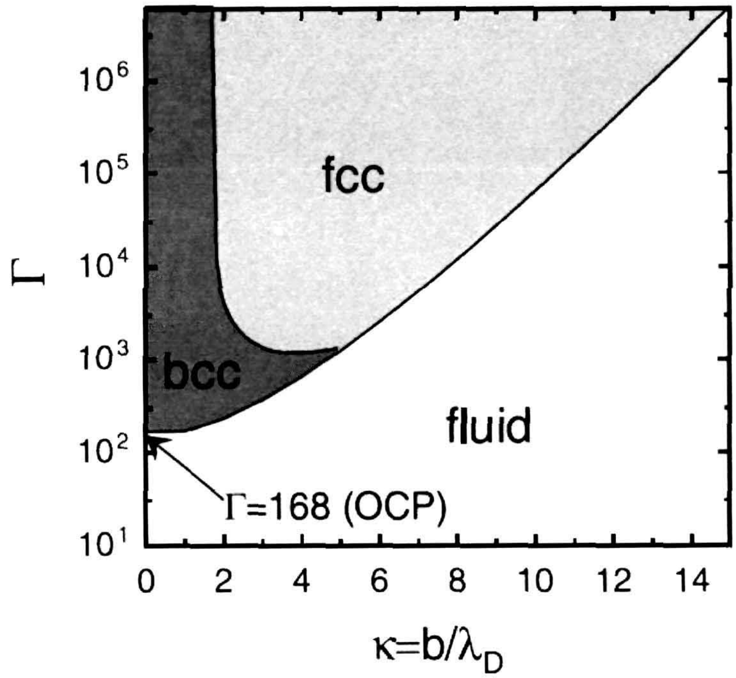

Figure 1.5: Phase diagram of Yukawa dusty plasma system in $\Gamma - \kappa$ plane.

solid-fluid transition strongly depends on the screening strength. The melting line increases almost exponentially with κ. The melting line of Yukawa system is approximated by an effective Coulomb coupling parameter $\Gamma_{c,eff} = \Gamma exp(-\kappa)$, where, it is assumed that the melting line exactly increases exponentially with increasing κ.

The charge on a dust is limited when all electrons are bound to the dust, i.e. $Z_{d,lm} = e\frac{n_i}{n_d}$, where, n_i and n_d represent number densities for ion and dust particle. It is interesting to find out the condition for values of the ion and dust density for Wigner crystallization. The ion density affects both the screening length λ_D and the dust charge limit. High ion density leads to increase in dust charge limit but at the same time causes strong screening.

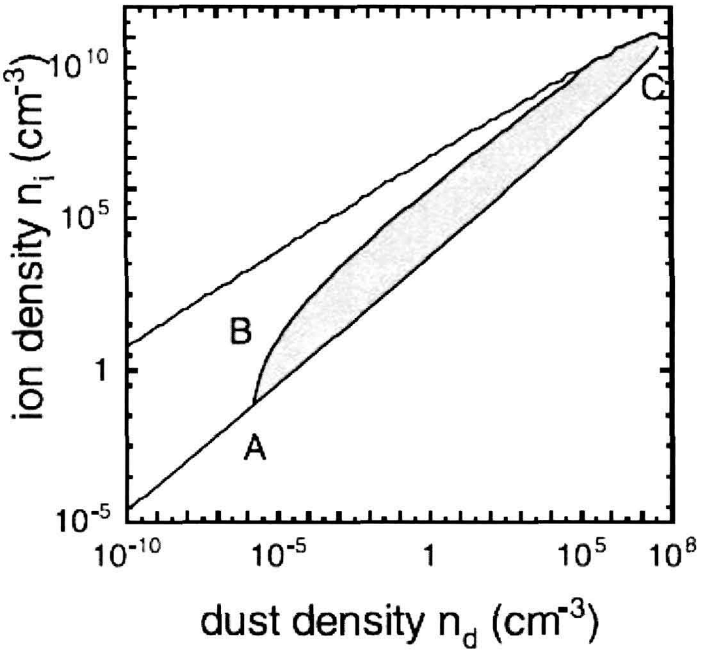

Figure 1.6: Existing diagram of Wigner crystal.

The dust density on the other hand affects the dust charge limit and the inter-particle distance. An increase in dust density results in lowering of maximum charge on dust but small inter-particle distance, which increases high coupling. Both parameters have counteracting effects. Taking into account both these effects, Wigner crystallization should be possible in the dark area ABC as shown in Fig.1.6.

In 1986, Hiroyuki Ikezi[119] predicted that dust particles in plasma could acquire enough charge such that Γ is large because of high density and small inter-particle spacing. The suspended dust particles due to their mutual Coulomb repulsion, can organize themselves into spectacular crystal-like arrays.

The formation of dust crystals has been demonstrated in several experiments and simulation. Dust crystals can be easily generated in rf discharge plasma. The observations of Coulomb crystals in dusty plasma were reported for the first time by two groups, one by Chu et al.[120] and the other by Thomas et al.[121]. In the experiment done by Chu and I, the strongly coupled dusty plasma was formed by suspending negatively charged SiO_2 fine particles with 10 μm diameter in weakly ionized rf Ar discharge. Coulomb crystals were observed by using an optical microscope. In the solid state, bcc, fcc, hcp and hexagonal cylinder structures were observed. The hexagonal cylinder is an interesting structure. The vertical particle alignment of the hexagonal cylinder structure is caused by the downstream ion flow induced vertical dipole. Horizontally, the system has triangular lattice structure. Particles along the same chain move together. It forms a quasi two-dimensional (quasi- 2D) structure. From the optical microscope mounted on top of the dusty plasma system, structures and motions of dusty particles at different state are easily observed and tracked. In their experimental observation of macroscopic Coulomb crystals, Thomas et al. investigated the structure of a cloud of charged particles levitated in a weakly ionized plasma. They did a numerical analysis of the image obtained from experiment and found that the observed particle structure is crystalline, which is consistent with a large value of the Coulomb coupling parameter.

The experimental observation of dust crystal has led to the basic question regarding the physical processes and corresponding to that, potentials that are responsible for binding together and arranging the dust grains in regular crystal-like arrangement. The primary condition for any self-organization in a many particle system is that the potential due to nearest-neighbor forces be greater than the thermal energy of the particles. The interaction among the plasma particles is mainly dominated by Debye-H*ü*ckel potential.

Hayashi and Tachibana[122] also observed a 3D dust cloud in rf plasma system. They investigated growth of spherical and mono-disperse carbon particles in a methane

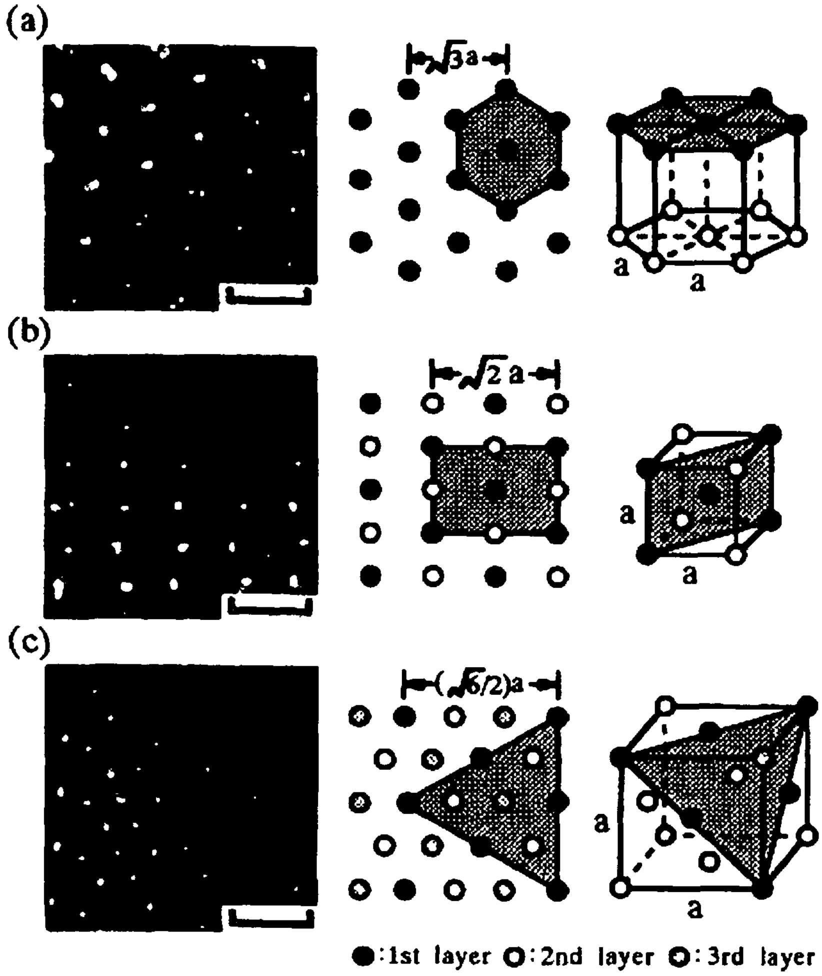
(a)
$\sqrt{3}a$
a
a
(b)
$\sqrt{2}\,a$
a
a
(c)
$(\sqrt{6}/2)a$
a
a
●:1st layer ○:2nd layer ○:3rd layer

Figure 1 7: Micrographs and sketches of different crystal structures (a) Hexagonal; (b) bcc; (c) fcc[120] plasma and found that the phase transition occurred when particle diameter becomes $1.3\mu m$ and the Wigner-seitz radius was about $90\mu m$. The 2D dusty plasma crystal with only 2-3 layers of dust suspended on the bottom electrode is also found by another group[123]. The melting of this kind of 2D crystal with only 2-3 layers of dust exhibits some special phases which are different from the ordinary 2D melting process. For example, a chain-like hopping process can start from some place, then disappear at a few 'a' (mean interparticle spacing) away. It implies that, there must be some mechanisms for the large compressibility of their 2D lattice, e.g., the vertical migration of the few layers mono-dispersive dust particles. Particle motion in vertical direction is possible according to their experiment.

The hexagonal cylinder lattice, which dust particles line up vertically, is also found especially for the large dust particles[124]. The attractive force in the vertical direction is so large that particles along the same vertical chain move together. A quasi-2D crystal with triangular structure in the horizontal plane is formed. The background plasma fluctuation plays a key role in the melting of the crystal. It randomly drives particles and destroys the ordering. Its amplitude can be increased as the rf power increases.

Fortov et al.[125], formed a quasi-crystalline structure using hollow thin wall spherical glass grains with diameter $50 - 63\mu m$ in the standing striations of a stationary glow discharge in Ne plasma. The crystalline structure did not occurr in the cathode sheath, but in the standing striations where the electric field intensity and the electron density both were high. Later, Nunomura et al.[126] formed plasma crystal in the DC Ar plasma sheath boundary at a very low pressure, generated by DC discharge between the hot filaments and the grounded vessel. A hexagonal structure of spherical grains of radius $2.5\mu m$ was formed on horizontal plane. In another experiment, Agarwal et al.[127] formed Coulomb dust cloud using spherical alumina dust grain with diameter $50 - 120\mu m$ in the sheath boundary of hollow cathode DC plasma. They

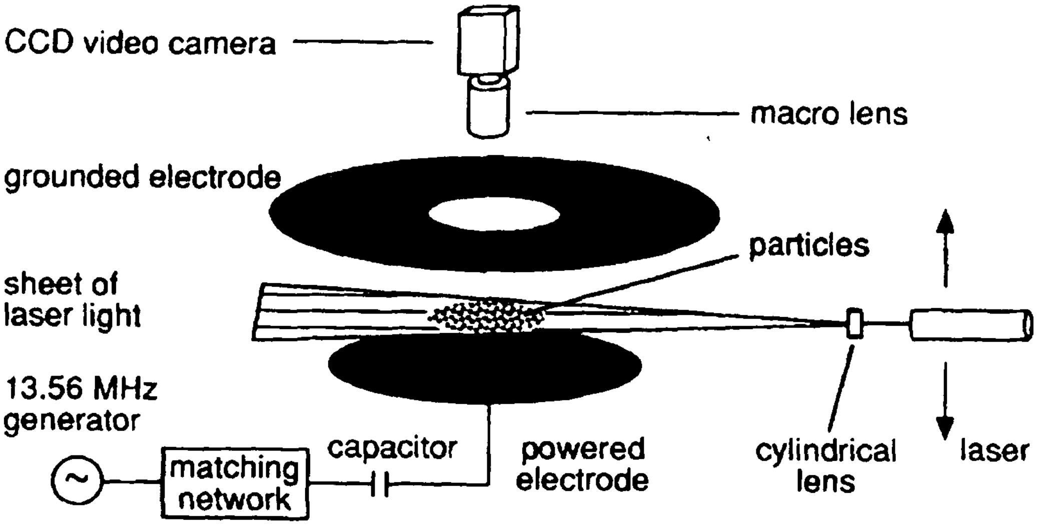
CCD video camera
macro lens
grounded electrode
particles
sheet of laser light
13.56 MHz generator
matching network
capacitor
powered electrode
cylindrical lens
laser

Figure 1.8: Experimental set-up for dusty plasma crystal[118].

attributed it to additional attractive force between the grains.

One major advantage of studying Coulomb crystal in dusty plasma is due to the fact that it can be easily produced. The properties of these crystals can be studied for a wide range of conditions by controlling the parameters like neutral gas pressure, rf power and type of gas and particles. Plasma crystal structure can be visualized with a CCD camera by illuminating the lattice layers with laser light. Particle positions can be stored on a video recorder with a high temporal and spatial resolution.

The study of phase transition is of great interest for condensed matter physics. It is very difficult to understand the mechanism of phase transition for real atomic or molecular systems. Dust crystal formation in strongly coupled plasma may be a very important platform to study the phase transition from crystalline to liquid and from liquid to gaseous state, self-organization etc. Detailed imaging and fine time resolution provides a good opportunity to study this process. Quinn et al.[128] attributed that the phase of the plasma crystal can be determined by calculating the pair correlation function $g(r)$ and the static structure factor. In their experiment Chu et al.[120] showed that a change in discharge parameters can decrease the relative strength of the Coulomb coupling and as a result of it the highly ordered crystal can be easily melted to the disordered liquid state. In the investigation of phase transition, Morfill et al.[129] have performed melting experiments from plasma crystal to its liquid and gaseous phase. They have observed a new intermediate phase, the so-called flow and floe stage between the solid and liquid phases. This has not been detected in normal phase transition from solid to liquid state. The flow and floe[118] state is characterized by the co-existence of islands of ordered crystalline structure (floes) and systematic directed particle motion (flows) and then vibrational followed by a disordered state. Vibrational state is more orientationally ordered structure, where vibrational amplitudes, thermal energy and vertical migration of particles increase and the translational order decreases. Beyond this, on further decrease of neutral gas pressure, particles attain a disordered state. It is characterized by complete vibrational and horizontal migration. There is no distinct translational or orientational order in this state. Thermal energy increases and the Coulomb parameter Γ reduces to a value of the order of unity or less. Melzer et al.[130] showed that plasma crystal exhibit phase transition either by increasing the rf power or by decreasing neutral gas pressure.

In simulation of Zheng and Earnshaw[131] it was observed that when the rf power was raised, dust grains moved more randomly. Many of these randomly moving grains appeared to have no equilibrium positions and cause melting of plasma crystal. Hayashi and Takahashi[132] observed a melting transition of 3D plasma crystal due to a change in the direction of force. They further quantitatively analyzed their results using the Monte-Carlo simulation. Nefedov et al.[133] proposed a model for the random motion of dust grains. They suggested that an anomalous increase in the part of the kinetic energy of these dust grains, cause the melting transition. They have verified their model with experimental results of Melzer et al.[130].

In determining the triple point, Hamaguchi et al.[134] applied molecular dynamics simulation of Yukawa system to strongly coupled plasma. They obtained the transition temperatures as functions of the screening parameter. Hammerberg et al.[135] used MD simulation to study the formation of dust crystals in three dimensions. In their study, the grain interaction potential consisted of three items: spherically symmetric Debye-Hückel potential, an asymmetric wake potential and an effective external trapping potential necessary to model grain dynamics consistent with laboratory experiments. Kharpak et al.[136] experimentally investigated the compressional waves in a complex plasma under a micro-gravity condition, where they observed the separation between two-species grains. It is of interest to study the behaviour of a 3D dusty plasma in the strongly coupled regime with the presence of dust with different parameters.

Plasma crystals of fine melamine formaldehyde dust grains of about $8.9\mu m$ diameter, suspended in the sheath of rf discharge, rotate under the influence of a vertical magnetic field has been studied by Konopka et al.[137]. Depending on the discharge conditions, they have observed two cases: a rigid body rotation and a sheared rotation. The dust grains reversed the direction of motion when the discharge voltage was sufficiently increased. A theoretical model based on azimuthal ion drag was proposed to explain the cluster rotation in a constant magnetic field. An experimental study of fine particles in magnetized plasma was done by Sato et al.[138]. They found that fine particles rotate in the azimuthal direction on the horizontal plane in presence of a magnetic field applied in the vertical direction. The strength of the magnetic field was varied between 0.4 kG (weak) and 40 kG. With an increase of the magnetic field, the rotation speed increased, being followed by subsequent saturation. In their

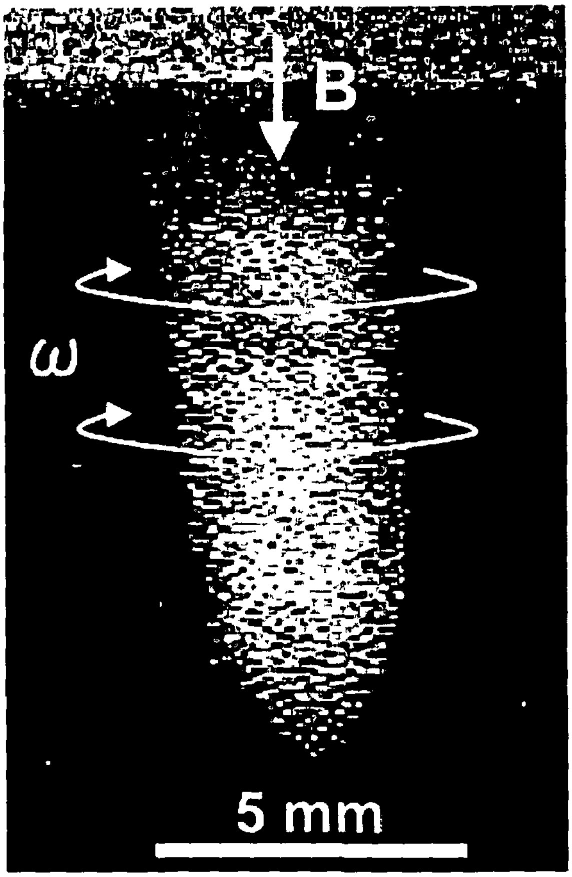

Figure 1.9: Rotation of dust particles in the azimuthal direction on the horizontal plane in presence of magnetic field applied in the vertical direction[138].

experiment, the rotation is induced under the condition that the particles are strongly coupled with very small inter-particle distance. Uchida et al.[139] on the otherhand, studied the wave dispersion relation in a two-dimensional strongly coupled plasma crystal by using both theoretical analysis and molecular dynamics simulation taking into account a constant magnetic field parallel to the crystal normal. Recently, Hou et al.[140,141] have developed a 2D-fluid model for a self-consistent treatment of the rf-sheath dynamics over a non-flat electrode with the perpendicular uniform magnetic field and have used it to simulate the formation and rotational behaviors of 2D dust plasma crystals.

Law et al.[142] observed rotation in plasma crystal induced by the biased probe immersed in a plasma in absence of magnetic field. It was suggested that ion wake fields generated due to the biased probe, giving rise to the space charge accumulation.

Arp et al.[143] have discovered "Coulomb balls", i.e. spherical particle clouds, in which hundreds or thousands of identical particle spheres are arranged in nested crystalline shells. Similar shell structures have been found in the halos of elliptical galaxies. As many as 20 shells have been discovered around one bright galaxy. It may be possible that the concentric shells in Coulomb balls of plasma and dark matter halos are controlled by similar mechanism of magnetic plasma. Magnetic plasma is pervasive throughout the universe.

The detailed knowledge about formation of Coulomb crystal in strong magnetic field may also be very useful in understanding certain phenomena in some astrophysical objects. Cores of white dwarfs and envelopes of neutron stars are ideal for formation of Coulomb crystals. The properties of Coulomb crystal may influence their pulsation frequencies, electron-phonon scattering and hence transport properties of their matter etc. Warm neutron stars with ultra strong magnetic fields, known as magnetars emit radiation in all ranges of electromagnetic spectrum[144]. They are

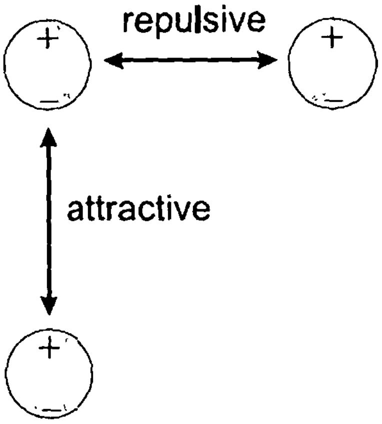

Figure 1.10: Repulsion and attraction for particles with a dipole moment; the + and - sign denote the charge imbalance between upper and lower side of the particle.

found to be source of quasi-persistent X-ray emission and giant bursts. These magnetars with high density may be suitable for Coulomb crystallization of charged dust particles. Proper investigation of Coulomb crystals in magnetized plasma may be very useful for understanding the mechanism of complex phenomena going on in magnetars.

Dust grains levitated in plasma also interact with each other through dust-dust attraction and they inturn give rise to ordered structure formation. Several mechanisms have been proposed to explain the causes of dust-dust attraction. They include electric field induced dipole interaction, asymmetry of charge between leading and trailing hemispheres of a dielectric grain in the flowing plasma, polarization of Debye sheath around the grain by external potential. Other mechanisms are based on focusing of ions flow in the sheath by dust grains, wake potential in the plasma, balance between attractive dipole-dipole field with repulsive monopole field, shadowing effect of one

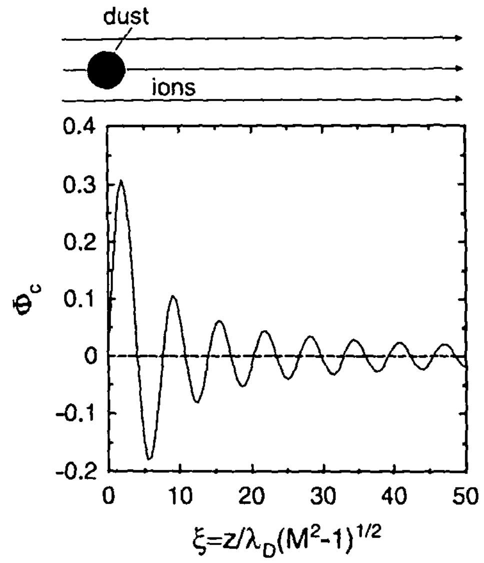

Figure 1.11: The ion weak potential in an ion flow. Downstream of the particle an oscillating potential is formed with alternating attractive ($\phi_c > 0$) and repulsive ($\phi_c < 0$) regions.

dust grain on the other, etc. When the dust grain sizes are large, there appears to be a strong intergrain attractive coupling which leads to the formation of distinct grain column along the sheath electric field. Mohideen et al.[145] attributed this to an electric field induced dipole-dipole interaction between the dust grains. Two mechanisms of dipole formation are possible: Induced dipoles by polarization due to the sheath electric field and the differences in the charging currents to upper and lower side of the particle may result in dipoles. The dipole-dipole interaction between the particles then results in attractive force component for vertically aligned pairs and a repulsive interaction for particles in the same plane. The attractive dipole-dipole force may be responsible for subsequent formation of dust structures and planetesimals. However, for small particles, this dipole effect is very small compared to the repulsion of the particles. The possibility of dipole-dipole interaction was also proposed by Lee et al.[146] by the analysis of phase diagram of coulomb crystals. The sheath electric field can also induce polarization on the dust grains with dipole moment $P = 4\pi\varepsilon_0 E r_d^3$, where r_d is the radius of the dust grain. It is clear that the dipole moment is very sensitive to the grain size and have a cubic dependence on it.

Nambu et al.[147] have proposed that collective interactions involving very low-frequency electrostatic waves in dusty plasmas can give rise to an oscillatory wake potential[148], which may cause grain attraction. It was assumed that the dust particles excite ion-acoustic waves of all frequencies in the ion stream. The oscillating wake field arises due to the resonance interaction between the DIA and DAW and a test charge that moves with a speed close to the dust ion acoustic or dust acoustic speeds. The oscillating ion wake potential Φ_c downstream of the dust particle is created with an alternating sequence of regions with enhanced positive and negative potential. The potential is attractive when $\Phi_c > 0$. This ion wake provides the attractive force that explains the vertical ordering of particles as shown in Fig.1.11. This mechanism is similar to cooper pairing of superconductors, in that the dust particle polarizes the surrounding medium, the plasma, which in turn leads to attraction of other particles. However, this model does not fully describe the dynamic behavior of plasma crystal.

Hou et al.[149] have performed MD simulation to illustrate the effect of Overlapping of Debye spheres (ODS) on properties of dusty plasmas. Like Shadowing force, ODS around dust grains produce an attractive force between them. Baruah et al.[150] have observed a clear difference between the effect of attractive potentials and Debye-Hückel interactions in crystal formation. The results of their study show a better agreement to the real experimental situation in case of the attractive potentials.

Chapter 2

Dissipative Drift Instability in Dusty Plasma

An investigation has been done on the very low-frequency electrostatic drift waves in a collisional dusty plasma The dust density gradient is taken perpendicular to the magnetic field $\overrightarrow{B_0}$*, which causes the drift wave In this case, low-frequency drift instabilities can be driven by* $\overrightarrow{E_1} \times \overrightarrow{B_0}$ *and diamagnetic drifts, where* $\overrightarrow{E_1}$ *is the perturbed electric field Dust charge fluctuation is also taken into consideration for our study The dust- neutral and ion-neutral collision terms have been included in equations of motion It is seen that the low-frequency drift instability gets damped in such a system Both dust charging and collision of plasma particles with the neutrals may be responsible for the damping of the wave Both analytical and numerical techniques have been used while developing the theory*

2.1 Introduction:

The presence of micron sized dust particles adds a new dimension to two-component plasma Various interesting phenomena occur in addition to normal wave modes and instabilities, due to the presence of dust particles Dust-acoustic wave[49], Dust lattice wave[51] are few such examples. The dust particles are relatively massive compared to electrons and ions and they may acquire a large negative charge and these two properties make them very special.

In the near past, the study of various low-frequency phenomena in dusty plasma has received much attention. The dust dynamics plays the key role in supporting these modes. Chu and I[66] reported about a very low-frequency ($\approx 12Hz$) mode with a wavelength of about 0.5 cm, which was detected in the motion of their strongly coupled charged grains. A study done by Praburam and Goree[68] revealed the existence of a pair of very low-frequency modes, termed as filamentary and great void modes. Rao et al.[49] predicted for the first time the existence of Dust Acoustic Wave (DAW) in dusty plasma. The DAW propagates as the normal mode when the phase speed is much larger than the dust thermal speed. Interpretations of DAW excitation in experiments have typically relied on collisionless inverse Landau damping mechanism[55,67]. However, a closer examination of experimental conditions revealed that waves are often excited when there is a significant background pressure of neutrals. It is therefore important to study the wave excitation theories into the collisional regime. In magnetized, homogeneous dusty plasma, the presence of charged dust can affect the electrostatic waves such as acoustic wave, electrostatic ion cyclotron waves and lower-hybrid waves[17].

The effect of charged dust on the propagation of low-frequency electromagnetic waves has been investigated by Pilipp et al. It was seen that the dispersion relation of such waves is significantly altered only near the dust gyro-frequency at which frequency, the waves are in resonance with the grains and hence can be damped by them. Rosenberg[55] investigated ion-acoustic and dust-acoustic instabilities using Vlasov theory for electrons, ions and dust of uniform mass and charge.

The study of drift instability is of great interest in plasma physics. Rosenberg and Krall[109] have done detailed study on low frequency drift instability in a dusty magnetized plasma both in presence of electron density gradient and dust density gradient opposite to each other. Possible applications of their results to dusty space plasmas are also discussed. Their study has motivated the present workers to study low-frequency drift instabilities taking into account the effect of collision of dust and neutral particles. Kaw et al.[151] have investigated instabilities of dust acoustic waves in a plasma with a significant background pressure of neutrals. They have demonstrated that the recombination of the background electrons and ions on the surfaces of dust particles and the momentum loss of ions to neutrals in the presence of a relative ion-dust drift act as new processes promoting the excitation of dust-acoustic instability in a collisional plasma. Ivlev et al.[152] have made study on acoustic modes in a collisional dusty plasma taking into account the influence of ion-neutral collisions, ion drag, and neutral friction. They have assumed that the frequency of ion-neutral collisions is greater than the frequency of ion dust collisions and have derived some interesting results.

It has been shown that the properties of the dissipative drift wave can be modified in the presence of charged dust grains[153] owing to the modification of the equilibrium quasi-neutrality condition and the dust particle dynamics. Dust charge fluctuations can also modify the properties of electrostatic drift waves. Using a kinetic approach, Benkadda et al.[154] have estimated the growth rate of a new type of drift instability, driven by the process of dust charging. From their study they have found that the growth rate is comparable to or much larger than the usual drift instability, even for a low dust density. By continuing this study using a hydrodynamics approach they have seen that a high rate of dissipation due to the charging of dust particles take place[155], which produces a high nonadiabaticity in the longitudinal electron motion which increases the range of unstable drift waves. Very recently, Shukla et al.[156] have investigated the existence of the drift dissipative instability in a non-uniform magnetoplasma whose constituents are the electrons, positive ions, negative ions and negatively charged dust grains that are stationary and non-uniformly distributed. They have given a fluid theory description. They have reported that the presence of the negatively charged, massive dust grains affects both the drift wave frequency and the growth rate of the drift dissipative instability. The dust particles may be spatially localized in laboratory dusty plasma. There may exist gradients in density of charged plasma species at the edge of the dust cloud in order to maintain overall charge-neutrality. In presence of a magnetic field, such plasma may lead to drift instability.

In this chapter, low-frequency dissipative drift instability is investigated in a plasma system consisting of electrons, ions, dust particles and neutrals on the basis of fluid theory. For the completeness of the theory, self-consistent fluctuation of charge on dust particles is also incorporated. The dust particles are like sinks of plasma particles. The dissipative effect arises due to charging of dust grains by plasma currents. The inhomogeneity in dust density in a direction perpendicular to the magnetic field $\overrightarrow{B_0}$ gives rise to drift wave. Electron density gradient is also taken into consideration along x-direction. If there is a feedback mechanism, then a drift instability occurs and the plasma becomes unstable. On the otherhand, in presence of collision and other dissipative effects, the wave damping might occur. The attempt has been made to study the effect of dust density gradient and ion- neutral collision on the damping of drift mode for low frequency regimes, where characteristic time scale is governed by dust inertia. The wave dynamics is governed by the relatively heavy dust grains. The theory is tested in a typical laboratory dusty plasma device. It is assumed that the perturbed electric field is constrained so as to produce negligible magnetic perturbation, so that the drift wave may be assumed to be electrostatic.

Many astrophysical plasma and plasma processing situations have significant amount of neutral pressure. In such cases collisionless theory is no longer valid. Experimental observations also reveal that the waves are often excited when there is high neutral pressure[151]. It is therefore necessary to consider full equation of motion for plasma species including the collisional terms instead of considering them as Boltzmann fluid. In this study we have considered full equation of motion for plasma species including dust taking into account ion-neutral collisional term. Effect of ion-neutral collision frequency is investigated on low-frequency drift wave.

The theoretical model and equations are discussed in section 2.2 of this chapter. Section 2.3 deals with the dispersion relation. In section 2.3, analysis of the general results are given along with discussion. The conclusions are summarized in section 2.4.

2.2 Theoretical model and equations:

We are interested in studying the low frequency drift wave in a dusty plasma consisting of electrons, ions, neutral particles and negatively charged dust particles both in presence of electron and dust particle inhomogeneity and collision between ions with neutral particles and dusts with neutral particles. The negatively charged dust particles have density gradient along -x direction (Fig.2.1). Since electrons are more mobile than the ions, more electrons are absorbed on the dust surface than ions. Hence an electron depletion takes place which results in an electron density gradient along + x direction. Ion density inhomogeneity may be neglected in this case. Overall charge neutrality implies that

$$\frac{dn_e}{dx} = -Z_d \frac{dn_d}{dx}$$

Where, it is assumed that the variation of Z_d with n_d (and therefore with x) is small compared with the variation of n_d with x. Ion number density is assumed to be uniform. An electric field $E_0\hat{x}$ arising due to an external field from the electrode configuration confines the negatively charged dust.

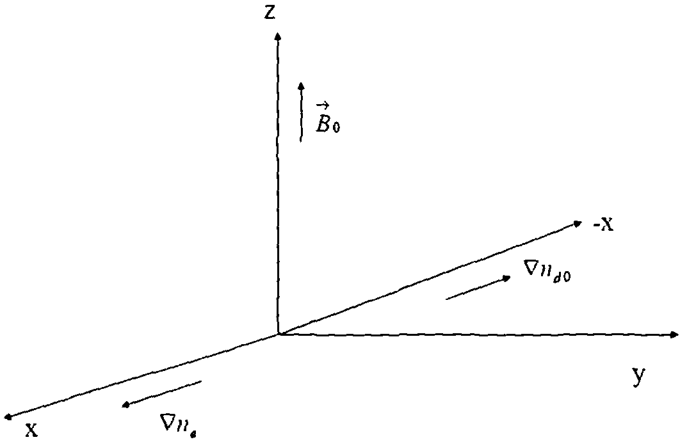

Figure 2.1: Schematic diagram showing the direction of magnetic field and density gradients in dusty plasma.

The governing equations for dust particles are

$$m_d n_d \left(\frac{\partial \overrightarrow{v}_d}{\partial t} + \overrightarrow{v_d}.\nabla \overrightarrow{v_d} \right) = n_d Q_d \left(\overrightarrow{E} + \overrightarrow{v_d} \times \overrightarrow{B_0} \right) - \overrightarrow{\nabla} p_d - \left(\overline{v}_d - \overrightarrow{v}_n \right) m_d n_d \nu_{dn} \tag{2.2.1}$$

$$\frac{\partial n_d}{\partial t} + \nabla \cdot \left(n_d \overrightarrow{v_d} \right) = 0 \tag{2.2.2}$$

where, $m_d, n_d, \overrightarrow{v_d}$ are the mass, density and velocity of dust particles, p_d is the dust pressure, whereas ν_{dn} is the collision frequency of dust particles of radius 'r_d' with the neutrals of mass m_n, density n_n and velocity v_n given as

$$\nu_{dn} = (4\pi/3)\, r_d^2 v_n n_n \left(m_n / m_d \right)$$

The density gradient of dust particles in presence of the magnetic field gives rise to diamagnetic drift. The expression for drift velocity can be obtained as

$$\overrightarrow{v}_{dD} = -\frac{1}{B_0} \frac{T_d}{Q_{d0} n_{d0}} \frac{\partial n_{d0}}{\partial x} \hat{y}$$

where, T_d is the temperature of the dust species. Due to the external field $E_{0x}\hat{x}$, the $\vec{E_0} \times \vec{B_0}$ drift is $\vec{u_E} = -\left(\frac{E_0}{B_0}\hat{y}\right)$.

Theory of dust charge fluctuation is taken into consideration. The charge Q_d on dust is treated as dynamical variable responding to electron and ion currents driven by self-consistent fields. The charging equation for dust particles is written as

$$\frac{dQ_d}{dt} = I_e + I_i \tag{2.2.3}$$

where

$$I_i = +\pi r_d^2 e\sqrt{\frac{8T_i}{\pi m_i}}n_i\left[1 - \frac{e(\Phi_{f0} - \Phi)}{K_B T_i}\right]$$

$$I_e = -\pi r_d^2 e\sqrt{\frac{8T_e}{\pi m_e}}n_e exp\left(\frac{e(\Phi_{f0} - \Phi)}{K_B T_e}\right)$$

and Φ_{f0} is floating potential, Φ is plasma surface potential. Φ_{f0} is determined by the condition that in equilibrium

$$I_{e0} + I_{i0} = 0$$

Equation of motion for ions is given as

$$m_i n_i\left(\frac{\partial \vec{v}_i}{\partial t} + \vec{v_i}.\nabla\vec{v_i}\right) = n_i e\left(\vec{E} + \vec{v_i} \times \vec{B_0}\right) - \left(\vec{v}_i - \vec{v}_n\right) m_i n_i \nu_{in} \tag{2.2.4}$$

where $\nu_{in} = n_n \sigma_{in} c_i$ is ion-neutral collision frequency, n_n is the neutral density and σ_{in} is the ion-neutral collisional cross-section and $c_i^2 = \frac{K_B T_i}{m_i}$

Continuity equation for ion is

$$\frac{\partial n_i}{\partial t} + \nabla \cdot (n_i \vec{v_i}) = 0 \tag{2.2.5}$$

Equations of motion for electrons are

$$m_e n_e\left(\frac{\partial \vec{v}_e}{\partial t} + \vec{v_e}.\nabla\vec{v_e}\right) = -n_e e\left(\vec{E} + \vec{v_e} \times \vec{B_0}\right) - \vec{\nabla} p_e \tag{2.2.6}$$

where, $\vec{\nabla} p_e = -T_e \nabla n_e$

$$\frac{\partial n_e}{\partial t} + \nabla \cdot (n_e \vec{v_e}) = 0 \tag{2.2.7}$$

Here, m_e, n_e and v_e are the mass, density and velocity of the electrons respectively. The governing equations for neutrals are

$$m_n n_n \left(\frac{\partial \vec{v}_n}{\partial t} + \vec{v_n}.\nabla \vec{v_n} \right) = -\left(\vec{v}_n - \vec{v}_d \right) m_n n_n \nu_{dn} - \left(\vec{v}_n - \vec{v}_i \right) m_i n_i \nu_{in} \tag{2.2.8}$$

$$\frac{\partial n_n}{\partial t} + \nabla \cdot \left(n_n \vec{v_n} \right) = 0 \tag{2.2.9}$$

The equations may be finally closed by Poisson's equation given as

$$\nabla^2 \Phi = 4\pi \left[e n_e + Q_d n_d - e n_i \right] \tag{2.2.10}$$

2.3 Dispersion Relation:

The normal mode analysis is used to solve the equations (2.2.1)−(2.2.10). We consider that the low-frequency wave is propagating in the yz-plane such that the perturbed quantities vary as $exp\left(i k_y \hat{y} + i k_z \hat{z} - i \omega t\right)$, where, $k_z \ll k_y$. Linearizing *equations* (2.2.1)−(2.2.10) *and taking Fourier transformation, we get the perturbed* parameters as

$$n_{d1} = \left(Q_{D2} E_{1y} + Q_{D3} E_{1z} + Q_{D4} Q_{d1} \right) / Q_{D1}(\omega) \tag{2.3.1}$$

$$n_{i1} = \frac{1}{\omega} \left[Q_{i1} n_{d1} + Q_{i2} E_{1y} + Q_{i3} E_{1z} + Q_{i4} Q_{d1} \right] \tag{2.3.2}$$

$$n_{e1} = \frac{1}{A_{e1}} \left[C_{e1} E_{1y} + D_{e1} E_{1z} \right] \tag{2.3.3}$$

$$Q_{d1} = \frac{1}{X} \left[A \left(1 + a_a Q_{d0} \right) n_{e1} \right] - \frac{B}{X} \left(1 - b_b Q_{d0} \right) n_{i1} \tag{2.3.4}$$

Substituting these first order perturbed quantities into the linearized Poisson equation $\nabla^2 \Phi_1 = 4\pi \left[e n_{e1} + Q_{d0} n_{d1} + Q_{d1} n_{d0} - e n_{i1} \right]$, we get the dispersion relation as

$$1 + \chi_e + \chi_d + \chi_i = 0 \tag{2.3.5}$$

Here,

$$\chi_e = -\frac{4\pi i e}{k^2 A_{e1}} \left(k_y C_{e1} + k_{z1} D_{e1}\right)$$

$$\chi_d = -\frac{4\pi i}{k^2} \left[\frac{Q_{d0}}{(\omega - Q_1)} \left(k_y Q_{dy} + k_z Q_{dz} + n_{d0} \left(\frac{k_y \alpha_y}{\alpha_d} + \frac{k_z \alpha_z}{\alpha_d}\right)\right)\right]$$

$$\chi_i = \frac{4\pi i e}{k^2} \left(k_y Q_{iy} + k_z Q_{iz}\right)$$

Where, the terms appearing in equations (2.3.1)–(2.3.5) are described in Appendix A.

2.4 Analysis of the Results and Discussions:

We consider the limit $\omega << \nu_{in}$ and $\omega < \nu_{dn}$. Then equation (2.3.5) reduces to

$$C_1\omega^5 + C_2\omega^4 + C_3\omega^3 + C_4\omega^2 + C_5\omega + C_6 = 0 \tag{2.4.1}$$

Where, the coefficients C_i $(i = 1, 2, 3, 4, 5, 6)$ are described in Appendix A. Assuming $\omega = \omega_r + i\gamma$, equation (2.4.1) is numerically solved for following values of the parameters obtained in typical dusty plasma laboratories:

$m_d = 4 \times 10^{13} m_p$, $n_{i0} = 5 \times 10^{16}$ m^{-3}, $n_{d0} = 1 \times 10^{14}$ m^{-3}, $n_{n0} = 10^{22}$ m^{-3}, $n_{e0} = 2.0 \times 10^{14}$ m^{-3}, $T_i \sim 0.7$ eV, $T_e \sim 3$ eV, $T_d \sim .03$ eV, radius of the dust $r_d \sim 10$ μm, $B_0 = 2$ Tesla, $Z_d = 5 \times 10^3$ and $\sigma_{in} \simeq 10^{-14}$ cm^2. The normalized values of real and imaginary parts of frequency i.e. (ω_r/ω_{pd}) and (γ/ω_{pd}) are plotted across $k_y\lambda_{Dd}$ in Figs (2.2 – 2.5), where

$$\lambda_{Dd} = \frac{\lambda_{De}\lambda_{Di}}{\sqrt{\lambda_{De}^2 + \lambda_{Di}^2}}$$

here, λ_{De} and λ_{Di} are the electron and ion Debye radii respectively. The negative values of γ indicate a dissipative, collisional drift instability in the regime $\omega_{pd} << \omega << \omega_{pi}$.

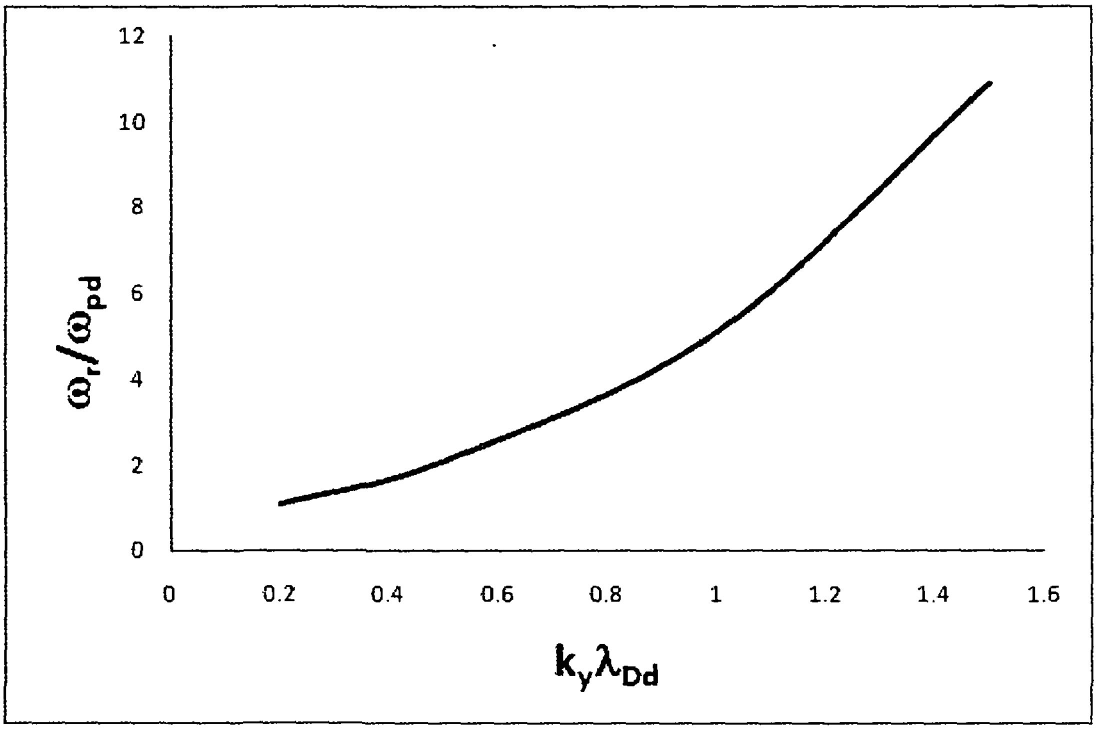

Figure 2.2: $\frac{\omega_r}{\omega_{pd}}$ vs. $k_y\lambda_{Dd}$, for $K\lambda_{Di} = 2.0$.

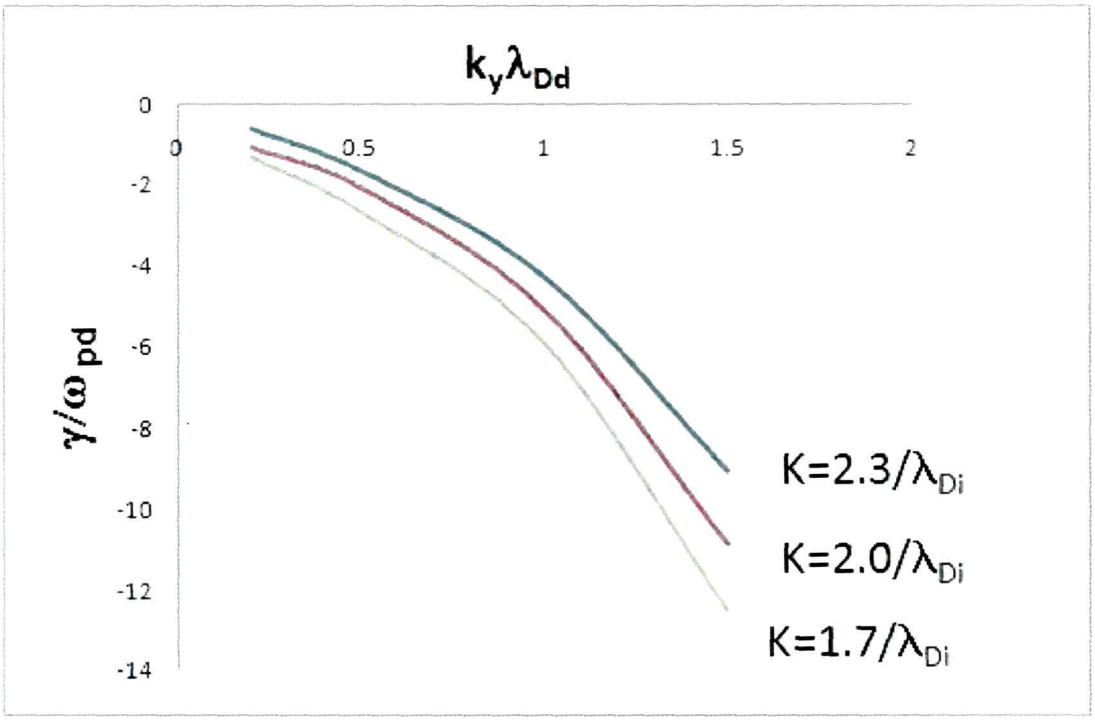

Figure 2.3: $\frac{\gamma}{\omega_{pd}}$ vs. $k_y\lambda_{Dd}$, for $K = 1.7/\lambda_{Di}$, $2.0/\lambda_{Di}$, $2.3/\lambda_{Di}$ respectively .

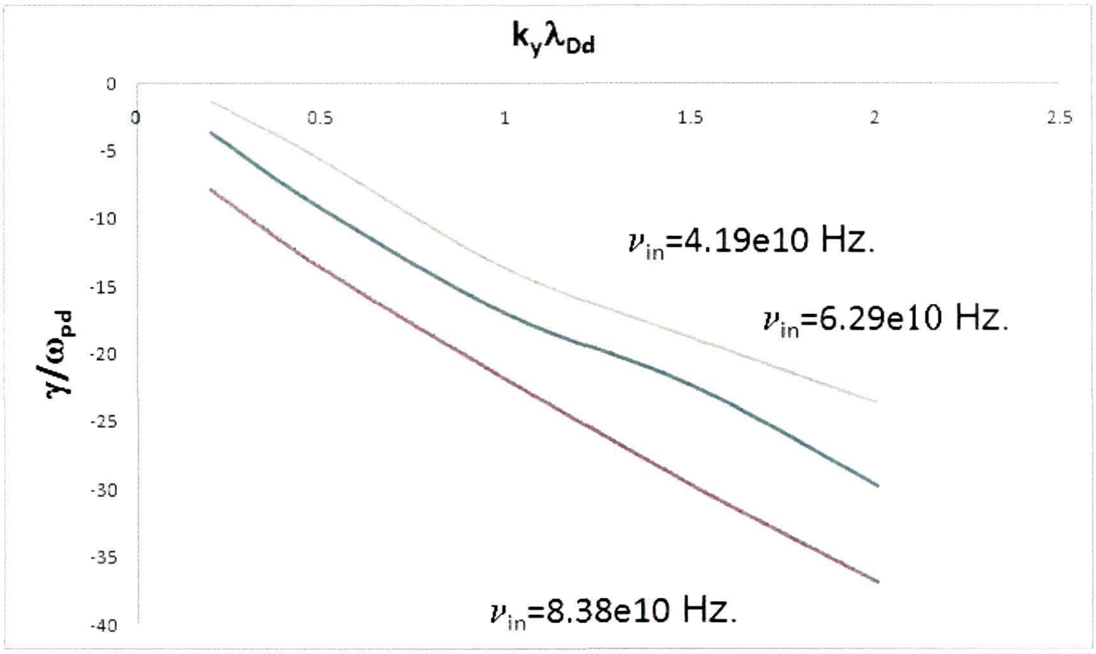

Figure 2.4: $\frac{\gamma}{\omega_{pd}}$ vs. $k_y\lambda_{Dd}$, for $\nu_{in} = 4.19\times10^{10}, 6.29\times10^{10}, 8.38\times10^{10}$ Hz. respectively

In order to see the role of density gradient scale-length on the dissipative instability, (γ/ω_{pd}) is plotted for different values of dust density gradient $K = \frac{n'_{d0}}{n_{d0}} = 1.7$, 2.0 and 2.3 respectively in the units of λ_{Di} in Fig.2.3. It is seen that with the increase in dust density gradient, damping of the wave decreases. Density inhomogeneity is the driving force for drift instability. However, due to the presence of dust and collisions between plasma particles with neutral, the wave is dissipated. This can be seen from Fig.2.4 where, (γ/ω_{pd}) is plotted for different values of ion-neutral collision frequency. This clearly shows that larger is the collision frequency, more is the dissipation rate. Low frequency drift mode gets damped in presence of high neutral pressure.

Fig.2.5 shows the dissipation rate of dusty plasma for different values of $\left(\frac{T_i}{T_e}\right)$.

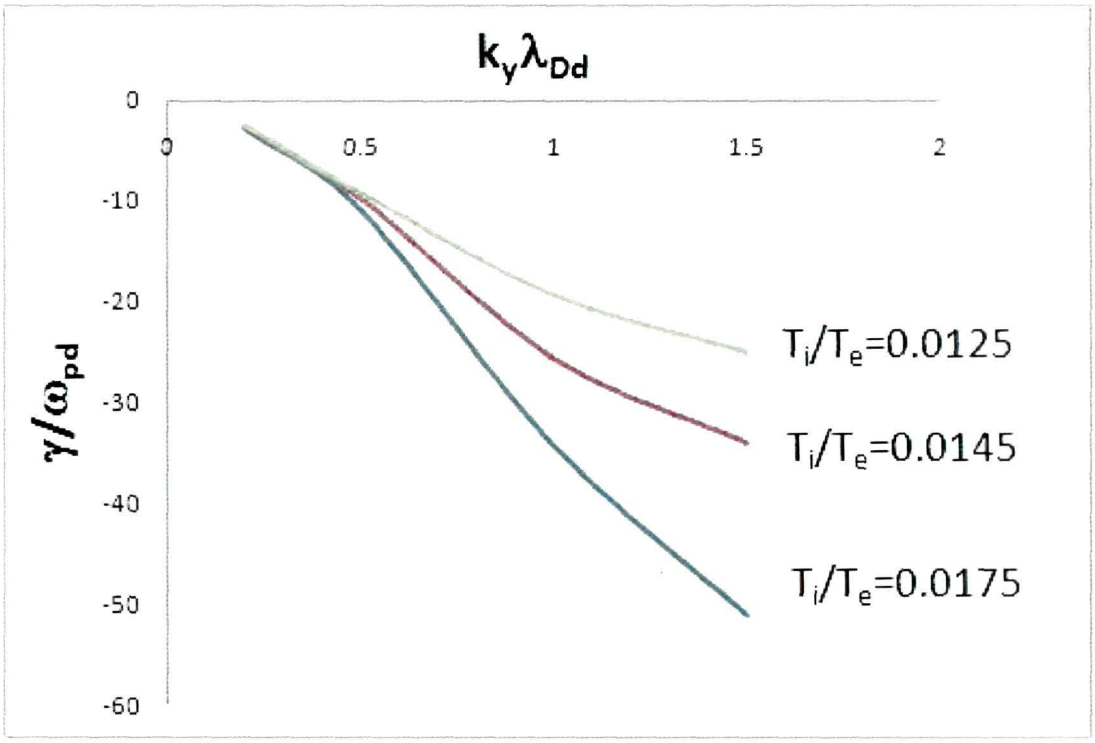

Figure 2.5: $\frac{\gamma}{\omega_{pd}}$ vs. $k_y\lambda_{Dd}$, for T_i/T_e = 0.0125, 0.0145, 0.0175 respectively.

The charging frequency for dust particles may be given as[155]

$$\nu_{ch} = \frac{\omega_{pi}^2 r_d}{v_{Ti}\sqrt{2\pi}}(1 + \tau + z)$$

where, $v_{Ti} = \sqrt{T_i/m_i}$ is the ion thermal velocity, $\tau = \frac{T_i}{T_e}$, $z = Z_d e^2/r_d T_e$. It is seen from our calculations that larger is the value of T_i/T_e higher is the charging frequency and higher is the damping. Charging of dust particles leads to dissipation of drift wave in plasma in the low frequency regime.

2.5 Conclusions:

We have presented a theory for low frequency dissipative drift instability in dusty plasma. Drift wave in such plasma arises due to inhomogeneity of dust density in presence of magnetic field. The dispersion relation has been obtained by normal mode analysis. The electron density gradient is in opposite direction to the dust density gradient. The drift wave gets damped due to self-consistent fluctuation of the charge on dust particles. Another wave damping mechanism that is discussed here is through ion-neutral collision. Our analysis clearly reveals that ion-neutral collision plays a major role in the process of the wave getting damped.

The study of dissipative drift wave is important in the ionosphere plasma turbulence, in astrophysical plasma and in edge plasma turbulence of tokamak.

Chapter 3

Molecular Dynamics Simulation of Dust Crystal Formation

In this chapter, a discussion has been made on crystal formation in complex plasma A molecular dynamics (MD) code is developed for this purpose and is used to study the crystal formation of the system The interaction potential among the dust grains is taken as Yukawa type The structure of the complex system is investigated by calculating Radial Distribution Function g(r) for different values of temperature, density and size of dust grains. It is very interesting to know the effect of these parameters on phase transition in complex plasma The long-range order is studied from the plot of the strength of lattice correlation with time The phase diagram obtained for the system shows the existence of three phases, solid(FCC), solid(BCC) and fluid

3.1 Brief introduction to Molecular Dynamics simulation:

Molecular Dynamics (MD) simulation is an important and powerful tool in the study of large collections of atoms and molecules[157] This computational method follows the evaluation of a many-body system by tracking the trajectory of every particle in the system by numerically integrating its equation of motion including all the forces acting on the particle. From the resulting information on the variation of the phase space (locations and velocities) of the particles, one can obtain the macroscopic properties (statistical, thermodynamics, and transport) of the system.

The first simulation of a liquid was carried out by Metropolis, Rosenbluth, Rosenbluth, Teller and Teller on the MANIAC computer at Los Alamos, using the Metropolis Monte Carlo method. The name *Monte Carlo simulation* had been coined earlier by Metropolis and Ulam, because the method makes heavy use of computer-generated random numbers, Almost at the same time, Fermi, Pasta and Ulam performed their famous numerical study of the dynamics of an an-harmonic, one-dimensional crystal. MD methods were originally conceived within the theoretical physics community during the 1950s. In 1957, Alder and Wainwright performed the earliest MD simulation using the so-called hard-sphere model, in which the atoms interacted only through perfect collisions. Many important insights concerning the transport behavior of simple liquids emerged from these studies. The first MD simulation of a model of a "real" material was reported in 1959 and published in 1960 by the group led by Vineyard at Brookhaven, who simulated radiation damage in crystalline Cu. A major advance appeared in 1964, when Rahman carried out the first simulation using a more realistic model potential for simulating liquid argon. The first MD simulation of a system of complex molecules was done in 1974 by Stillinger and Rahman in their study of liquid water[158]. The first protein simulations appeared in 1977 with the simulation of the bovine pancreatic trypsin inhibitor (BPTI)[159]. Much of the methodology of computer simulations has been developed since then, although it is fair to say that the basic algorithms for MC and MD have hardly changed since the 1950s.

Today in the literature, one routinely finds molecular dynamics simulations of solvated proteins, protein-DNA complexes as well as lipid systems addressing a variety of issues including the thermodynamics of ligand binding and the folding of small proteins. The number of simulation techniques has greatly expanded; there exist now many specialized techniques for particular problems, including mixed quantum mechanical - classical simulations, that are being employed to study enzymatic reactions in the context of the full protein. Molecular dynamics simulation techniques are widely used in experimental procedures such as X-ray crystallography and NMR structure determination. MD simulations can also be used for testing of novel statistical as well as dynamic models, such as the interaction potential between two or more particles of certain type. Recently, MD simulation was employed to clarify the plasma maser effect in the classical quasilinear theory of weak turbulence[160], modelling of laser ablation of matter[161], investigating the dynamics and pattern behavior of granular objects such as sand and colloids[162] etc. Beside these, the study of MD simulation involves a large variety of problems, including fundamental studies of equilibration, tests of molecular chaos, kinetic theory, diffusion, transport properties, size-dependence, tests of models and potential functions etc.; in the field of phase transitions, it involves the study of first and second order phase transition, phase coexistence, order parameters, critical phenomena etc. MD simulation involves the study of decay of space and time correlation, coupling of translation and rotation, vibration, dielectric properties etc.; in the study of complex fluid, it can be used to study structure and dynamics of molecular liquids, glasses, liquid crystals, ionic liquids, films and monolayers etc.; MD simulation also can be used to study defect formation and migration, fracture, structural transformations, friction, molecular crystals, epitaxial growth etc.[163]. MD simulation can provide accurate information about the relationships between the bulk properties of matter and the underlying interactions among the constituent atoms or molecules in the liquid, solid or gaseous state. The ever-increasing power of computers makes it possible to calculate ever more accurate results about larger and larger systems.

3.2 Development of code for the study of crystal formation:

3.2.1 Equations of motion:

Molecular dynamics simulation consists of the numerical, step-by-step, solution of the classical equations of motion may be written as,

$$m_i \ddot{\vec{r_i}} = F_i = \sum -\nabla\phi(r_{ij}) \tag{3.2.1}$$

where $i \neq j$ and $j = 1, 2, 3, ..., N$, $\vec{r_i}$ is the position vector of a particle denoted by i, m_i is the mass of the i^{th} particle, F_i is the total force on it, N is the total number of particles to be simulated and $\phi(r_{ij})$ is the inter-particle potential between the i^{th} particle and the j^{th} particle at a distance $r_{ij} = \mid r_i - r_j \mid$ apart. Molecular Dynamics does exactly this even for very small N, or for complicated forms of $\phi(r_{ij})$. Because the classical N-body problem lacks a general analytical solution, in MD simulation the trajectory of each particle in the system is followed by solving its equation of motion.

Solving the above equations on a computer has the following limitations[164]:

(1) The limitation of the time step being around a femtosecond to simulate materials, so as to determine numerical stability.

(2) The number of atoms simulated is limited between 100 and 10^9, depending on the type of potential used and speed of computers.

In pure MD there is no way to increase the time step above $10 fs$ in atom systems in any real material at ordinary temperatures (77 K and up). According to the rule of thumb the atoms can not move more than 1/20 of the nearest-neighbor distance during one time step. Usually Δt is constant throughout the simulation in case of ordinary equilibrium MD. But if during the simulation the maximum velocity of the atoms changes a lot then a variable time step can be used, so that it increases with the decrease in the maximum velocity.

In MD simulation the physical properties of the system is governed by the total interaction potential, ϕ_{total}, which can be expressed as

$$\phi_{total} = \sum_{i=1}^{N}\sum_{j>i}^{N}\phi(r_{ij}) + \sum_{i=1}^{N}\sum_{j>i}^{N}\sum_{k>j}^{N}\phi(r_{ijk}) + ... \tag{3.2.2}$$

where $\phi(r_{ij})$ and $\phi(r_{ijk})$ denote the pair and triplet interaction potentials respectively. Since the many-body interaction is usually either theoretically unknown or computationally too time-consuming, a practical approximation is to use the pair term alone. Having specified the potential energy function the next step is to calculate the atomic forces. Numerous numerical algorithms have been developed for integrating the equations of motion, including Verlet algorithm, Leap-frog algorithm, Velocity Verlet and Beemans algorithm. Of these existing algorithms we use in our MD calculation the efficient Velocity Verlet algorithm to find out particle positions and velocities at each time step and according to which the new particle positions and velocities can be find out as

$$\begin{aligned} r_i(t+\delta t) &= r_i(t) + \delta t v_i(t) + \frac{1}{2}\delta t^2 a_i(t) \\ v_i(t+\delta t) &= v_i(t) + \frac{1}{2}\delta t[a_i(t) + a_i(t+\delta t)] \end{aligned} \tag{3.2.3}$$

where δt is the time step of the integrator.

We introduce a set of dimensionless MD units in which all physical quantities will be expressed, so that, instead of extremely small values normally associated with the atomic scale, we can work with numerical values that are almost equal to unity. Another benefit for using such units is that the equations of motions become simplified and a single model can describe a whole class of problems.

Boundary conditions:

As mentioned earlier the computation time of MD simulation depends on the number of atoms in the simulation, so one would want to use minimum number of atoms without compromising on the accuracy of the results. For this reason use of boundary condition is important. To simulate homogeneous bulk systems, periodic boundary conditions (PBCs) are used.

A system that is bounded but free of physical walls can be constructed by resorting to periodic boundary conditions. Periodic boundaries is equivalent to considering an infinite space-filling array of identical copies of the simulation region. To implement this boundary condition two things have to be done.

1. In the first case, an atom which passes through a particular boundary face of simulation region comes back on the opposite face.
2. In the second case, atoms lying within a distance r_c of a boundary interact with atoms near the opposite boundary[163].

Fixing macroscopic parameters:

Molecular dynamics simulations generate information at the microscopic level, including atomic positions, velocities, individual kinetic and potential energies etc. The conversion of this microscopic information to macroscopic observable such as temperature, pressure etc., requires statistical mechanics, which provides the mathematical expressions that relate macroscopic properties to the distribution and motion of the atoms and molecules of the N-body system. Molecular dynamics simulations provide the means to solve the equation of motion of the particles and evaluate these mathematical formulaes.

In the case of crystalline solids the initialization of atomic positions are defined by the crystal symmetry and positions of atoms within the unit cell of the crystal, which is then repeated to fill up the desired dimensions of the system. The initial velocities are set by assuming a Maxwell-Boltzmann distribution for velocities along the three dimensions by using Gaussian distributed random numbers multiplied by a mean square velocity given by $\sqrt{2K_BT_d/m_d}$ in each of the three directions and verify that the system has total momentum equal to zero. Therefore the initial temperature is fixed by the velocity distribution. The total energy of the system is given by the sum of the total kinetic energy KE_{Total} the total potential energy PE_{Total} of the system given by

$$KE_{Total} = \sum_{i=1}^{N} \frac{1}{2} m_d \left(v_{x,i}^2 + v_{y,i}^2 + v_{z,i}^2\right) \tag{3.2.4}$$

$$PE_{Total} = \sum_{i=1}^{N} \phi_i(r_i) \tag{3.2.5}$$

here, $v_{x,y,z}$ being the velocities, r being the positions of atoms, i being the index that sums over all the atoms N in the system and $\phi_i(r_i)$ is the potential energy of the atom due to all other atoms in the system. Depending on the type of ensemble simulated, various macroscopic parameters of the simulation like temperature, pressure, specific heat at constant pressure or at constant volume, etc. can be determined.

3.3 MD code for Yukawa crystal in dusty plasma:

Plasma is known to have disordered nature. Yet some regular crystal like arrangement of particles is possible in dusty plasma when certain conditions are satisfied. A dusty or complex plasma consists of micron-sized charged particulate in addition to normal electrons and ions. It is well known that micron-sized dust particles immersed in plasma acquire very large negative charge. If the kinetic temperature of the grain, $T_d <<$ interaction potential (ϕ), the grains are strongly coupled and are self organized into a crystalline configuration. Ikezi[119] predicted that if Coulomb's coupling parameter, defined as

$$\Gamma = \frac{Z^2 e^2}{4\pi\epsilon_0 a K_B T_d} \tag{3.3.1}$$

exceeds a critical value, $\Gamma_c \simeq 170$, Coulomb lattice may be formed. Here, $a = \left(\frac{3}{4\pi n_d}\right)^{\frac{1}{3}}$ is the mean inter-particle distance, T_d is the temperature of the dust grains. Besides this condition, the lattice parameter (the ratio of the particle separation to the Debye length) has to be smaller than unity.

In this chapter, we intend to investigate the structural properties of a three-dimensional (3D) dusty plasma system using molecular dynamics (MD) simulation. In section 3.3.1, we are describing the theoretical model for our system. The results of our study are discussed in section 3.3.2. Section 3.3.3 deals with the conclusions drawn from the study. The dust grains are allowed to evolve according to Newton's law of motion with a model dust-dust Yukawa interaction potential. The structure of the complex system is investigated by calculating Radial Distribution Function (g(r)) and the presence of long-range order. We are mainly interested to study how the dust size, density and temperature affects the crystal formation and the phase transition from fluid to solid and solid(FCC) to solid(BCC) states.

3.3.1 Theoretical Model:

We consider a 3D dusty plasma system of identical, spherical particles of mass m_d and charge Q_d immersed in a neutralizing background plasma. In such a system, the interaction potential between the dust grains is usually described by Screened Coulomb or Yukawa potential

$$\phi(r_{ij}) = \frac{Q_d^2}{4\pi\epsilon_0 r_{ij}} \exp\left(-\frac{r_{ij}}{\lambda_D}\right) \tag{3.3.2}$$

where, r_{ij} is the distance between two particles, λ_D the Debye length of the background plasma defined as

$$\lambda_D = \left(\frac{q_i^2 \bar{n}_i}{\epsilon_0 K_B T_i} + \frac{e^2 \bar{n}_e}{\epsilon_0 K_B T_e}\right)^{-\frac{1}{2}}$$

where, q_i, $-e$, $\bar{n}_i$, $\bar{n}_e$, T_i and T_e denote the ion charge, charge of electron, ion mean density, electron mean density, temperature of ions and electrons respectively. We assume that the mass, size and charge of all the grains are the same.

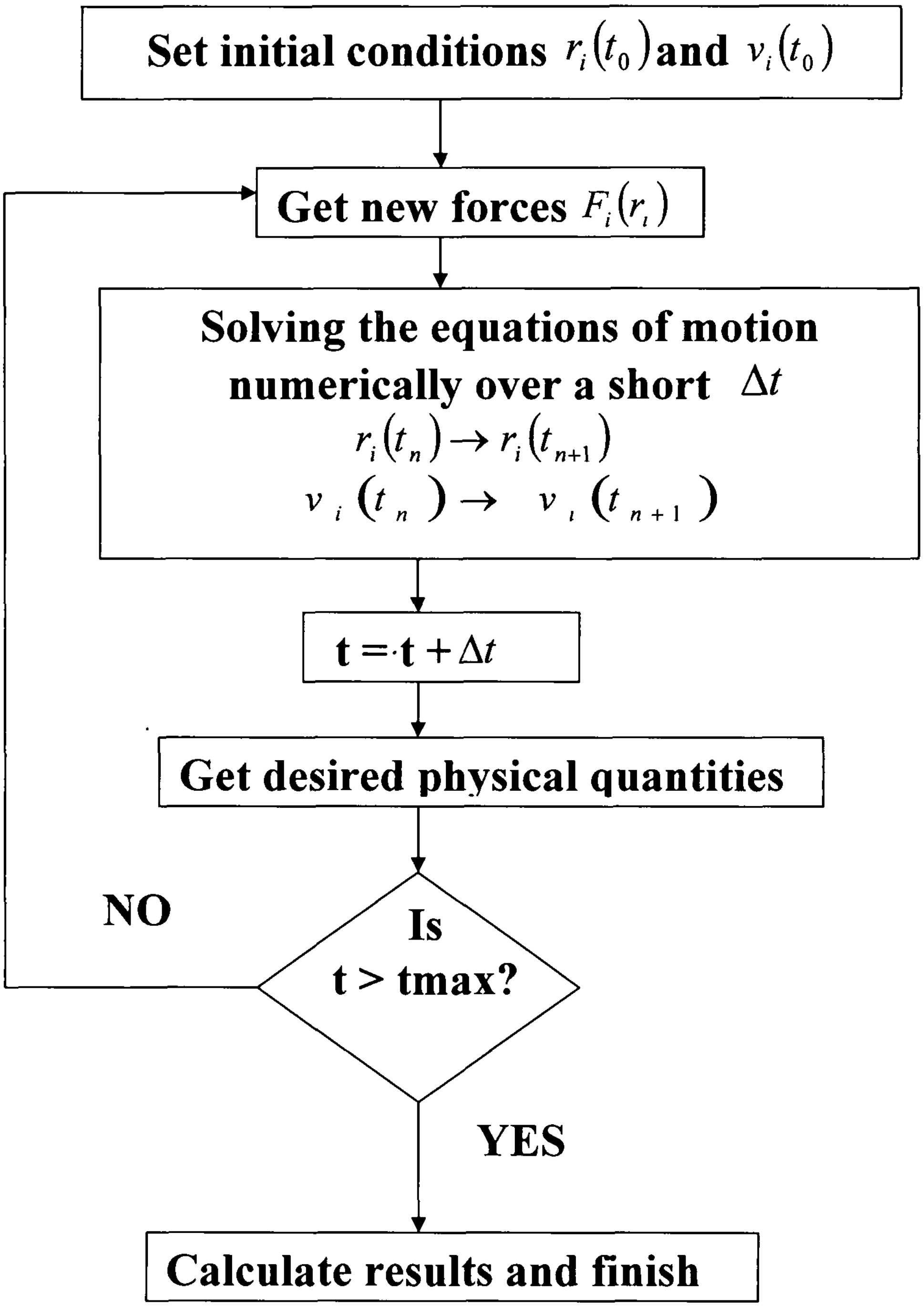
Set initial conditions $r_i(t_0)$ and $v_i(t_0)$
Get new forces $F_i(r_i)$
Solving the equations of motion numerically over a short Δt
$r_i(t_n) \to r_i(t_{n+1})$
$v_i(t_n) \to v_i(t_{n+1})$
$t = t + \Delta t$
Get desired physical quantities
NO
Is t > tmax?
YES
Calculate results and finish

Figure 3.1: Basic MD Algorithm.

To study this problem we have developed a Molecular Dynamics (MD) code by learning and implementing the basic MD algorithm (Fig. 3.1), to observe the crystalline pattern formed by the dust grains, and then see the effects of different dust parameters on phase transition.

Although different kinds of interaction potential may exist among the dust grains, we have considered here the existence of an effective Yukawa potential only. In physically bounded or otherwise confined systems, different kinds of regular arrangements like crystals and clusters can be formed even if the inter-particle interaction is purely repulsive, because of the competition between physical packing and the repulsive interaction force. The time scale of dust dynamics is very long, so that electrons and ions can be treated as to be in local thermodynamic equilibrium. Therefore, it is sufficient to simulate only one species of particles, whose interaction obeys an effective interaction potential. This automatically accounts for the fast moving electrons and ions in a time averaged manner.

In the MD simulation of a system of N number of charged dust grains, the equation of motion of each of the N interacting particles is solved numerically. The evolution of the trajectory of each of the particles is tracked by integrating Newton's law of motion denoted by equation (3.2.1). In the present work, the simulations are performed with 686 particles for BCC crystal structure and 500 particles for FCC crystal structure, under periodic boundary conditions, in a 3D cubic simulation box of side L. These lattices are used as initial conditions. The interaction of a given particle, say i with other particles j and the periodic images of particles j in other neighbor boxes is considered to calculate the electrostatic potential in the MD simulations. Each grain is assigned an initial velocity (random in magnitude and direction) such that the average kinetic energy corresponds to the chosen temperature T_d. Velocity Verlet algorithm is used to compute the new positions and velocities from the computed forces. In this present problem, the space, mass, time, velocity and energy are normalized by λ_D,

m_d, $\sqrt{\frac{m_d \lambda_D^2}{K_B T_d}}$, $\sqrt{\frac{m_d}{K_B T_d}}$ and $K_B T_d$. Here λ_D is the screening length of the background plasma, m_d is the mass of the dust grain, T_d is the dust temperature, K_B is the Boltzmann constant. In this problem we use constant temperature MD to simulate structural properties which is achieved by NVT (standing for controlled number, volume and temperature) runs so that the system achieve equilibrium state. The conservation of energy and momentum is verified to check whether the simulation is self consistent, and can be used for new interaction models.

Normally, the thermodynamics of the system can be characterized by two dimensionless parameters. One is the Coulomb coupling parameter (Γ) defined as in equation (3.3.1) and the other parameter is the screening constant

$$\kappa = \frac{a}{\lambda_D} \tag{3.3.3}$$

The parameter Γ determines the possibility of formation of dusty plasma crystals. Different parameters such as dust particle density, temperature, density of neutral gas, particle size play very important role in deciding whether a dusty plasma will be strongly coupled or not.

To find out structural correlation of the grains, pair correlation function $g(r)$ is calculated. It is the probability of finding a pair of particles at a distance r from a chosen particle. One finds that

$g(r) \rightarrow 1$ for $r \rightarrow \infty$

since one will always find a particle at large distances, and

$g(r) \rightarrow 0$ for $r \rightarrow 0$

since particles cannot come infinitely close to each other. Here, $g(r)$ is calculated by choosing one particle as a center point and counting the particles in concentric spheres of definite radii around center point at regular intervals. This number in each shell is normalized by the volume of each shell, which gives the average density of atoms in the system, at the end of the simulation. For an isotropic system, this function can be averaged over angles and this leads to radial distribution function (RDF), that describes the spherically averaged local organization around any given atom. Mathematically, in 3D this function is defined by

$$g(r) = \frac{V}{N}\frac{N(r,\Delta)}{4\pi r^2\Delta} \tag{3.3.4}$$

where, V is the volume of the simulated region, N is the number of simulated particles, and $N(r,\Delta)$ is the number of particles located in a shell of infinitesimal thickness Δ from $r-\frac{\Delta}{2}$ and $r+\frac{\Delta}{2}$. From the study of RDF, local structure of the grains can be analyzed. The sharp RDF peaks indirectly indicate the existence of long-range crystalline order.

In order to check the presence of lattice structure, long-range order is studied. In a crystal, atomic positions exhibit this long-range order property, which means, positions repeat in space in a regular array or we can say that remote portions of the sample exhibit correlated behavior. In a solid the atoms are strongly correlated with each other, which means presence of long-range order. In order to test presence of long range, the local density at a point r_i can be expressed as

$$\rho(r_i) = \sum \delta\left(r_i - r_j\right)$$

and it's Fourier transform is

$$\rho(k) = \frac{1}{N}\sum \exp(-ik.r_j) \tag{3.3.5}$$

which represents the strength of lattice correlation. Here, k denotes the reciprocal lattice vector of the ordered state, which can be any linear combination of vectors appropriate for the expected lattice. So, $k = \left(\frac{2\pi}{l}\right)(a_1, b_1, c_1)$, where, l is the unit cell edge and (a_1, b_1, c_1) is the set of Miller indices appropriate for the expected lattice structure. In our present work, if $\mid \rho(k) \mid \approx 1$, we can conclude that the system is almost fully ordered.

3.3.2 Results and Discussions:

We have studied the structural properties of 3D dust clusters by means of MD simulation. In the present work we have identified solid, liquid and gas-like phases by analyzing the pair correlation function. The effect of various dust parameters such as temperature of dust grains, size of the dust grain and dust number density on it has been studied. The code is tested for the presence of long-range order.

We have calculated $g(r)$ for different initial dust temperatures for $n_d = 3.74 \times 10^{10}$ m^{-3}, $n_i = 1.0 \times 10^{14}\, m^{-3}$, $n_e = 1.415 \times 10^{14}\, m^{-3}$, $T_e = 2320$ K, $T_i = 300$ K, $r_d = 2.0 \mu m$ and $m_d = 4.0 \times 10^{-15}\, kg$ as shown in Fig.3.2 and Fig.3.3. From the plot (Fig.3.2) we see that the peaks of $g(r)$ for different initial dust temperatures $T_d = 5K$, $T_d = 10K$, $T_d = 50K$ respectively are at the same locations, which means that the physical structures of the dust clusters are similar. However, the height of the peaks for all the three cases are different. It is because, at a low temperature, for the same r there is higher chance to find a dust pair than at a high one.

Fig.3.3 reflects crystalline, fluid, and gas-like states. In the solid state, for low dust temperature ($T_d = 5K$), the peaks of $g(r)$ are very pronounced and more peaks can be identified which indicates presence of more ordered structure. The first peak in g(r) plot is due to the neighboring particles, further peaks are due to the next neighbors. In the liquid state ($T_d = 500K$) one pronounced maximum is found, which correspond to the nearest neighbor distance. This corresponds to an ordering at small distances. For $T_d = 7000K$, the pair correlation is almost flat, which means no correlation among dust grains exists at all and we can conclude that the dust system is now in gas-like state. In this phase, the particle velocities are very high and as a result, no regular structure exists and system becomes chaotic. We also observe that in comparison with the plot of $g(r)$ at lower initial dust temperature, the peak of g(r) plot at higher initial dust temperature is shifted to a smaller inter-particle

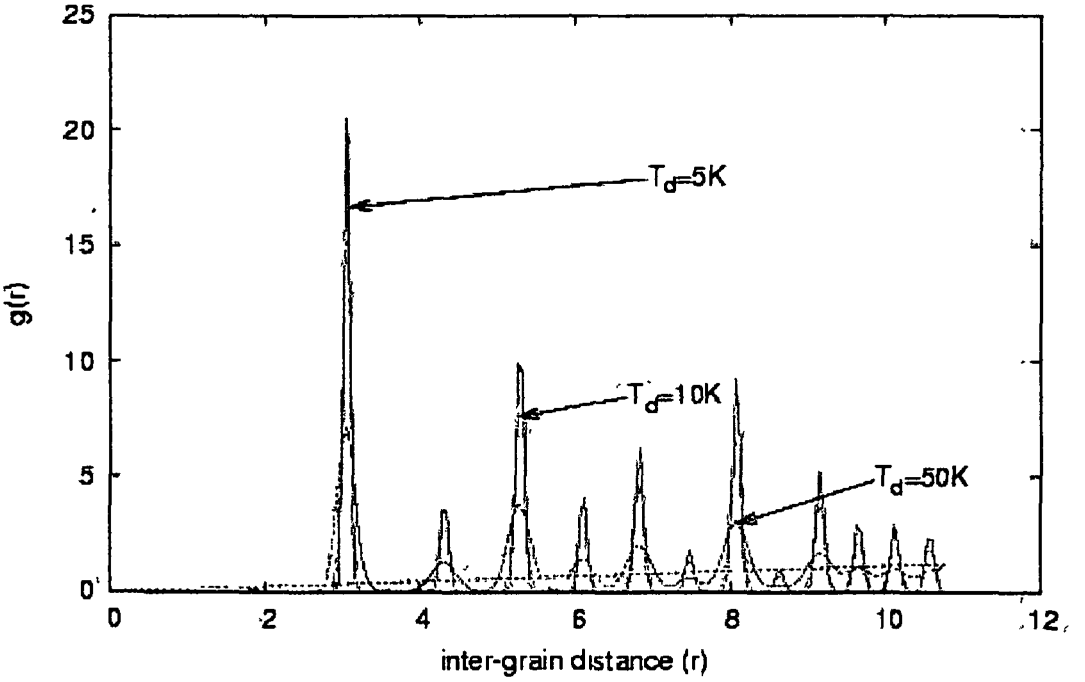

Figure 3.2: Plot of $g(r)$ vs. r for dust temperatures $T_d = 5K, 10K, 50K$ respectively.

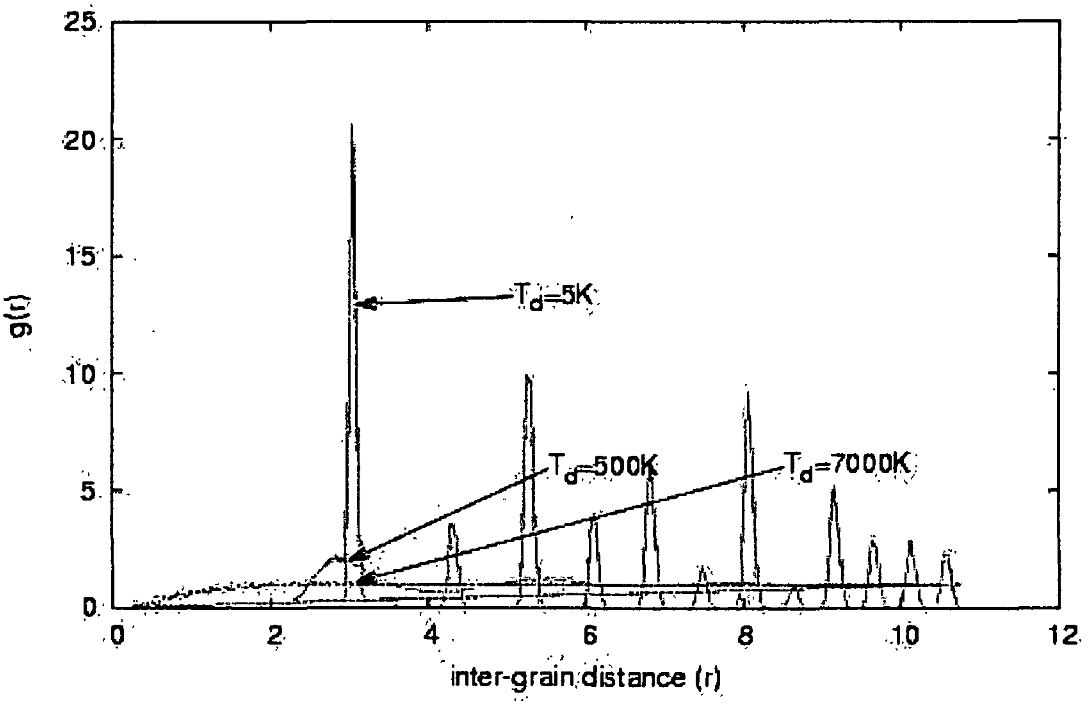

Figure 3.3: Plot of $g(r)$ vs. r for dust temperatures $T_d = 5K, 500K, 7000K$ respectively.

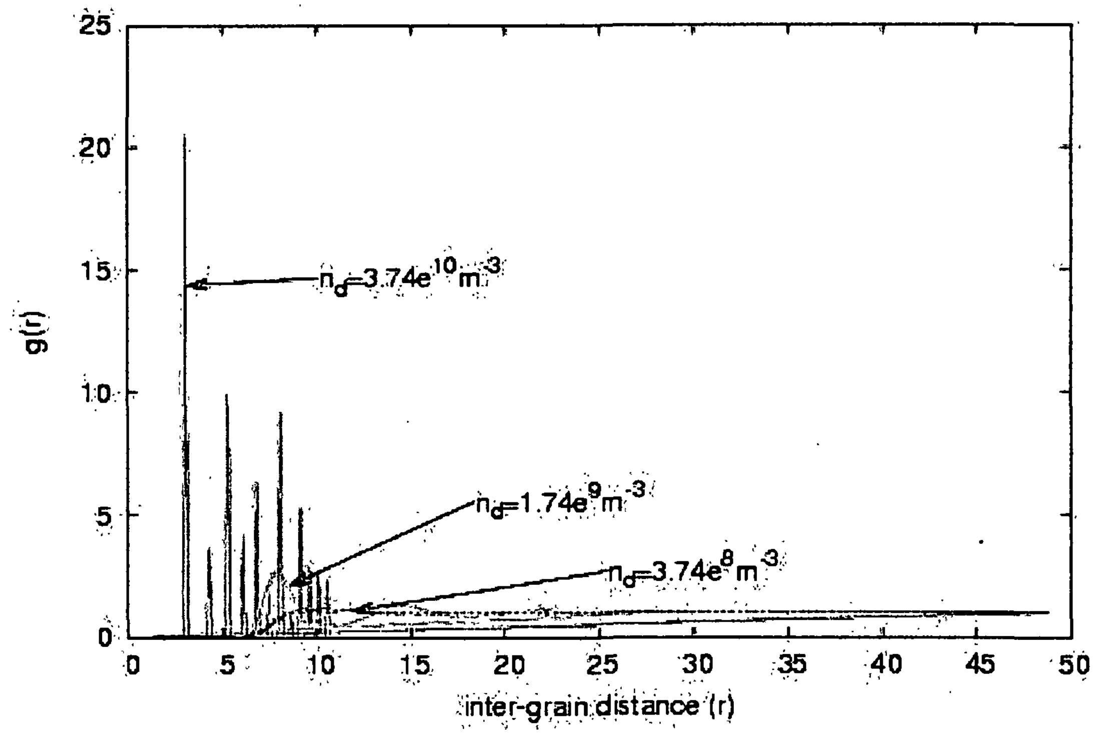

Figure 3.4: Plot of $g(r)$ vs. r for different values of dust number densities at T_d=5K.

distance. This is because at higher temperatures, the dust grains have higher kinetic energies such that they can come to a closer distance.

From Fig.3.4 we observe that for relatively low dust density ($n_d = 3.74 \times 10^8 m^{-3}$) only a very small hump appears in $g(r)$ plot, which means there is a lack of strong order in the system and one can find particles at all distances larger than the inter-particle distance. When dust number density increases to $n_d = 1.74 \times 10^9 m^{-3}$ the nearest neighbor peak and the peaks of next neighbors grow, indicating increased order of the system. Further increase of the dust number density ($n_d = 3.74 \times 10^{10} m^{-3}$) results in shifting of the peak of $g(r)$ towards smaller inter-particle distance with some prominent additional peaks, which indicate that the particles pack around

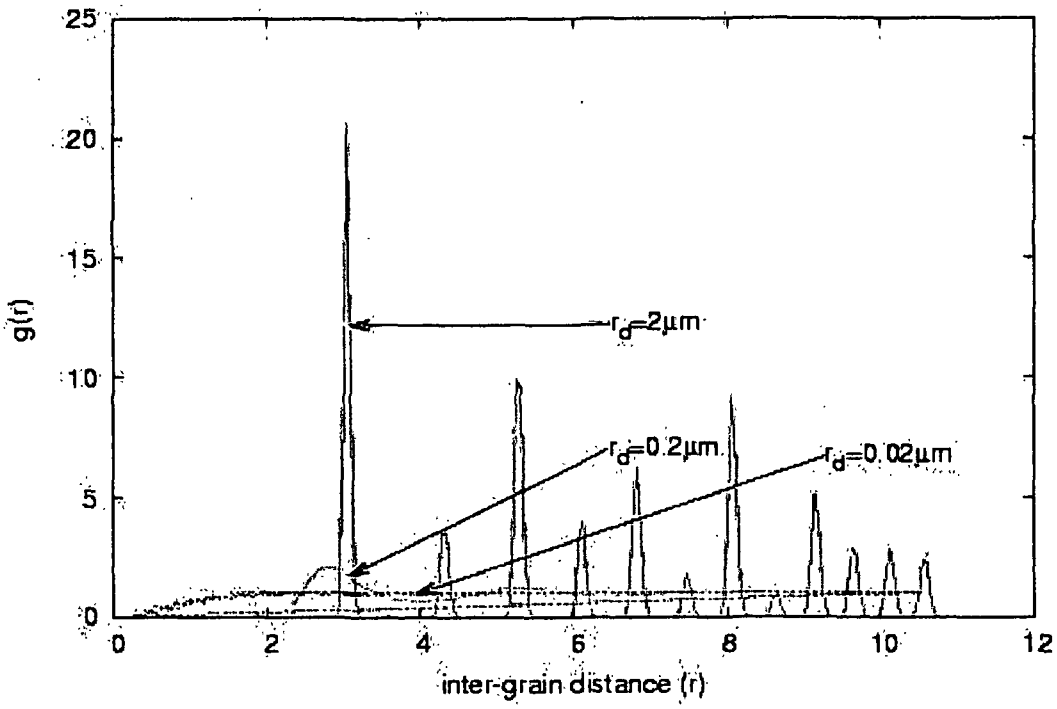

Figure 3.5: Plot of $g(r)$ vs. r for different dust sizes.

each other in neighboring shell. As density increases, these shells become distorted. As a result the additional peaks in the g(r) plot appear when the lattice structure of the solid phase begins. With the increasing value of dust number density, the density of the grains in the concentric shell increases and as a result of it, the inter-particle distance decreases.

Plot of $g(r)$ with different size of the dust grains ($r_d = 2\mu m, 0.2\mu m, 0, 02\mu m$) appears in Fig.3.5. For dust grains with size $2\mu m$, some pronounced peaks can be identified which represent an ordered structure. With size $0.2\mu m$ one pronounced peak at next neighbor distance is observed, which corresponds to an ordering at small distances and the system is in liquid like state. But with dust grain of size

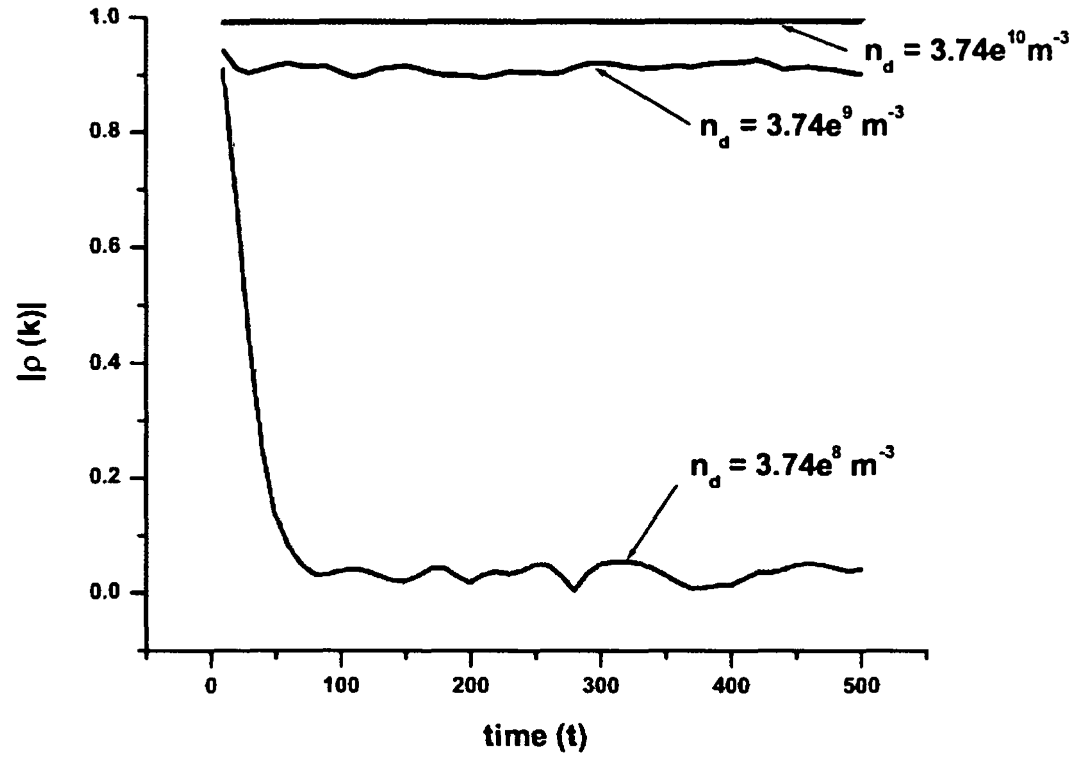

Figure 3.6: Time dependence of long-range order for different dust number densities.

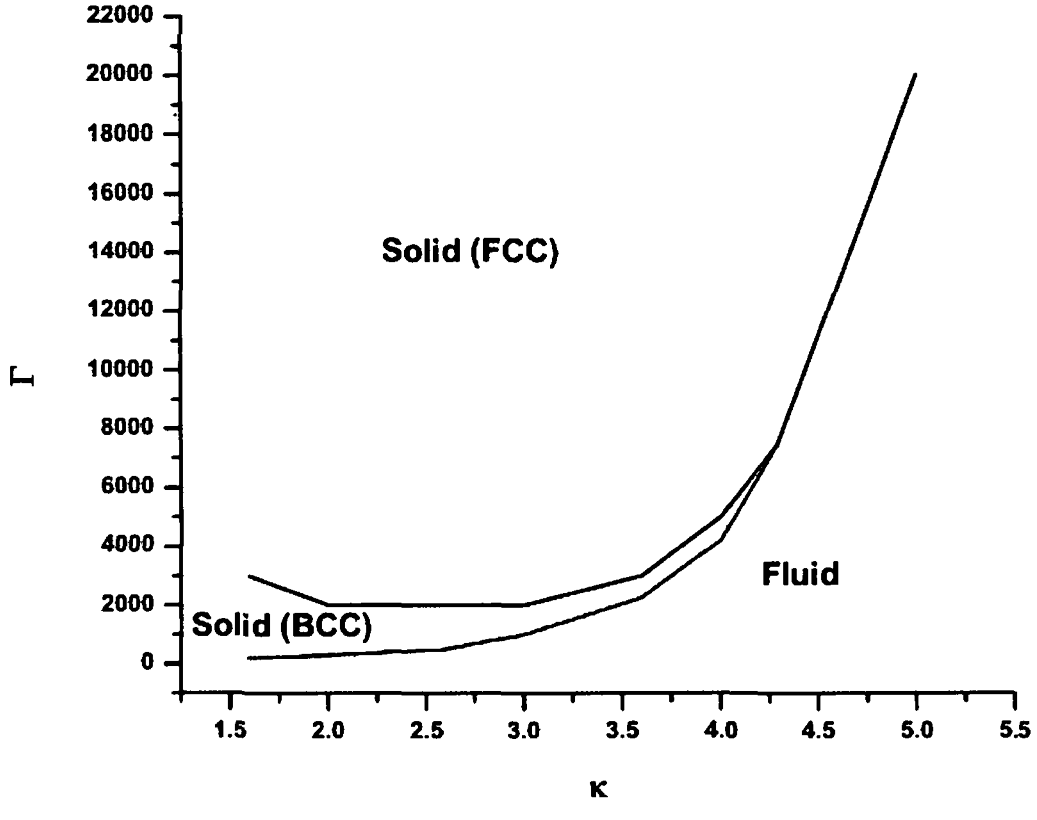

Figure 3.7: Phase diagram of Yukawa system in the (κ, Γ) plane.

the $g(r)$ plot is almost flat, which means no correlation exists at all. This reflects the gas-like characteristics of this particle arrangement. From this plot we observe that with the increase of the dust grain size the first maximum of $g(r)$ plot is shifted towards longer inter-particle distance.

Usually pair correlation function gives an idea about the local structure. It does not give direct information as to whether long-range crystalline order exists. The time dependence of long-range order in our system with dust number densities $n_d = 3.74 \times 10^8 m^{-3}$, $n_d = 3.74 \times 10^9 m^{-3}$, and $n_d = 3.74 \times 10^{10} m^{-3}$ has been analyzed in Fig.3.6. From this figure, we see that at higher densities a moderate to high degree of order exists throughout the observation period, where as at the lowest density the long-range order rapidly vanishes.

Fig.3.7 represents the phase diagram of Yukawa systems. The strength of lattice correlation is plotted in the (κ, Γ) plane. This diagram clearly shows the existence of the phases solid(BCC), solid(FCC) and fluid. The triple point is found to be at $\kappa = 4.29$ and $\Gamma = 7.443 \times 10^3$. The triple point obtained from our study is close to the one obtained by Hamaguchi et al.[134]. In their study of Yukawa system using MD simulation they included the infinite sum for periodic boundary conditions which is valid in the strong screening regime and they observed the triple point at $\kappa = 4.28$ and $\Gamma = 5.6 \times 10^3$.

3.3.3 Conclusions:

We have studied the fluid-solid phase transition and BCC-FCC phase transition in a dusty plasma using MD-simulation. The interaction potential among the particles is assumed to be Yukawa type. The structure of the Coulomb crystal is studied from the plot of radial distribution function. The plot of the long-range order clearly shows that the system attains a solid-like form for certain parameters of the dusty plasma system. The code is developed to study the effect of dust temperature, density and size on the crystal formation. It is seen that as the temperature of dust T_d is reduced, the structure becomes highly ordered. The results of our simulation with particles of radius r_d=2μm show that the system behaves as fluid for temperature ranging from T_d=330K to T_d=7000K with $n_d = 3.74 \times 10^{10} m^{-3}$. For values of T_d varying from 5K to 320K, it shows regular arrangement and behaves as solid. The system attains an ordered solid state for dust density larger than $n_d = 1.78 \times 10^{9} m^{-3}$ for r_d=2μm and T_d=5K and disordered fluid state for n_d below that value. It is seen that even a slight change in the size of dust particles affects the structure to a large extent. The crystal formation becomes more probable with grains of relatively large size. The system shows solid like behaviour for dust radius r_d=0.25μm for T_d=5K, $n_d = 3.74 \times 10^{10} m^{-3}$, whereas it behaves as fluid for r_d=0.23μm. With this code, it is possible to study the pattern of the structure formed for wide range of values of different parameters of dusty plasma system. The phase diagram of Fig.3.7 clearly shows three distinct phases: solid(FCC), solid(BCC) and fluid state. The triple point is found to be at $\kappa = 4.29$, $\Gamma = 7.443 \times 10^3$. This study will help to identify accurately the parameters suitable for the formation of Coulomb crystal in a Yukawa dusty plasma system.

The code developed here has a scope for modification in future to incorporate the effect of an attractive potential among the dust particles on the structure.

Chapter 4

Role of Shadowing force in formation of 3D dust crystal

Here, molecular dynamics (MD) simulational study on the role of attractive force on Coulomb crystal formation has been done. The interaction attractive potential among the dust grains is taken as Shadowing force that is caused by asymmetrical ion flow to the grains. A comparative study has been made for the effects of purely repulsive Yukawa and the combined Yukawa-Shadowing potential on phase transition of dust crystal by calculating pair-correlation function, for different values of Coulomb coupling parameter Γ*, screening constant* κ*, and grain radius* r_d*.*

4.1 Introduction:

The physics of dusty plasmas has recently attracted considerable interest due to their applications in many phenomena e.g , in the acceleration of particles and in the formation of dust particles into regular crystalline structures. The formation of dust crystals in plasma is relatively a new area of research Plasma crystals are example of strongly coupled system With the development of plasma crystal, it has become possible to study self-organization of many body system with high resolution imaging.

Chaotic motion of particles can be investigated by studying the interaction among few particles and their response to external forces[165]. Some of the major advantages of plasma crystals are charge neutrality, fast response, easy experimental control, detailed imaging, fine time resolution of the dynamics of individual particles[166].

In this chapter we have studied the effect of attractive Shadowing force on the dynamics of dust particles immersed in plasma using a molecular dynamics code. The interaction potential among the grains is assumed to be consisted of two parts, Yukawa potential and the attractive Shadowing potential. Due to the Yukawa potential, the grains arrange themselves in crystalline pattern. However, this arrangement will be modified in presence of the attractive Shadowing force. A comparative study has been made for the role of purely repulsive Yukawa (Debye-Huckel) and the combined Yukawa- Shadowing potential on phase transition of dust crystal from solid to fluid and then to gaseous states.

The attractive Shadowing force between the particles may arise due to asymmetrical ion flow to the surface of the dust grains. The ions when collide with grains, they transfer momentum to the grains. For an isolated dust, the ion flow would be symmetric and net transfer of momentum is zero. If there are two isolated grains, the plasma flow becomes asymmetric and that results in an attractive force. This theory was developed by Tsytovich et al.[167] and the force is known as shadowing force or the LeSage gravity, after the French scientist who proposed a similar explanation of universal gravitation in the 18th century[168]. The origin of Shadowing force is sketched schematically in Fig.4.1.

Although the Shadow force is caused by the redistribution of the ion momentum flux, its magnitude is proportional to the electron temperature. The reason is that the electron temperature determines the grain charge and, accordingly, the net current of the absorbed ions. Since the electric potential of the grain behaves asymptotically as $1/r^2$, at large distances, the electric repulsion changes with the shadow attraction. In

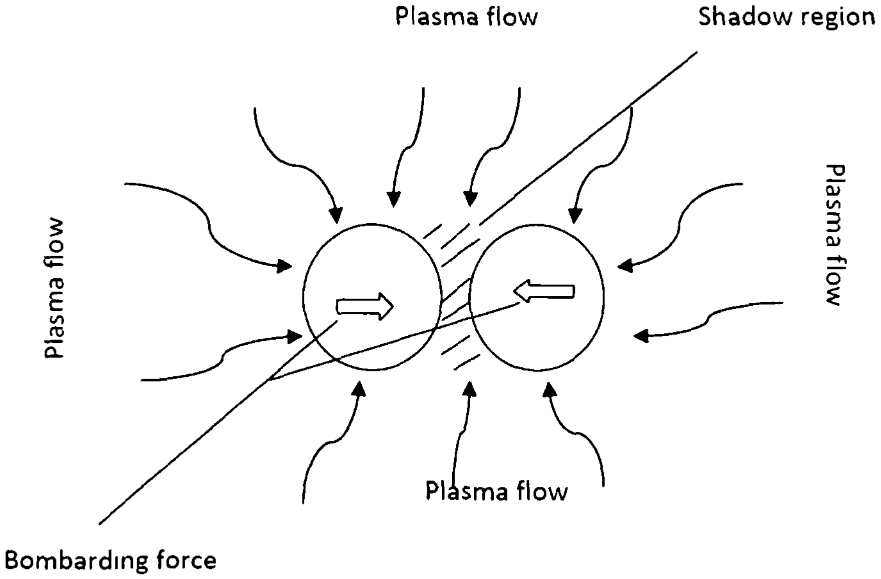
Plasma flow
Shadow region
Plasma flow
Plasma flow
Plasma flow
Bombarding force

Figure 4.1: Shadow interaction between two dust grains. The ions with velocities lying within the shadow region do not reach the grains.

their study, Khodataev et al.[169] presented both analytically and numerically the dependence of the Shadowing interaction force on the distance. The attraction between two isolated grains has not yet been observed experimentally; however, Samsonov et al.[170] have made an experimental study of long-range attractive and repulsive forces between the negatively charged particles of a monolayer plasma crystal and a negatively biased wire. It has been reported that the particles close to the wire were repelled from it electrostatically, while the far particles were attracted due to the drag of the ion flow deflected toward the wire.

A number of other mechanisms of grain interaction that may be responsible for binding them together and organizing them in regular crystal-like fashion have been discussed in the literature.

The concept of the wake field in dusty plasmas was introduced by Nambu et al.[171]. In recent years, this theory of the wake potential[172,173] has attracted much attention. For dust Coulomb crystals Takahashi et. al.[174] have experimentally demonstrated the role of the wake potential in a plasma with a finite ion flow. Vladimirov and Nambu[173] first showed that the collective interaction of the static dust particulate with low frequency oscillations in the ion flow in a dusty plasma can provide an attractive oscillatory wake potential along the ion flow direction. Vlamidimirov and Ishihara[175] and Ishihara and Vlamidimirov[176] extended this theory to consider periodic structures along and perpendicular to the ion flow direction. Recently, Nasim[177] studied wakefield excitations in a multi-component dusty plasma by using the fluid as well as the Vlasov-Poisson model. The form of the wake field was found to critically depend upon the size of the test charge velocity relative to the dust acoustic speed. More recently, Ali[178] has studied attractive wake field formation due to an array of dipolar projectiles in a multi-component dusty plasma for modified dust acoustic waves.

The dust grains formed in laboratory and astrophysical environments may have any shape and size. Elongated dust grains are assumed to be formed by coagulation of smaller particulates in partially or fully ionized plasmas by some attractive forces[179,180], the details of which are not fully understood. However, it is thought that inelastic, adhesive, and collective interactions between micrometer-sized dust particles give rise to kilometer-sized bodies, which are known as planetesimals. Recently, Shukla[181,182] has investigated the formation of wake potentials in an unmagnetized dusty plasma consisting of electrons, ions, and elongated dust grains, by neglecting the dust particle dynamics.

In a strongly coupled dusty plasma, attractive force between the particles may also arise due to dipole-dipole interactions[145,183,184,185,186]. The attractive dipole-dipole force may be responsible for attracting large, irregular shaped particles and for subsequent formation of dust structures[145], as well as planetesimals or planetary seedlings[179,187].

Here in this Chapter, the modelling of the system and simulation are written in section 4.2. Section 4.3 deals with the calculated results and discussions. Conclusions of this study are included in section 4.4.

4.2 Formulation:

It is well known that dust particles in plasma acquire a significant negative charge, which causes strong interaction between the dust particles themselves and between dust and plasma particles. These negatively charged micro particles attract the ions surrounding them, leading to a constant flow of ions to the surface. If two grains are close to each other, the plasma flux onto one grain is shaded by the other one. This results in difference in pressure exerted by the plasma particles between the outer and inner sides, which gives rise to the attractive Shadowing force between the two grains. This Shadowing force is given as[167,188]

$$F_{shadow} = -\frac{3}{8}\frac{r_d^2}{\lambda_{Di}^2}\frac{Z_d^2 e^2}{r_{ij}^2} \tag{4.2.1}$$

where r_d, Z_d, λ_{Di} and r_{ij} represent the grain size, number of charges residing on the dust grain surface, the ion Debye screening length and inter-particle distance respectively. The Shadowing forces are λ_{Di}^2/r_d^2 times less than the Coulomb forces and, thus, not being screened, can operate only at distances larger than the Debye screening length and may play a major role in the process of dust crystal formation. However, statistical Shadowing from many dust grains in a plasma can substantially reduce the Shadowing force. The Shadowing force is proportional to r_d^4 and increases sharply with an increase in the grain size. The size of dust particles is growing slowly but continuously in many existing experiments (e.g. on plasma etching) and the role of the Shadowing force in these conditions increases with time.

In this Chapter, we have studied the structural properties of the 3D dusty system of identical, spherical particles of mass m_d and charge Q_d immersed in a neutralizing background plasma by developing a molecular dynamics (MD) code. In such a system, the interaction potential between the dust grains is usually described by screened Coulomb or Yukawa potential given by equation (3.3.2) in Chapter 3.

The effect of the attractive Shadowing force on the structure of strongly coupled dusty plasma is studied by comparing Yukawa potential and combined Yukawa-Shadowing potential given by

$$\phi(r_{ij}) = \frac{Q_d^2}{4\pi\epsilon_0 r_{ij}} exp\left(-\frac{r_{ij}}{\lambda_D}\right) - \frac{3}{8}\frac{r_d^2}{\lambda_{Di}^2}\frac{Q_d^2}{r_{ij}} \tag{4.2.2}$$

In MD scaling the combined Yukawa-Shadowing potential can be expressed as

$$\phi'(r'_{ij}) = \Gamma\kappa\left(\frac{1}{r'_{ij}} exp(-r'_{ij})\right) - \Gamma\kappa\left(\frac{3}{8}\frac{r_d'^2}{\lambda_{Di}'^2}\frac{1}{r'_{ij}}\right) \tag{4.2.3}$$

where $r'_{ij} = r_{ij}/\lambda_D$, $r'_d = r_d/\lambda_D$ and $\lambda'_{Di} = \lambda_{Di}/\lambda_D$. The simulations are performed with 686 particles for BCC crystal structure and 500 particles for FCC structure, by using the following plasma parameters $n_e = 4.39 \times 10^{13} m^{-3}$, $n_i = 1.0 \times 10^{14} m^{-3}$, $T_i = 300K$, $T_e = 2320K$, $r_d = 0.7 \times 10^{-6} m - 2.7 \times 10^{-6} m$, $n_d = 3.74 \times 10^{10} m^{-3}$, $T_d = 100K$. To find out structural correlation of the grains, pair correlation function $g(r)$ is calculated for this system in presence of both the Yukawa force and combined Yukawa-Shadowing forces. A comparative study between the two forces has been made for different values of κ, Γ and grain size r_d.

4.3 Results and Discussions:

In this Chapter we have compared the results found from both the Yukawa and combined Yukawa-Shadowing forces. In our results, the pair correlation factor $g(r)$ has been plotted for Yukawa potential and then they are plotted for combined Yukawa and Shadowing potential. In Fig.4.2, g(r) has been plotted for κ=1.6 and Γ=130, 300, 444 and 1389 respectively. The black line represents the effect due to combined Yukawa and Shadowing force, whereas the red line represents that due to the Yukawa force only.

With the increase in the Coulomb coupling factor, it is expected that dusty system transits to ordered crystalline state. The plots for both Yukawa and coupled Yukawa-Shadowing forces show solidification with the increase in the value of Γ. It is seen from the graphs that the sharpness of the peaks becomes more prominent for combined Yukawa-Shadowing force than for Yukawa force alone with the increase in Γ. A slight shift in the position of the peaks towards smaller value of inter-particle distance is observed for coupled Yukawa-Shadowing force. In MD scaling, the combined Yukawa-Shadowing potential is expressed in terms of coupling parameter Γ, as given in equation (4.2.3). Due to this dependence, the sharpness of the peaks due to coupled Shadowing-Yukawa force may increase. In our simulation, the coupling pa-

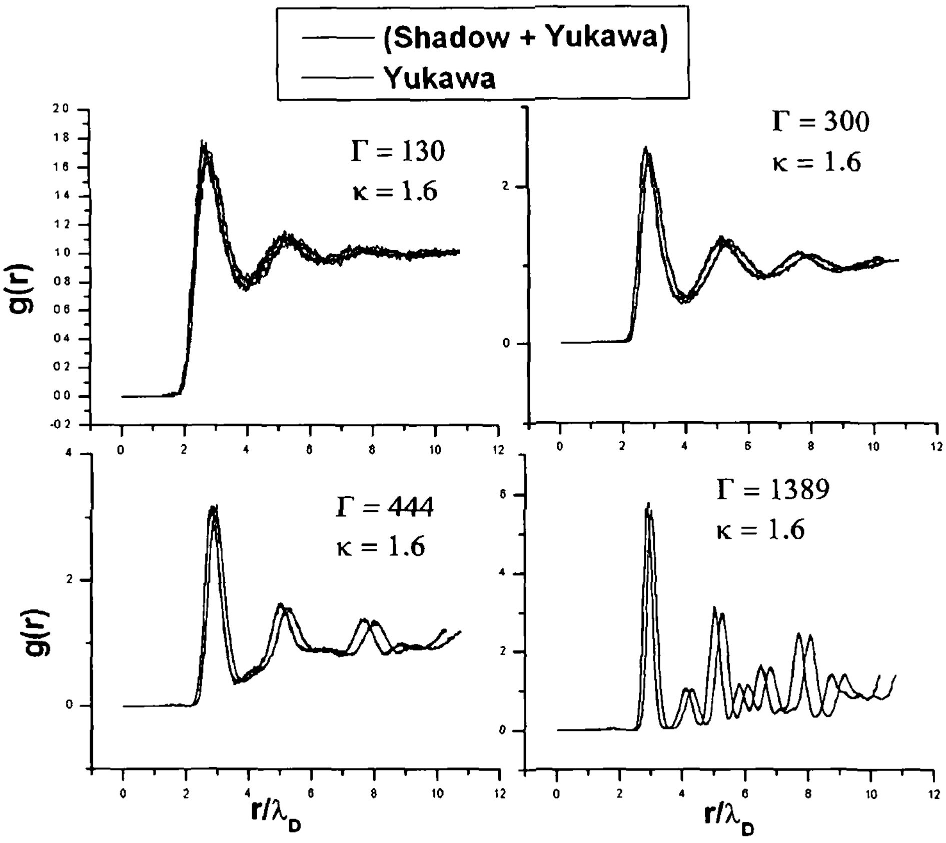

Figure 4.2: Plot of $g(r)$ vs. r/λ_D for κ=1.6 and Γ=130, 300, 444, 1389 respectively.

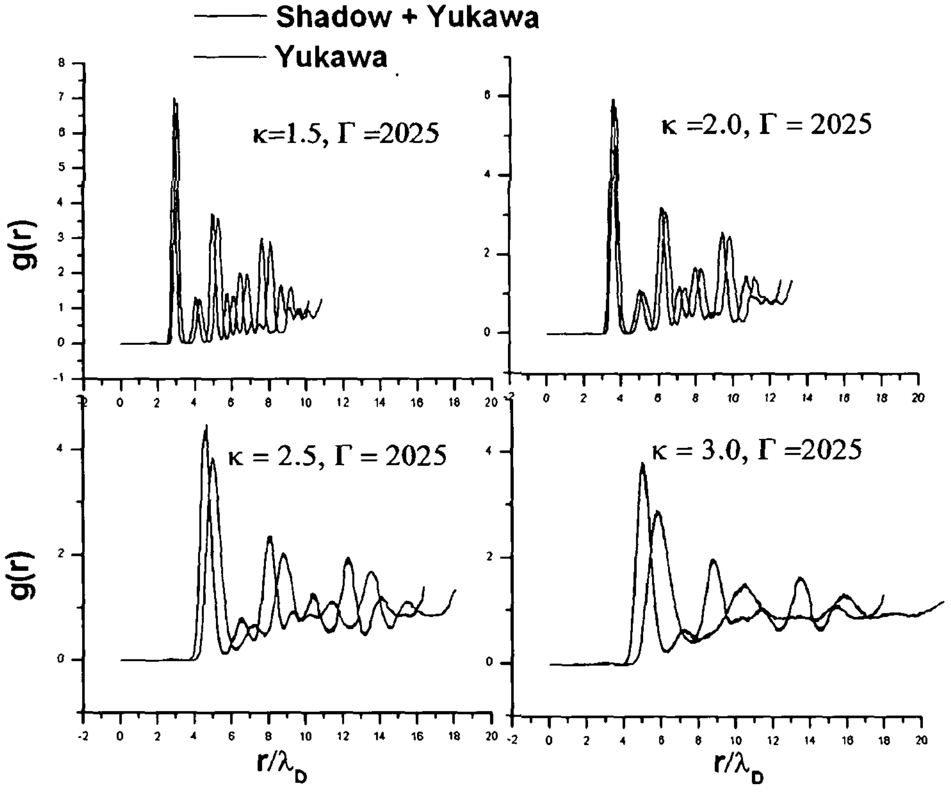

Figure 4.3: Plot of $g(r)$ vs. r/λ_D for Γ=2025 and κ=1.5, 2.0, 2.5, 3.0 respectively.

rameter is controlled by temperature of the dust particles T_d. The velocity of particles increases with the rise in temperature. The Shadowing force may become ineffective for particles moving with high velocity, and as a result the plots of $g(r)$ overlap with each other for the two potentials for smaller values of Γ.

In Fig.4.3, we have compared the effect of the screening parameter on crystal formation taking into account the existence of attractive Shadowing force along with the Yukawa force for $\Gamma = 2025$ and κ=1.5, 2.0, 2.5 and 3.0 respectively. It is seen from the plot that for small values of κ both the curves almost overlap and Shadowing force is not much effective. However, as the value of κ increases, the two sets of RDF's are quite different in peak height and shape. The positions of peaks for combined Yukawa-Shadowing force shift towards smaller value of inter-particle distance. Thus κ plays a major controlling role over Shadowing force. Contrary to the Coulomb force, Shadowing force is not screened and dominate for distances larger than the Coulomb field screening length. Yukawa force decreases exponentially with the increase in the value of κ, whereas the absolute value of Shadowing force increases with screening parameter. For κ = 3.0,the g(r) plot shows that dust particles transit to fluid state when only Yukawa force is considered. The results of combined Yukawa-Shadowing potential shows that the particles still occupy ordered crystalline state. The Shadowing force might significantly exceed the electrostatic force at large distances, which results in the attraction of the particles.

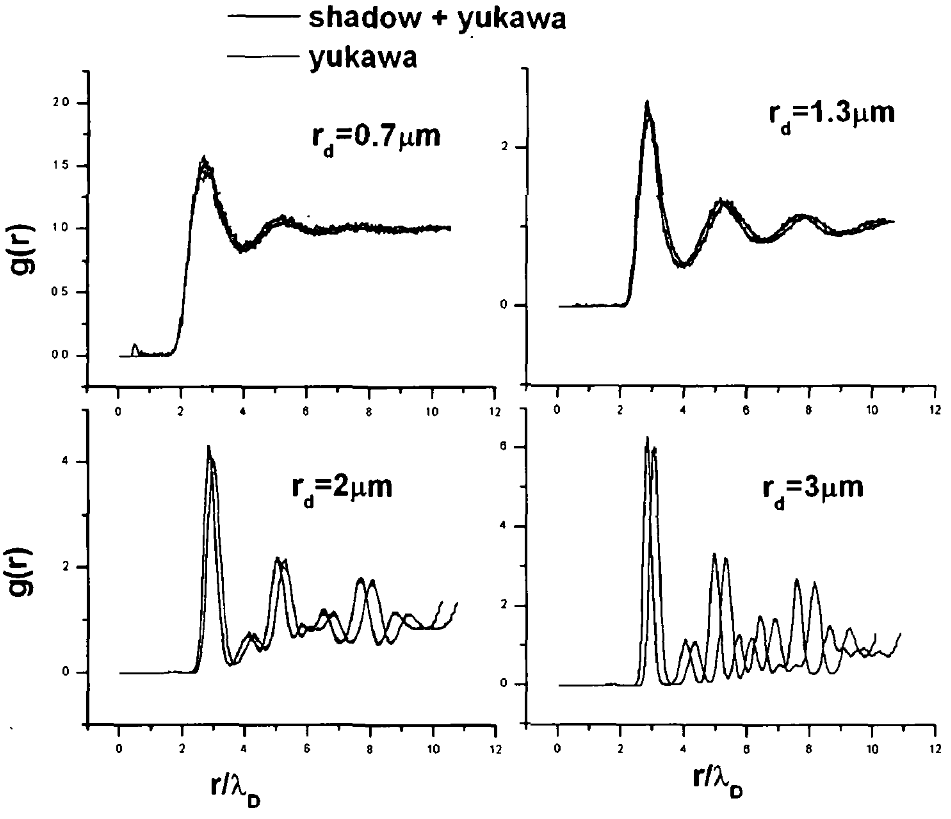

Figure 4.4: Plot of $g(r)$ vs. r/λ_D for grain radius r_d=0.7, 1.3, 2.0, 3.0 μm respectively.

Fig.4.4 shows the plots for g(r) for four different values of radius of the grain. For r_d.= $0.7\mu m$, the dust particles are in fluid state. As the grain size is increased, the system gradually transits to solid state. The charge on the dust particle depends on its size. Hence the height of the peak increases when size is increased, indicating more ordered arrangement of the particles. It is observed from the figures that the Shadowing force becomes more and more dominant with the increase in radius. The positions of the peaks gradually shift towards shorter inter-particle distance. Since the Shadowing force is proportional to fourth power of the grain radius, influence of Shadowing force is more for grains with larger size. The Shadowing force is attractive in nature and the particles with large size, may come closer to each other resulting in the shifting of positions of peaks towards smaller inter-particle distance.

4.4 Conclusion:

In this Chapter, by using MD simulation a comparative study has been made between the effects of Yukawa force and the coupled Yukawa-Shadowing force on dust crystal formation. The interaction among the dust grains consists of two parts: normal Yukawa force and then the Shadowing force that arises due to asymmetrical current flow to the grain. From our study it is observed that the attractive Shadowing force plays a dominating role for grains with large size and for large screening parameter. The Coulomb coupling parameter does not have significant effect on Shadowing force. These observations confirm the theoretical and experimental studies made on the role of Shadowing force in crystal formation.

Chapter 5

Study of effects of attractive potentials on Coulomb crystal formation

In this chapter, a comparative study between the effect of coupled Yukawa-Shadowing potential and Overlapping Debye Sphere (ODS) potential on 2D dust crystal formation has been done by using MD simulation. The structure of the system is investigated by calculating Radial Distribution Function ($g(r)$) for different values of Γ, κ *and dust number densities* n_d. *The results for Yukawa-Shadowing and ODS potential are compared with experimental results and a close agreement is obtained for attractive Shadowing force.*

5.1 Introduction:

The formation of dust crystal is a wellknown phenomenon in dusty plasma physics. Due to large negative charge, dust particles immersed in plasma can turn plasma into a strongly coupled system. Dusty plasma exhibits interesting phenomena such as the formation of a liquid or solid structure when the coupling is sufficiently strong[121,189]. Dust crystals have been produced experimentally and their structural and dynamical behaviours are studied in many laboratories[120,122,123,190,191]. The discovery of plasma crystals has encouraged the plasma physics community to work in this area. Dusty plasmas provide a model system for crystalline structures to study phase transitions, melting process etc. in condensed matter. Plasma crystal offers ideal tool to observe phase transition at kinetic level due to two factors; direct visualization of individual particles and short restoring time that offers the particles required to reach equilibrium after a perturbation.

One outstanding problem of dust crystal is that the average interaction potential between two dust particles is not known precisely. Shielding of dust particle and resulting interaction potential are not explored properly. It is usually assumed that the average interaction potential between two dust particles is of the Debye-Hückel or Yukawa type. It is now well established that dust particles form Coulomb crystal in presence of strong repulsive forces[134,192]. However, a question generally arises regarding existence of any attractive force between the grains. The mechanism of interaction among grains in plasma is a complex phenomenon and it needs substantial amount of research both at theoretical and experimental levels to understand it. For system where inter-particle distance is larger than Debye length, it may not be sufficient to consider Debye-Hückel potential as the interaction potential among the dust grains. The effect of attractive force like Shadowing force or overlapping Debye sphere can not be ignored in such cases.

In dusty plasma, the overlapping Debye spheres around dust grains produce an attractive force[149,193,194]. The interaction energy of the sheath of one grain with the bare charge of the other grain can be expressed as

$$\phi_{ODS}(r_{ij}) = -\frac{Q_d^2}{4\pi\epsilon_0 2\lambda_D} \exp\left(-r_{ij}/\lambda_D\right) \tag{5.1.1}$$

where λ_D represents the Debye length of the background plasma. Here, the grains are assumed to have identical charges. The result of this potential is a weak attraction at larger distances (beyond a critical radius $r_c = 2.73\lambda_D$). Very recently Hou et al.[149] have used molecular dynamics simulation to study the effect of overlapping Debye sphere on structure of 2D dusty plasma. For this, they have made a comparison between the normal Yukawa potential and potential due to overlapping Debye spheres. Their results show a clear difference between the two potentials for large screening parameter κ or at low dust density.

Shadowing force is exerted between neighboring particles due to mutual distortion of ion or neutral flux to the particles, detail of which is discussed in Chapter 4. The existence of an attractive component in the force between dust particles was experimentally studied and verified by several methods[174,195,196]. It was suggested by Tsytovich et al.[167] that the grains create flux of plasma particles towards their surface and the shadow of the plasma flux to one of the interacting grains by another grain creates an attractive force. Since these forces are not screened, they can dominate Coulomb repulsion force at distances larger than the ion Debye screening length. This attractive force may play a major role in the formation of dust crystal. Ramazanov et al.[197] investigated the interaction between dust particles in a plasma on the basis of experimental pair correlation function. They confirmed existence of an attractive component in the interaction potential of dust particles.

Shukla and Rao[148] have discussed the possibility of Coulomb crystallization under an attractive force between charged dust grains in a multi-component dusty plasma whose constituents are tenuous electrons, streaming ions and negatively charged dust grains. They have shown that these could be a far-field non-Coulombean potential that may be responsible for bringing the like particulates together that leads to microscopic Coulomb crystallization in dusty plasma. Quasi-lattice structures may be formed under such attractive forces between like polarity dust grains. Resendes et al.[193] have suggested a static screening mechanism for the formation of plasma molecules in the bulk plasma and in the plasma sheath. They identified correlation

Coulomb energy as the mechanism responsible for plasma crystals. They suggested that each grain is correlated with its own Debye sheath and the interaction takes place between the dressed grains.

Tsytovich[198] pointed out that the observed values of the critical coupling constant in most of the experiments are not consistent with the physical and theoretical estimates of this quantity. He suggested a new physical model for phase transition in a dusty plasma. He has shown that the balance between nonlinear screening at short distances and collective attraction at large distances determines the mean interparticle distances corresponding to the values observed in the transition to the crystalline state. Ishihara et al.[199] have shown that a like-charge attraction could align dust particles along the equipotential line on a void boundary perpendicular to the ion flow in the complex plasma. Tsytovich et al.[200] have reported about some of their interesting results regarding helical dust structures. They have performed molecular dynamics (MD) simulations to demonstrate that a random distribution of grains, interacting via a potential with shallow attractive well and experiencing background friction and stochastic kicks, forms spherical grain crystals.

Although there exist different theories about attractive interactions among dust grains in plasma, a clear understanding of the mechanism is still lacking. There are few experimental studies that investigate about the interactions among the particles. Melzer et al.[195] performed an experiment where they had demonstrated that attractive binding forces between the negatively charged dust exist. They found by laser manipulation of dust particles that net forces between the particles can be reversibly changed between attraction and repulsion.

Here in this chapter, a molecular dynamics code is developed to study phase transition of 2D Coulomb crystals in presence of Shadowing and Overlapping Debye sphere (ODS) potentials. The study has shown some interesting results. Both shadowing and ODS potential have distinct roles to play for different parameter regimes of the dusty system. In section 5.2 of this Chapter, the theoretical and simulational model used to study this problem have been discussed. Results are discussed in section 5.3. Section 5.4 deals with the concluding remarks of the present investigation.

5.2 Theoretical modelling and simulation

Here, a 2D dusty plasma system is considered consisting of identical, spherical particles of mass m_d and charge Q_d immersed in a neutralizing background plasma. It is assumed that the average interparticle potential between two dust particles separated by a distance 'r_{ij}' is of Debye-Hüchel or Yukawa type, given by Eq.(3.3.2) in 3rd chapter. It is well known that because of large charge on dust particles, dusty plasma easily attains strongly coupled regime and when the value of the Coulomb coupling parameter Γ exceeds a certain critical value, the dust pericles may crystalline into solid-like structure. The phase transition of such a system are determined by two basic parameters Γ and screening parameter $\kappa = a/\lambda_D$. Here, a represents the mean-interparticle distance.

It has been already discussed that role of attractive force in forming plasma crystal cannot be ignored. In this Chapter, we intend to have a comparative study between effects of Shadowing potential and ODS potential on Coulomb crystal formation. It is interesting to find out regimes of dominance of the two attractive potentials.

We examine the effect of coupled Debye-Hückel and Shadowing potential

$$\phi(r_{ij}) = \frac{Q_d^2}{4\pi\epsilon_0 r_{ij}} exp\left(-\frac{r_{ij}}{\lambda_D}\right) - \frac{3}{8}\frac{r_d^2}{\lambda_{Di}^2}\frac{Q_d^2}{r_{ij}} \tag{5.2.1}$$

and Yukawa potential combined with ODS potential

$$\phi_{Yu,ODS}(r_{ij}) = \frac{Q_d^2}{4\pi\epsilon_0 r_{ij}} exp(-r_{ij}/\lambda_D) - \frac{Q_d^2}{4\pi\epsilon_0 2\lambda_D} exp(-r_{ij}/\lambda_D) \tag{5.2.2}$$

on pair correlation function of the dusty system. The first term of both the above expressions represents Debye-Hückel potential, whereas the second term of equation (5.2.1) is due to the Shadowing potential. In equation (5.2.2) the second term arises due to interaction of sheath of one grain with the bare charge of the other grain.

Here the already developed MD code is implemented to study 2D crystal formation. The combined potentials : Yukawa-ODS and Yukawa-Shadowing have been incorporated to derive the interacting force among the particles. Simulations have been performed for wide-range of the parameters such as Coulomb coupling parameter Γ, screening constant κ, dust density n_d and dust radius r_d. The simulations are performed with 900 particles for FCC crystal structure for following plasma parameters : $n_i = (1.5 \times 10^{14} - 4.0 \times 10^{14})/m^3$, $T_e = 2320K$, $T_i = 300K$, $T_d = 40K$ to $1000K$. This lattice is used as initial condition. Each grain is assigned an initial velocity (random in magnitude and direction) such that the average kinetic energy *corresponds to the chosen temperature* T_d.

Newton's equation of motion is solved numerically using velocity Verlet algorithm for interaction potentials mentioned above. In MD scaling Newton's equation for the two cases take the following form:

Yukawa-Shadowing

$$\frac{d^2r'_i}{dt'^2} = \Gamma\kappa\left[\left(1+\frac{1}{r'_{ij}}\right)\frac{1}{r'_{ij}}exp(-r'_{ij}) - \left(\frac{3}{8}\right)\left(\frac{r'^2_d}{\lambda'^2_{Di}r'^2_{ij}}\right)\right] \tag{5.2.3}$$

Yukawa-ODS

$$\frac{d^2_{,}r'_i}{dt'^2} = \Gamma\kappa exp(-r'_{ij})\left[\frac{1}{r'_{ij}}\left(1+\frac{1}{r'_{ij}}\right) - \frac{1}{2}\right] \tag{5.2.4}$$

where $r'_{ij} = r_{ij}/\lambda_D$, $r'_d = r_d/\lambda_D$ and $\lambda'_{Di} = \lambda_{Di}/\lambda_D$. From these results pair correlation function may be calculated that gives a picture of the structure of the particles. The pair-correlation function in 2D is defined as

$$g(r) = \frac{A}{N}\frac{N(r,\Delta)}{2\pi r\Delta} \tag{5.2.5}$$

where 'A' is the area of the simulated region, N the number of simulated particles, $N(r, \Delta)$ is the number of particles located in a circle of infinitesimal thickness Δ from $r - \Delta/2$ and $r + \Delta/2$. One may study the solid, liquid, and gaseous phases of the system under different conditions from the above simulation.

5.3 Results and Discussions:

It is already mentioned that in this chapter a comparative study has been done between the Shadowing potential and ODS potential, keeping basic interaction as due to Yukawa potential. It is well known that dusty plasma described by Yukawa potential as described here transits from organized crystalline state to fluid state as the value of Coulomb parameter Γ decreases. Fig.5.1 shows variation of $g(r)$ for different values of Γ. It is seen that larger the value of Γ, more pronounced are the peaks of RDF plot. The effect of both ODS and Shadowing force is to increase the height and sharpness of the peaks of RDF's. For almost all the values of Γ, the contributions of Shadowing and ODS force almost overlap with each other. However, it is seen that Shadowing force is slightly more dominating than the ODS for relatively small values of Γ. For large values of Γ, the difference in the peak heights for the two cases is almost negligible.

Fig.5.2 shows the plot of RDF's both for Shadowing and ODS forces for different values of screening constant κ. The simulations are performed keeping the value of 'Γ' fixed at 6.409×10^3. For $\kappa = 1.66$, the two plots of RDF almost overlap with each other. The dust particles with this value of κ arrange themselves in crystalline state. With the increase in the value of κ, a drastic change appears to the plots of RDF's. The contribution of Shadowing force no longer is same as that of ODS. It is seen that Shadowing force is not that affected with the increase in the value of κ. The

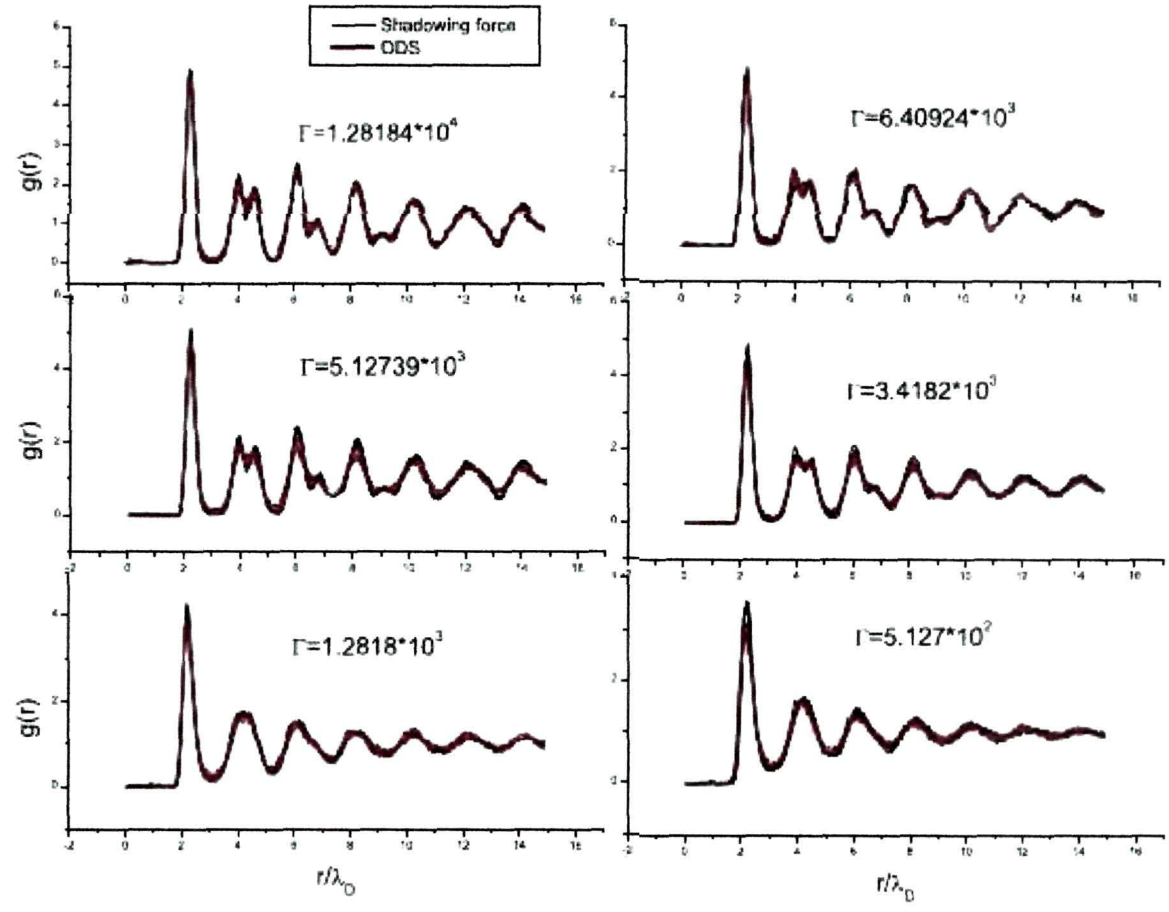

Figure 5.1: Plot of $g(r)$ vs. r/λ_D for Shadowing force and ODS for different values of Γ, taking κ=1.6

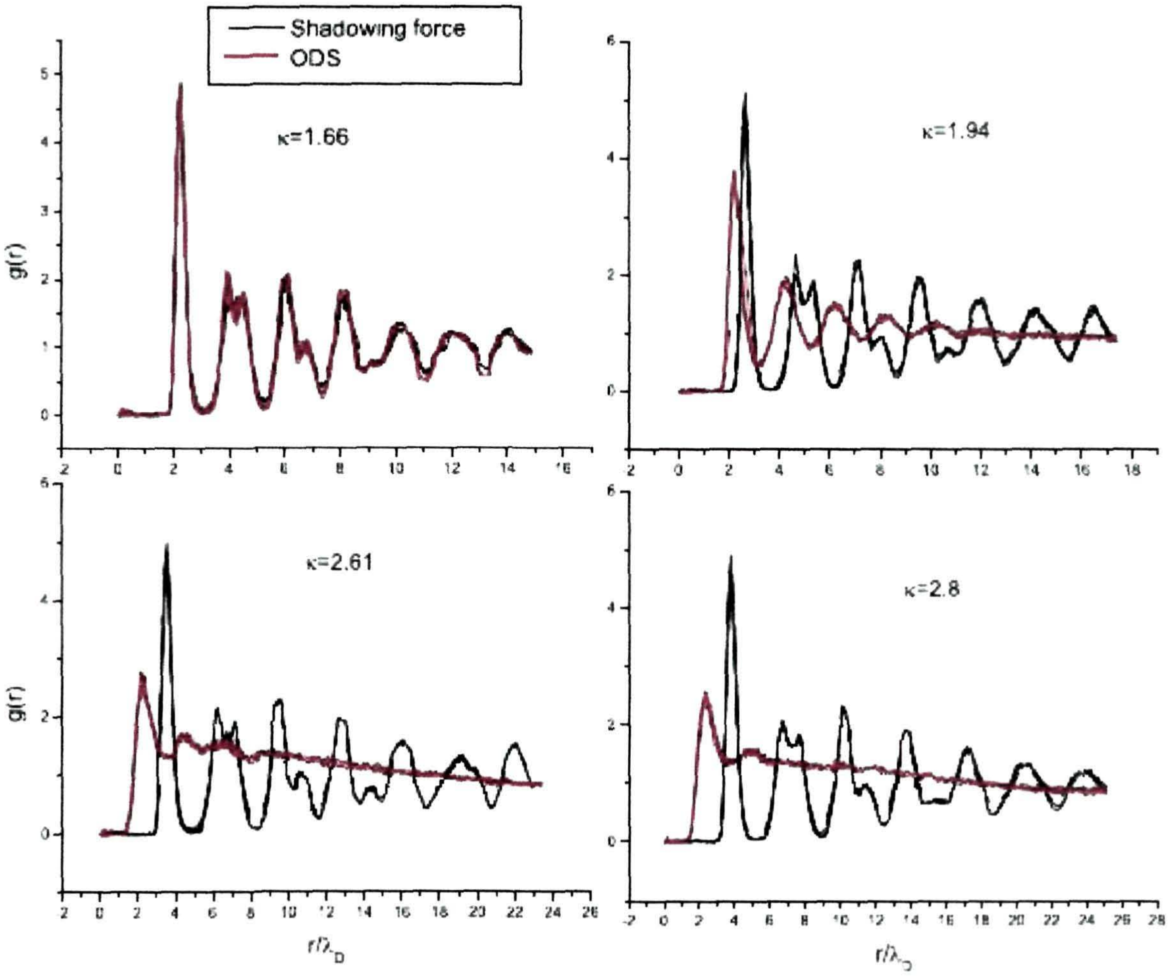

Figure 5.2: Plot of $g(r)$ vs. r/λ_D for Shadowing force and ODS for different values of κ with $\Gamma = 6.40924 \times 10^3$

shielding does not have much effect on Shadowing force. However, ODS potential has the tendency to take the system to gaseous state. For larger values of κ, the difference in both the peak height and shape, for the two cases, Shadowing and ODS is quite prominent. While the contribution of Shadowing force is still to maintain the crystalline state, that of ODS is completely opposite.

It is clear from these results that both Shadowing and ODS facilitate the formation of Coulomb crystal for $\kappa < 2$. The increase in κ results in reduction in the values of shielding length λ_D. In ODS term, the exponential factor $exp(-r_{ij}/\lambda_D)$ dominates over the term $Q_d^2/2\lambda_D$ for small λ_D. The result is that ODS potential decreases very sharply with the decrease in the value of λ_D. Due to screening effect, Yukawa potential also decreases with the rise in κ. The effect of combined Yukawa and ODS potential is to cause phase transition of the crystalline state of dust particles to disordered gaseous state for large values of κ.

A reverse effect is observed for combined Yukawa and Shadowing force. Although with the rise in the value of κ, Yukawa potential decreases exponentially, the combined Yukawa and Shadowing forces still maintain the crystalline pattern. The absolute value of Shadowing force increases with the rise in κ and the term due to this force plays the dominating role.

Thus it is seen that upto mean inter-particle distance $a = 1.608173 \times 10^{-4}m$ $(\lambda_D = 5.72927 \times 10^{-5}m, \kappa = 1.66)$ the combined Yukawa-Shadowing and Yukawa-ODS overlap with each other and equally facilitate the process of crystallization. With the increase in inter-particle distance, the effect of ODS becomes gradually weak. However, even then shadow effect predominates and crystallization is possible with this term. It may be concluded that for large κ ($\kappa > 2$), crystallization is possible only due to the effect of Shadowing force. The role of attractive force thus can not be neglected in dust crystal formation.

Fig.5.3 shows the comparison of RDF's for combined Yukawa-Shadowing and

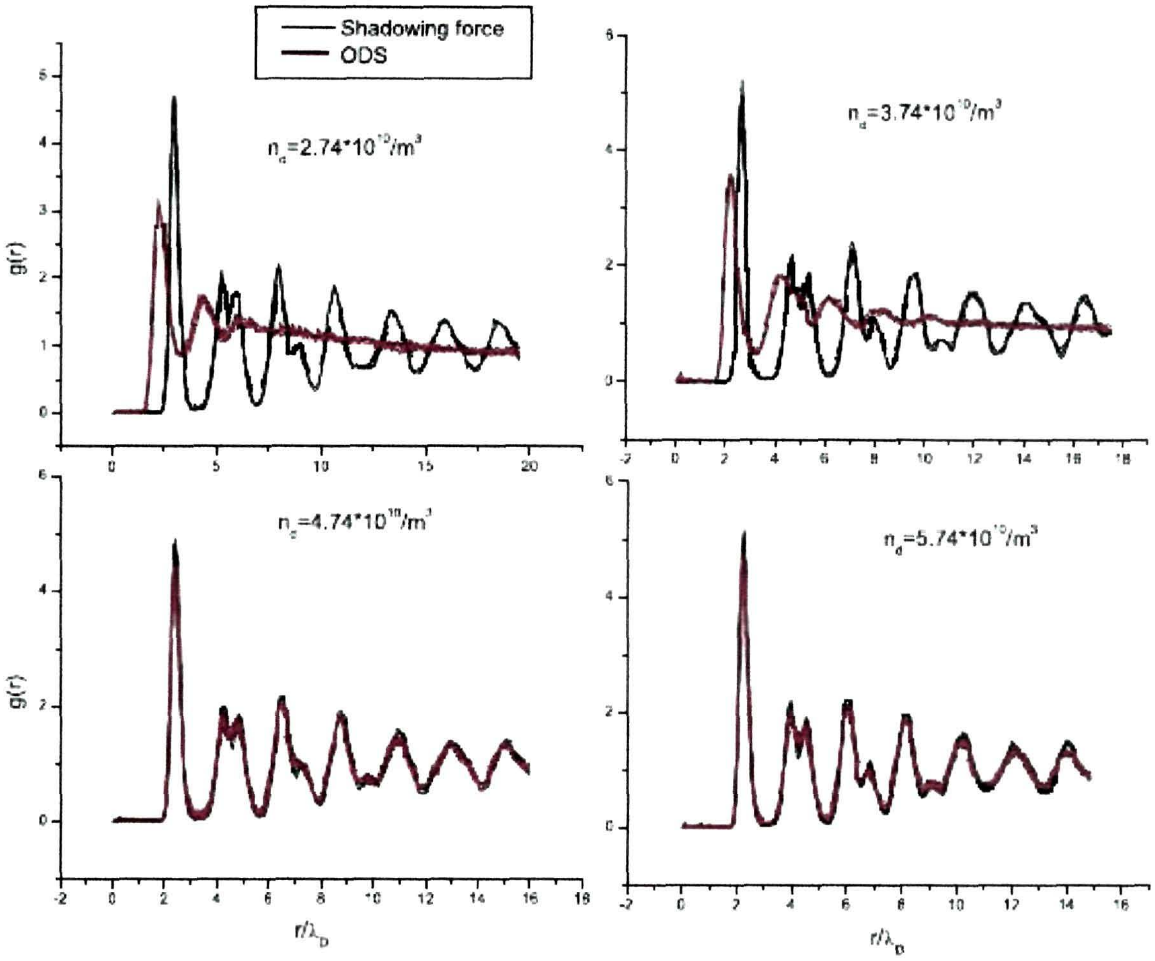

Figure 5.3: Plot of $g(r)$ vs. r/λ_D for Shadowing force and ODS for different values of dust number density

Yukawa-ODS for four different values of dust density $n_d = 2.74 \times 10^{10}/m^3, 3.74 \times 10^{10}/m^3, 4.74 \times 10^{10}/m^3$, and $5.74 \times 10^{10}/m^3$ respectively. It is known from earlier studies that higher the values of dust density, more is the probability of crystal formation. For large values of n_d ($> 4 \times 10^{10}/m^3$), the effects due to Shadowing and ODS almost overlap with each other. Large values of dust density usually facilitate the process of crystallization. For relatively small values of dust density, the peak heights and positions for the two cases differ from each other. The Shadowing force shows sharper, prominent peaks with peak height higher than that of ODS. It is also seen that the peaks due to combined Yukawa-ODS shift towards smaller inter-particle distance. The dust particles attain gaseous state for Yukawa-ODS potential, whereas it is still showing crystalline pattern for Yukawa-Shadowing force. For small values of n_d, the contribution due to Shadowing force is very strong compared to ODS force.

When dust density is small, the particles are far apart from each other. Although Coulomb force is screened, Shadowing force can still be significant for distances larger than the Coulomb field screening length. The effect of combined Yukawa-Shadowing force is very strong to maintain the crystalline state of the particle. For ODS on the otherhand, closer the particles more effective is the overlapping and hence the attractive force. It is clear from the expression for ODS that small value of n_d results in large inter-particle distance and hence small Yukawa-ODS potential. Simulation results also show that average inter-particle distance for the case $n_d = 5.74 \times 10^{10}/m^3$ is $1.6 \times 10^{-4} m$. It may be inferred that beyond $a = 1.6 \times 10^{-4} m$, Shadowing force dominates over ODS and becomes effective in Coulomb crystal formation. Both Shadowing and ODS potential are very sensitive to the change in dust density.

Results of our simulation have been compared with the plots of RDF obtained experimentally by Ramazanov et al.[197]. They determined RDF from experiments carried out in a dc glow discharge set up. The experimental curves by Ramazanov et

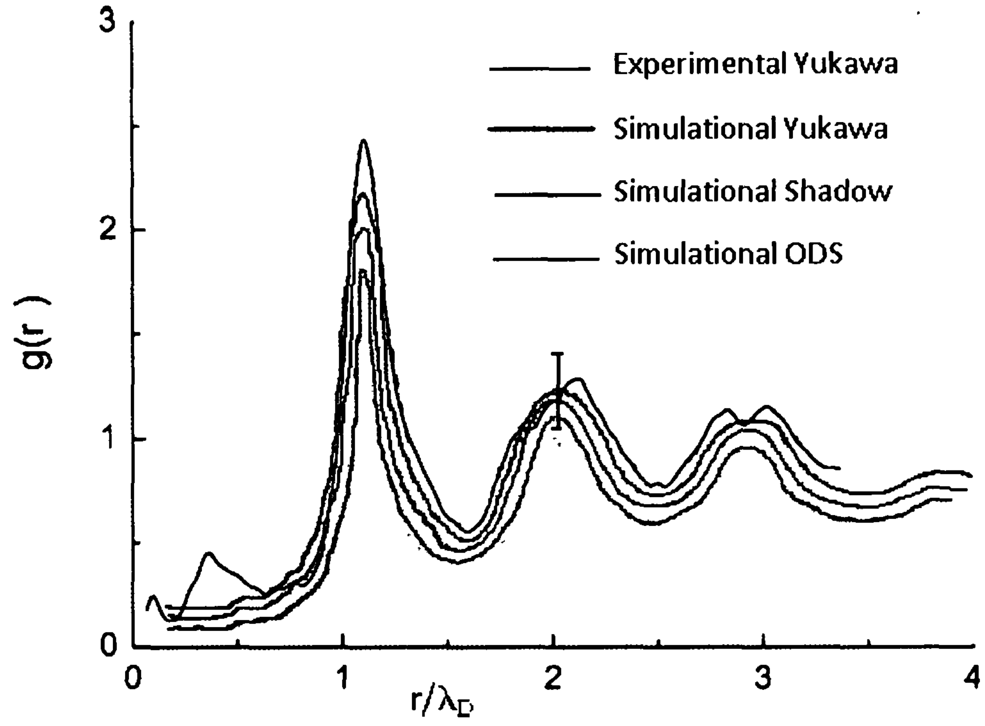

Figure 5.4: Experimental and Simulational $g(r)$ vs. r/λ_D for Γ=121, κ=1.79, $n_d = 14300 cm^{-3}$, $n_e = 2.69 \times 10^{10} cm^{-3}$, $Z_d = 2.1 \times 10^4$

al. have been compared with RDF's obtained for normal Yukawa potential, Yukawa-Shadowing and ODS potentials in our simulation and results are plotted in Fig 5.4 - 5.7.

Experimental data, based on which simulations are performed have been listed in Table.5.1. From all the figures of 5.4 - 5.7, it is clearly seen that RDF due to Yukawa-Shadowing potential is closer to the experimental curve than the curves due to ODS potential or Yukawa potential. The curve due to Yukawa-Shadowing potential is almost within the experimental errors (10-15 percent) mentioned in Ramazanov's plots.

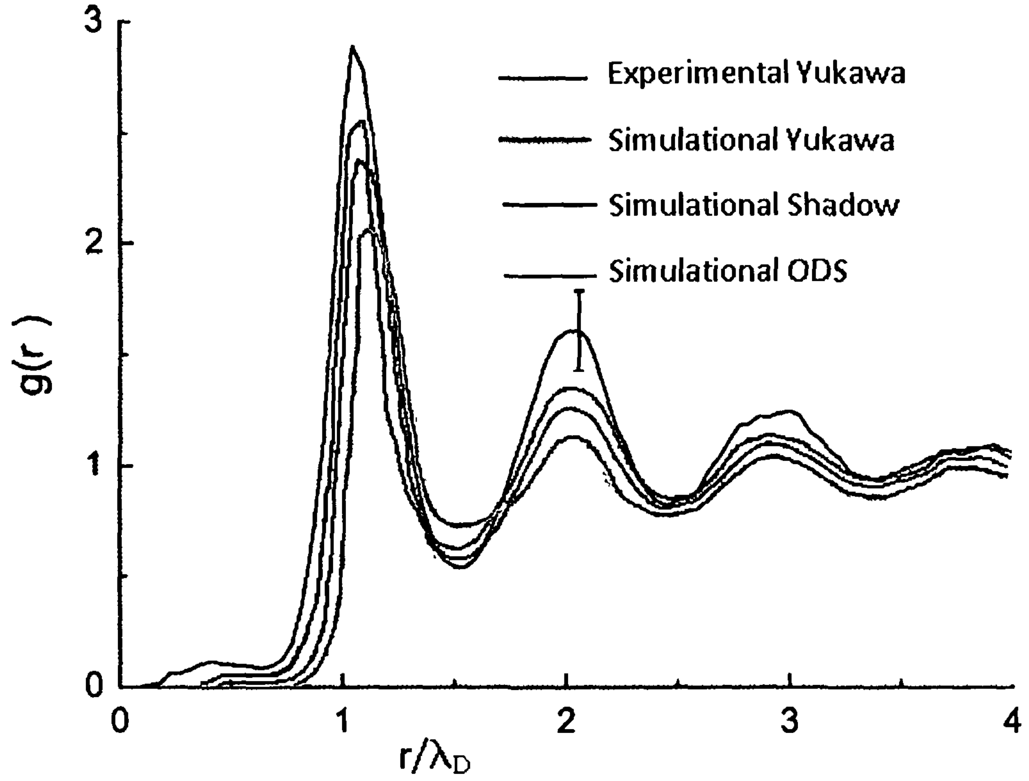

Figure 5.5· Experimental and Simulational $g(r)$ vs. r/λ_D for Γ=239, κ=2.67, $n_d = 3940cm^{-3}$, $n_e = 2.1 \times 10^{10}cm^{-3}$, $Z_d = 2.1 \times 10^4$

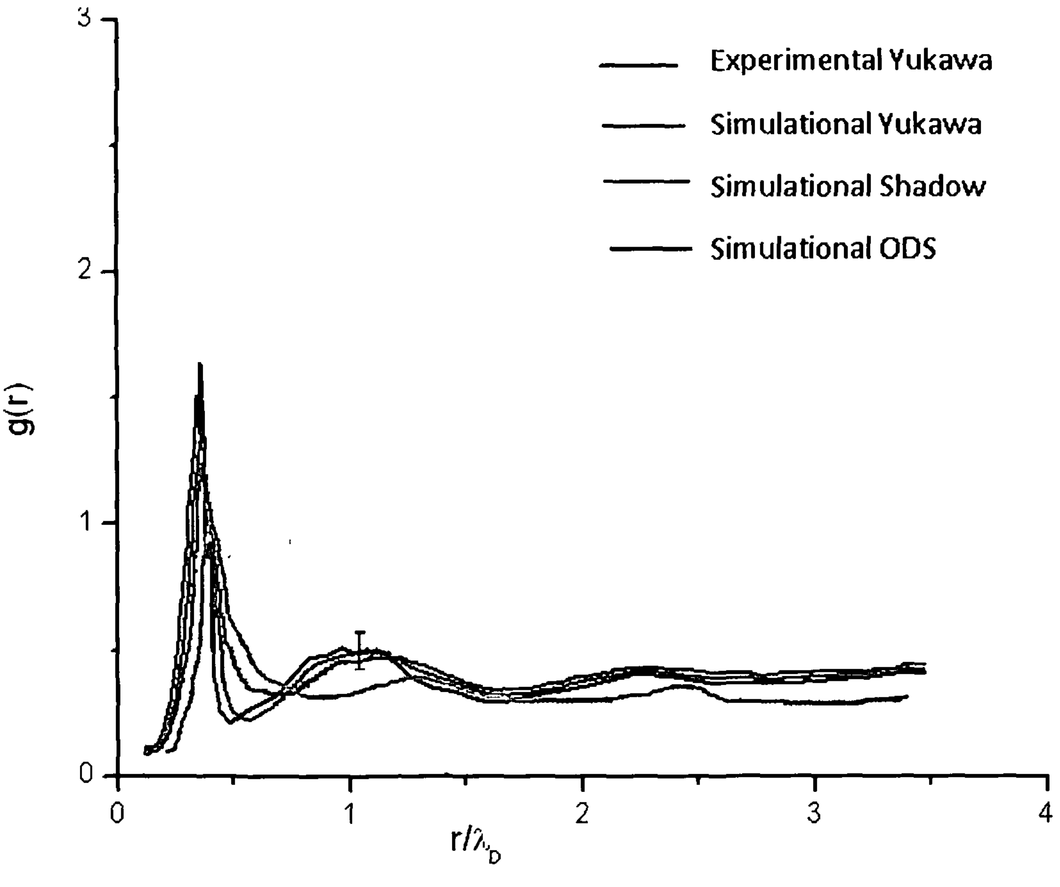

Figure 5.6: Experimental and Simulational $g(r)$ vs. r/λ_D for Γ=68.50, κ=1.68, $n_d = 10712 cm^{-3}$, $n_e = 2.4 \times 10^{10} cm^{-3}$, $Z_d = 2.1 \times 10^4$

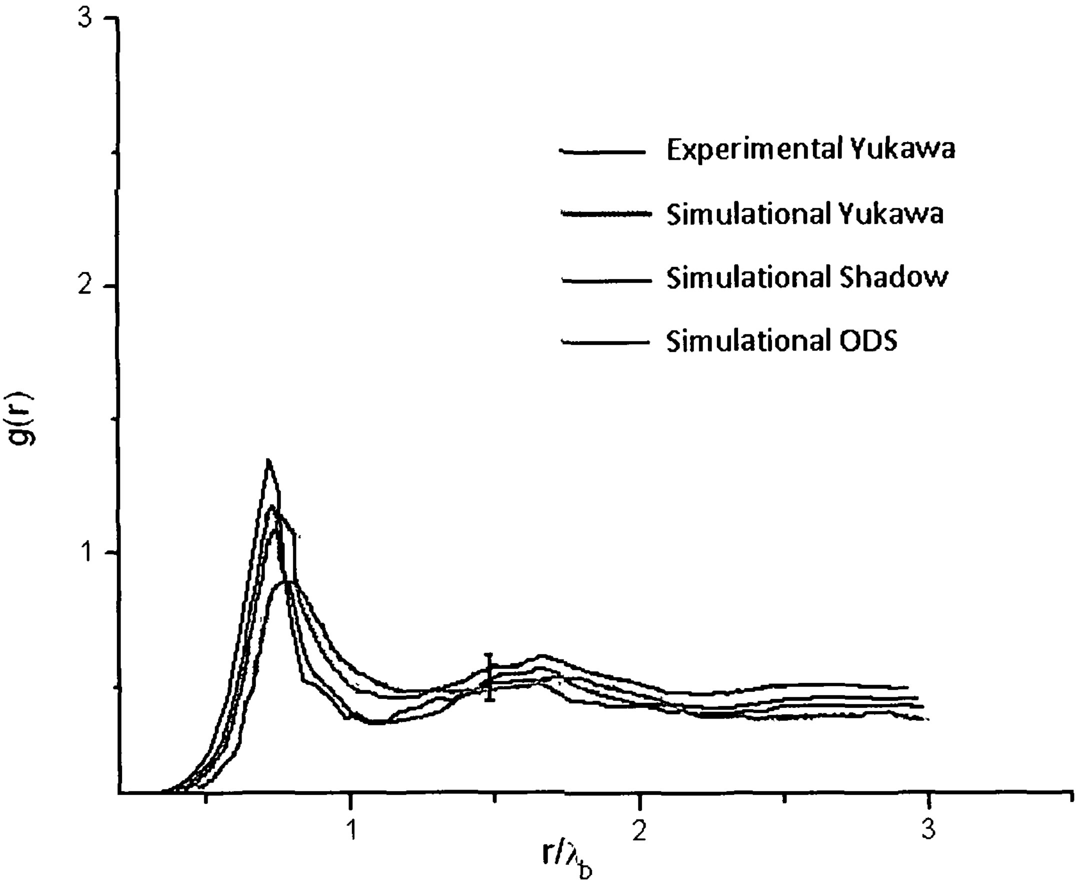

Figure 5.7: Experimental and Simulational $g(r)$ vs. r/λ_D for Γ=40.68, κ=1.48, $n_d = 20995 cm^{-3}$, $n_e = 2.4 \times 10^{10} cm^{-3}$, $Z_d = 2.1 \times 10^4$

Table 5.1: Summary of simulational data.

Z_d	Dust number density	Electron number density	Ion temperature	Coulomb coupling parameter Γ	Screening constant κ
$Z_d = 2.1\times 10^4$	$n_d = 1.4300 \times 10^{10} m^{-3}$	$n_e = 2.96 \times 10^{16} m^{-3}$	$T_i = 203K$	121	1.79
$Z_d = 2.1\times 10^4$	$n_d = 3.940 \times 10^{10} m^{-3}$	$n_e = 2.1 \times 10^{16} m^{-3}$	$T_i = 168K$	239	2.67
$Z_d = 2.1\times 10^4$	$n_d = 1.0712 \times 10^{10} m^{-3}$	$n_e = 2.4 \times 10^{16} m^{-3}$	$T_i = 221K$	68.50	1.69
$Z_d = 2.1\times 10^4$	$n_d = 2.0995 \times 10^{10} m^{-3}$	$n_e = 2.4 \times 10^{16} m^{-3}$	$T_i = 240K$	40.67	1.49

It is also seen that for relatively small values of Γ and κ, the curves corresponding to experiment, Shadowing potential and ODS potential almost overlap with each other. The deviation from the experimental curve is maximum for pure Yukawa potential. For $\gamma = 239$, $\kappa = 2.67$, the deviation from experimental curve is found to be maximum (Fig. 5.5). However, in almost all the cases, the results due to Yukawa-Shadowing potential agree with the experimental results. From this analysis it is clear that attractive potentials like Shadowing potential and ODS potential play a major role in determining crystal structure. Consideration of Yukawa-Shadowing potential or ODS potential leads to better agreement with the experimental results rather than mere Yukawa potential.

5.4 Conclusion:

In this Chapter, the effect of attractive ODS and Shadowing potential on structure of 2D strongly coupled dusty plasma has been compared. The results have clearly showed that both ODS and Shadowing potentials equally dominate for small values of screening parameter κ and large values of dust density. On the otherhand, Shadowing potential plays a dominating role over ODS potential for large values of screening parameter κ and small values of dust density. For relatively large values of κ, Shadowing potential can dominate Yukawa repulsive potential and ODS attractive potential. For a dusty system considered here, it is seen that crystal structure is no longer maintained beyond an inter-particle distance $r_{ij} = 1.6029 \times 10^{-6} m$ with Yukawa-ODS as the interaction potential. On the otherhand, Yukawa-Shadowing potential maintains the crystal structure even beyond this distance. For longer inter-particle distance, Shadowing attractive potential becomes more effective and cannot be ignored. The comparison of this simulational results with the experimental observation clearly reveal that Yukawa-Shadowing force is close to the real situation.

Chapter 6

The effect of magnetic field on the structure of dust crystal in magnetized plasma

In the presence of the magnetic field Yukawa interaction potential among the dust grains gets modified and becomes anisotropic. It is very interesting to study the dust crystal formation and phase transition in presence of magnetic field using a molecular dynamics code. To characterize the structural properties of the dusty plasma for different values of magnetic field strength, the pair correlation function has been calculated. For different values of magnetic field strength the phase diagrams for the system have been plotted in $\Gamma - \kappa$ *plane.*

6.1 Introduction:

Plasma shows a variety of rich phenomena in presence of dust particles; one of these is the so called dust crystallization. As mentioned earlier, under certain conditions, the charged dust particles may organize in regular crystal like structure. On cooling, the plasma may pass through phase transition from ionized state to a liquid state and then even to a solid state. Important properties about dusty plasma system and its structure can be derived by applying external influence on such system. The application of magnetic field is one such mechanism that brings out lot of information about such system. The motion of electron and ion get affected due to the presence of magnetic field. This subsequently affects the flow of particles to dust, charge on dust and interaction potential among the charged dust particles. An external magnetic field applied to strongly coupled dusty system may cause transition from ordered crystalline state to disordered gaseous state.

Dust particles are produced in fusion devices by various plasma-surface interaction mechanisms. The study of dusty plasma in presence of magnetic field may be useful for understanding the behaviour of dust particles in the wall plasma of tokamaks. The magnetic field plays an important role for many dusty plasma environments. The study of dust crystal formation in magnetized plasma is relevant for astrophysical bodies like white dwarfs. Coulomb crystallization plays an important role in the evolution of compact stellar remnants[201]. Microscopic properties of Coulomb crystals may control the electron-phonon scattering in white dwarfs and neutron stars[202,203]. Proper study of dust crystal in magnetized plasma may give much insight into this subject.

Shukla and Mendonca[204] presented a theory on Dust Quasi-atom structure in magnetoplasma. They found that the magnetic field modifies the Debye-Hückel interaction potential and the screening radius of a test dust charge and introduces new eigenstates of electron density oscillations within the modified Debye sphere. They pointed out that a dust quasiatom can contain internal energy associated with upper-hybrid plasma oscillations, which can be resonantly coupled to external magnetic field. In the paper reported by Liu et al.[205], MD simulation has been done to study the structure of a two-dimensional dusty plasma in an external magnetic field. In their study, they incorporated the term $Q_d(\vec{v} \times \vec{B})$ due to force on a dust particle in presence of the external magnetic field. However, they did not consider that the

Debye-Hückel potential would be modified due to the presence of the magnetic field.

From their experimental study on strongly coupled plasmas in a magnetic field, Kaw et al.[206] observed that the dust component exhibits a rigid rotation of order a fraction of a radian/s. It was observed that, the rotation arises spontaneously and seems to be in the direction of ion rotation, which in turn is determined by a competition between $\overrightarrow{E} \times \overrightarrow{B}$ and diamagnetic rotations of the ions in the collisional magnetized plasma. Krasheninnikov et al.[207] have presented a novel mechanism for spinning of a charged dust particle in a magnetized plasma.

The magnetic field affects the motion of plasma particles in such a way that it may lead to rearrangement of dust particles and subsequently may cause phase transition of the system. In the experiment performed by Dzlieva et al.[208], it was found that application of magnetic field to a dusty plasma structure causes a phase transition : liquid-ice phase to vibrational phase and then to disordered phase. They found that upto 160 G, the magnetic field can change the type of the crystal lattice of the dusty plasma formation, increasing the fraction of a hexagonal phase. They also found that further increase in the magnetic field results in destruction of the crystal lattice.

In this chapter, we investigate the problem of phase transition in presence of external magnetic field. The modified potential as found by Shukla et al.[204] is considered as the interaction potential among dust grains. The shielding of a dust charge will depend on the surrounding plasma particles. The magnetic field affects the dynamics of the plasma particles that take part in the shielding process. It is important to understand the effect of modified potential on crystal formation and the phase transition.

In section 6.2, the theoretical model that is used to study this problem is described. The expression of modified Debye-Hüchle potential in presence of external magnetic field as well as the modified Coulomb coupling parameter and screening constant are also written here. All these parameters and the triple points at different κ and Γ are numerically evaluated for different values of magnetic field strength in section 6.3. Results are also discussed in this section. In section 6.4, the concluding remarks of our investigation are added.

6.2 Theoretical Model:

In plasma the interaction potential among the dust particles depends on their size, charge, temperature and also on the dynamics of the plasma particles. The presence of an external field leads to further modification of potential. In absence of any external influence the interaction potential among the dust grains may be of Yukawa type, given by Eq.(3.3.2) in 3rd chapter. From experimental and simulational studies[120,121,134], it is observed that the dust particles may be organized into BCC and FCC structures, under the influence of Yukawa potential.

Shukla and Mendonca[204] have developed an expression for modified Debye shielding potential around a stationary dust grain in presence of an external magnetic field $B_0\hat{z}$, where B_0 is the magnitude of the external magnetic field and $\hat{z}$ is the unit vector along the z-axis as

$$\phi(r_{ij}) = \frac{Q_d}{4\pi\epsilon_0 r_{ij} f} \exp\left(-\frac{r_{ij}}{\rho_s}\right) \tag{6.2.1}$$

where Q_d is the charge of a test dust charge, $f = \left(\omega_{pi}^2/\omega_{ci}^2\right)$, ω_{pi} and ω_{ci} being the ion plasma and ion gyro-frequencies respectively, $\rho_s = \sqrt{f}\lambda_{De} \equiv (C_s/\omega_{ci})$ is the ion-acoustic gyro-radius, λ_{De} is the electron Debye radius, and $C_s = \lambda_{De}\omega_{pi}$ is the ion-acoustic speed. In deriving above expression, authors assumed that electrons thermalize along $\hat{z}$-direction and establish a Boltzmann distribution in the shielding potential.

In our model it is assumed that in presence of external magnetic field, force-field no-longer remains isotropic. In this case, the shielding potential has the direction

Table 6.1: Values of f for different values of magnetic fields

B_0 in Tesla	0.5	1.0	2.0	3.0
f	7.556188×10^{-2}	1.889047×10^{-2}	4.722618×10^{-3}	2.098941×10^{-3}

dependence. The motion of the plasma particles is not affected along z-direction. Hence, Yukawa potential, which is considered to be the mutual interaction energy among the dust grains, will not be affected by the presence of the magnetic field along z-direction and the plasma particles can move freely the direction of $\overrightarrow{B_0}$. However, the interaction potential among the dust grains is given by modified Yukawas potential defined as,

$$\phi(r_{ij}) = \frac{Q_d^2}{4\pi\epsilon_0 r_{ij} f} exp(-r_{ij}/\rho_s) \tag{6.2.2}$$

in the x-y plane, i.e. the plane perpendicular to the magnetic field where the motion of the plasma particles will be influenced by the magnetic field. Based on this idea, we have calculated radial distribution function $g(r)$.

The effect of modified Yukawa potential on crystal formation has been studied for magnetic field ranging from $0.5T$ to $3T$. In our work, this analysis has been done based on the data given in the paper of Chu et al.[120]. For the simulation, following data have been used, $n_d = 3.74 \times 10^{10}$ m^{-3}, $n_i = 1.0 \times 10^{14}$ m^{-3}, $m_d = 4.0 \times 10^{-15}$ kg, $r_d = 2.0\mu m$, $T_d = 300$ K, $T_i = 300$ K, $T_e = 2320$ K. The value of 'f' is tabulated in Table.6.1. It is clear from this table that $f << 1$, which is the condition for ion-magnetized plasma. It is interesting to study the behaviour of phase transition and the triple point due to the modification of the interaction potential in presence of magnetic field.

Due to the anisotropy in the potential, Coulomb coupling parameter Γ and screening constant κ that are used to characterize the strongly coupled dusty plasma, will have direction dependence property. In the x-y plane, the effective Coulomb coupling parameter and effective screening strength may be defined as

$$\Gamma_m = (\Gamma/f) = Q_d^2/(4\pi\epsilon_0 a K_B T_d f) \tag{6.2.3}$$

and

$$\kappa_m = (a/\rho_s) = a/(\sqrt{f}\lambda_{De}) \tag{6.2.4}$$

Γ and κ will still play the role of coupling parameter and screening constant along the direction of the magnetic field. An increase in the magnetic field results in an increase of the modified Coulomb Coupling parameter and the screening strength κ_m. Due to the exponential behaviour of $(-\kappa_m)$ in the expression for potential, the strength of the shielded potential reduces with increase in B_0 and higher value of Coulomb Coupling parameter is required to enter the crystalline regime.

To observe the role of modified Yukawa potential and the effect of the magnetic field on crystal formation an MD code has been developed. In MD scaling the expression for modified potential energy is

$$\phi'(r'_{ij}) = \frac{\Gamma}{f}\frac{\kappa}{r'_{ij}} exp\left(-\frac{r'_{ij}}{\rho'_s}\right) \tag{6.2.5}$$

where $r'_{ij} = (r_{ij}/\lambda_D)$, $\rho'_s = (\rho_s/\lambda_D)$ and λ_D is the screening length of the background plasma. The simulations are performed with 686 particles for BCC crystal structure and 500 particles for FCC crystal structure. The particles are put inside a simulation box of side L with periodic boundary conditions. These lattices are used as initial conditions. Due to the presence of the anisotropic interaction potential these structures are not spherically symmetric. These structures exist among the grains under the condition for strong coupling and low dust temperature. The length, mass, time, velocity, energy and external magnetic field strength are normalized by λ_D, m_d, $\sqrt{(m_d\lambda_D^2)\,/\,(K_BT_d)}$,$1/\sqrt{m_d/K_BT_d}$, K_BT_d and $\sqrt{(m_d/4\pi\epsilon_0 a^3)}$. Each grain is assigned an initial random velocity such that the average kinetic energy corresponds to the chosen temperature T_d. Velocity Verlet algorithm is used to calculate the new position and velocities from the computed forces. Constant temperature MD is used to simulate structural properties of a 3D dusty plasma. The conservation of energy and momentum is verified to check whether the simulation is self consistent. The structural properties of the system are measured by calculating the pair correlation function $g(r)$ and long-range order $\rho(k)$. Due to the anisotropy in the potential, the pair-correlation function $g(r)$ will also have direction dependence. We have calculated this parameter on the x-y plane, perpendicular to the magnetic field. The plot of $g(r)$ versus inter-particle distance gives the idea how the particles may transform into crystal-like structure under the influence of the modified Yukawa potential. In x-y plane, RDF is defined as

$$g(r) = \frac{A}{N}\frac{N(r,\Delta)}{2\pi r\Delta} \tag{6.2.6}$$

where 'A' is the area of the simulated region, N is the number of simulated particles, $N(r,\Delta)$ is the number of particles located in a circle of infinitesimal thickness Δ from $r-\Delta/2$ and $r+\Delta/2$.

6.3 Results and Discussions:

Molecular Dynamics simulation has been performed to investigate the formation of dust crystal and phase transition in presence of magnetic field. In Fig. 6.1, the pair correlation function $g(r)$ has been plotted against inter-grain distance for magnetic field strength of 1.0 Tesla, 2.0 Tesla, and 3.0 Tesla respectively. The plot shows solid like behaviour with very pronounced peak, for magnetic field strength $B_0 = 1.0T$. With the increase in magnetic field, the peaks get flattened. At $B = 3.0T$, the particles become completely disordered with flat $g(r)$ plot. This observation is also supported by the plot of Fig.6.2, where the variation of the long-range order with external magnetic field is plotted. From this figure, we see that a moderate to high degree of order exists throughout the observation period at lower value of the magnetic

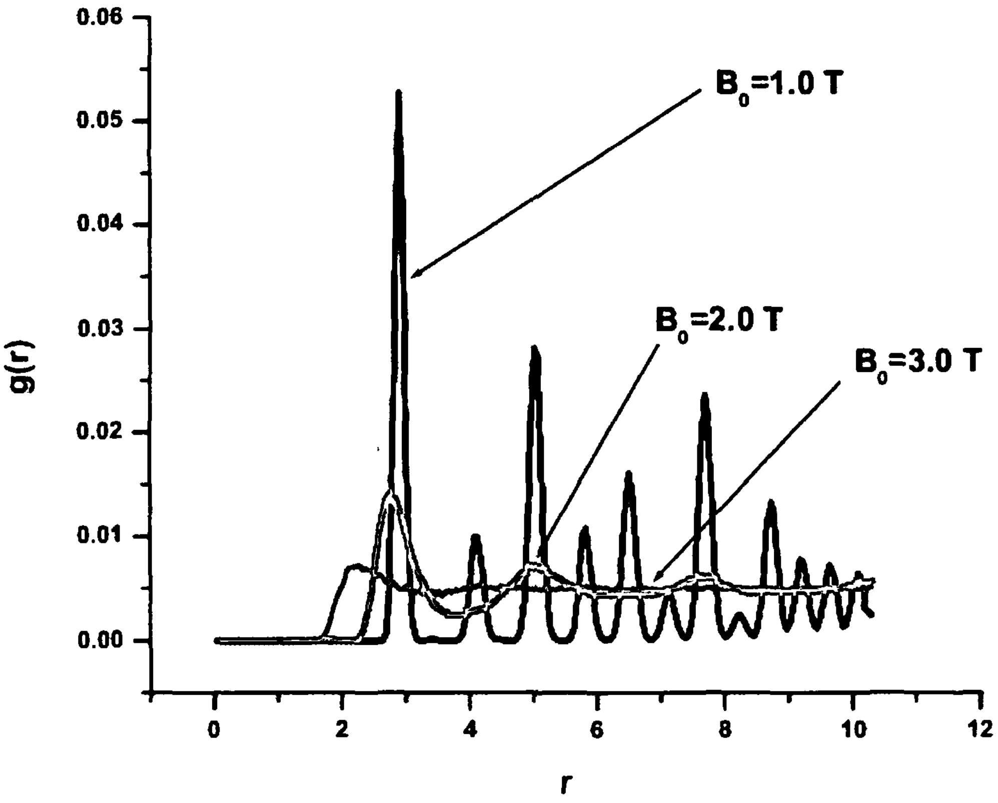

Figure 6.1: Plot of $g(r)$ vs. r for external magnetic field strength of $B_0 = 1.0, 2.0$ and $3.0T$ respectively.

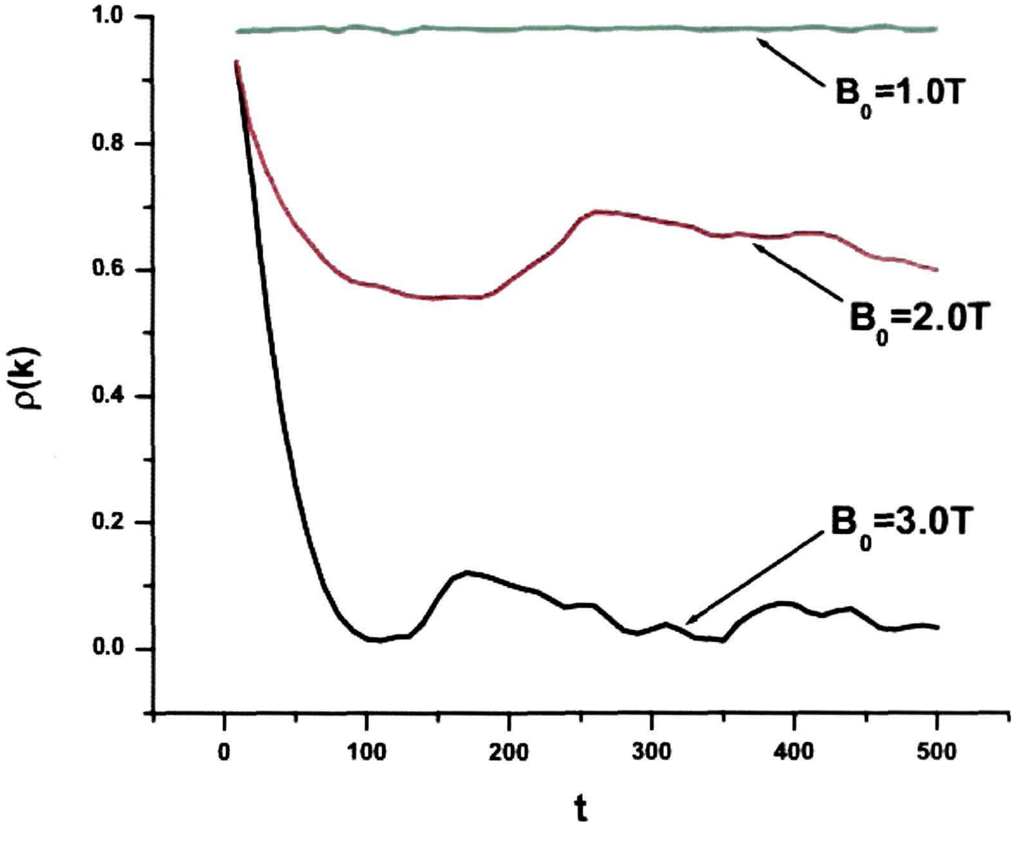

Figure 6.2: Plot of time dependence of long-range order for external magnetic field strength of $B_0 = 1.0, 2.0$ and $3.0T$ respectively.

Table 6.2: Variation of P.E. with magnetic field

B_0in Tesla	Γ_m	κ_m	P. E. in MD scaling
1.0	1.960917×10^4	3.10463	2.716719×10^3
2.0	7.84366×10^4	6.2092	2.500603×10^3
3.0	1.764825×10^5	9.31389	2.495990×10^3

field strength, whereas the long-range order rapidly vanishes at the highest value of magnetic field.

With the increase in the value of the external magnetic field, the modified Coulomb Coupling parameter and modified screening constant, given by Eq.(6.2.3) and Eq.(6.2.4) respectively, increase, since f is inversely proportional to square of B_0. However, the term $\exp(-\kappa_m)$ in Eq.(6.2.2) decreases with the rise in the value of B_0. As a result, the interaction potential among dust particles decay very rapidly at a distance a from it with the increase in the value of B_0. This is clearly shown in Table.6.2. This is also the reason why the long-range order decreases from a value of the order of 0.9 for $B_0 = 1.0T$ to less than 0.1 for $B_0 = 3.0T$. Since from Table.6.2, it can be observed that with the increase in B_0, potential energy decreases, the effective Debye radius decreases, and as a result of it the particles come closer to each other, which leads to the shifting of the peaks of $g(r)$ towards lower values of inter-particle distance.

Figures 6.3, 6.4 and 6.5 represent the phase diagrams of modified Yukawa system for magnetic field strength of $B_0 = 0.5T, 1.0T$ and $1.5T$ respectively. These diagrams clearly show the existence of the Solid(FCC-like), Solid(BCC-like) and fluid phases. In our system solid(FCC-like) and solid(BCC-like) crystalline pattern are seen for dust density $n_d = 3.74 \times 10^{10}m^{-3}$, temperature of the dust grain $T_d = 300K$, dust grain of radius $r_d = 2.0 \times 10^{-6}m$ and $Z = 10^3$, where 'Z' is the number of electrons embedded on dust. The triple points obtained at different κ and Γ for various values

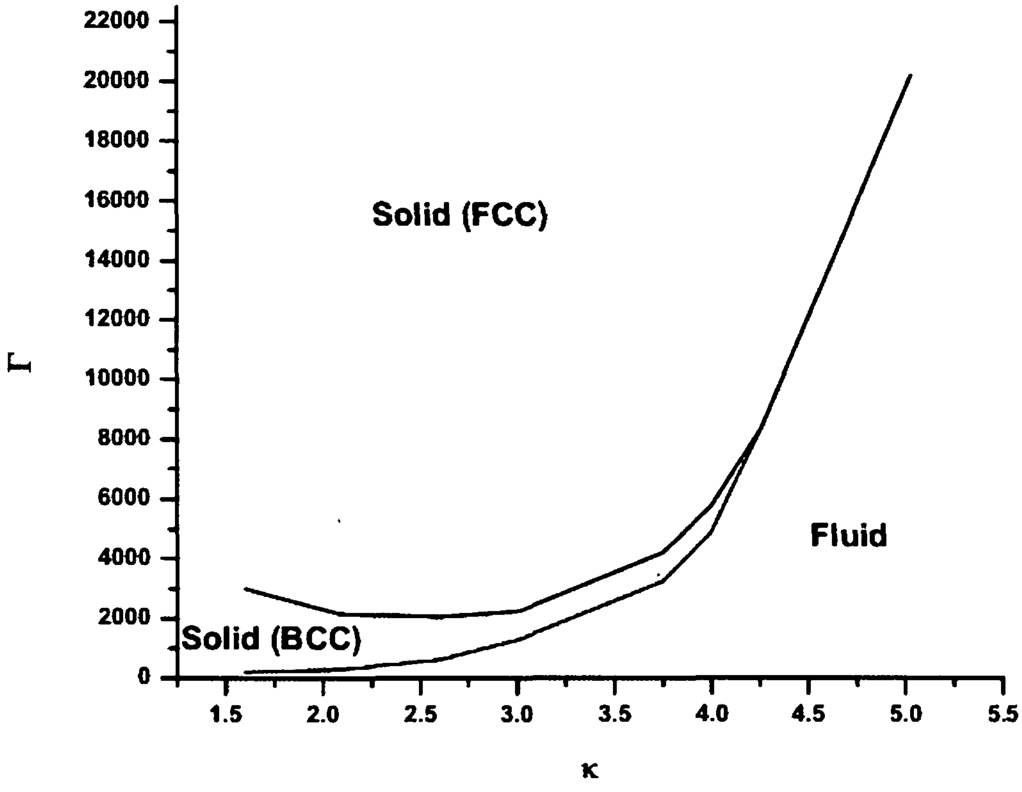

Figure 6.3: Phase diagram of modified Yukawa system in (Γ, κ) plane using magnetic field $B_0 = 0.5T$.

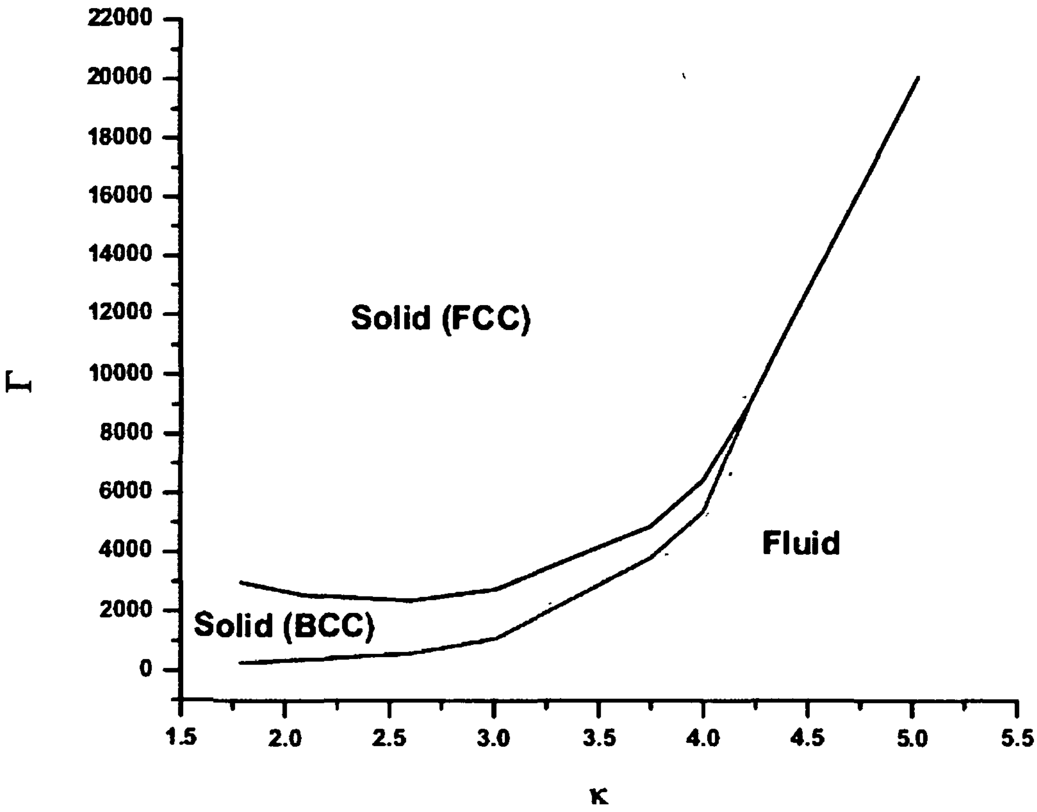

Figure 6.4: Phase diagram of modified Yukawa system in (Γ, κ) plane using magnetic field $B_0 = 1.0T$.

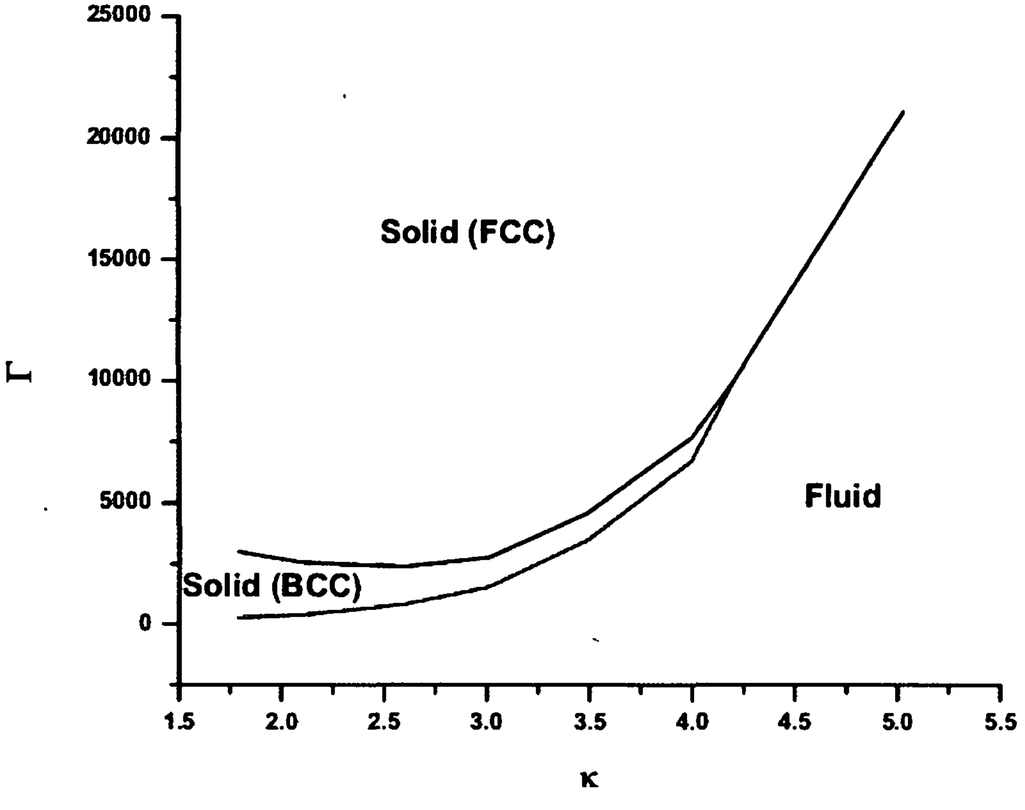

Figure 6.5: Phase diagram of modified Yukawa system in (Γ, κ) plane using magnetic field $B_0 = 1.5T$.

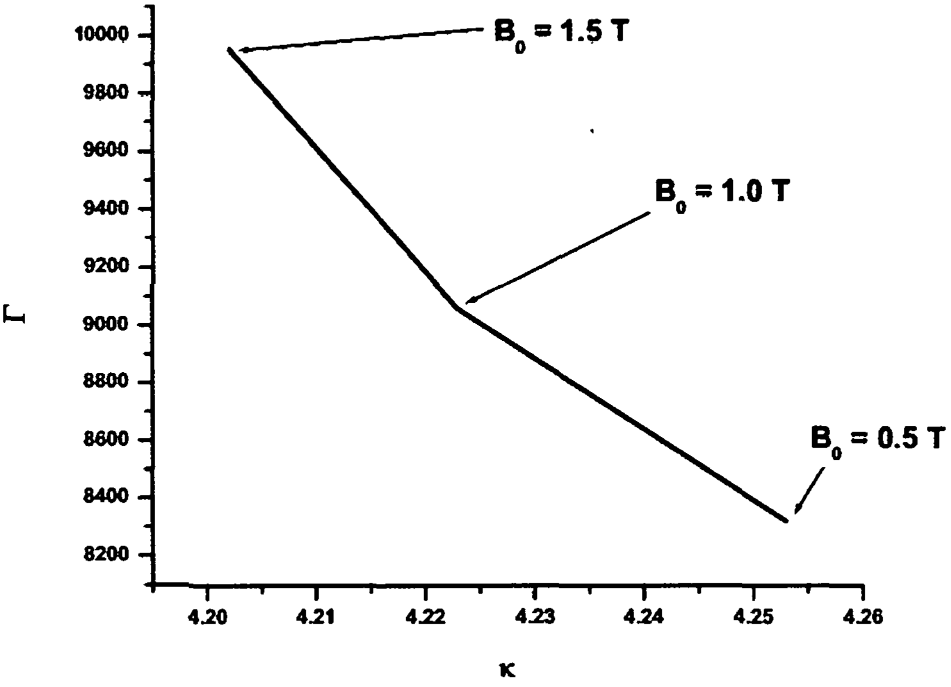

Figure 6.6: Plot of shifting of the triple point towards lower value of κ, higher value of Γ with increase in B_0.

of the magnetic field are tabulated in Table 6.3.

The phase diagrams also reveal that higher the value of the magnetic field, the triple point shifts towards lower value of κ, but higher value of coupling parameter. This shifting of the triple points is also supported by the plot of Fig.6.6. Higher value of dust density and lower value of dust temperature would be required to attain the crystalline state with the application of magnetic field.

Table 6.3: Values of κ and Γ at which triple points appear with magnetic field strength

B_0 in Tesla	κ	Γ
0.5	4.253	8322
1.0	4.223	9059
1.5	4.202	9956

6.4 Conclusions:

The structure of a three-dimensional dusty plasma system in presence of magnetic field using a molecular dynamics code has been studied here. Stress has been given to observe the structural behaviour and triple point of the system with magnetic field. The density, size and temperature of dust particles are chosen in such a way that the charged dust particles organize themselves in crystalline pattern in absence of magnetic field. Once the parameters ideal for crystal formation are identified, an external magnetic field is applied and its strength is gradually increased. The effect of the field is incorporated by modifying the interaction potential among the dust grains in the plane perpendicular to the magnetic field. It is assumed that the magnetic field influence the dynamics of shielding particles in x-y plane so that the shielding potential gets modified and becomes anisotropic. The simulation result shows that for a particular value of coupling parameter, the system undergoes phase transition from fluid to solid and solid (FCC-like) to solid (BCC-line) states, with the increase in magnetic field. The strength of the shielding potential decreases exponentially with B_0, and results in the observed phase transition. The triple point of the transition shifts towards higher value of coupling parameter and lower value of screening strength. In the present analysis, the direct effect on dust grains due to the magnetic field has not been taken into account. It is discussed in the next chapter.

Chapter 7

Determination of Critical Magnetic field for phase transition of Coulomb crystal

In this Chapter, the structure and phase transition of dust crystal in presence of magnetic field has been investigated in more detail. It is considered that the interaction potential among the dust grains no longer remains isotropic in presence of magnetic field. For low magnetic field it is seen that the crystallinity of dust particles is facilitated with the rise in magnetic field. However, for moderately strong magnetic field, there exists a critical magnetic field, application of which causes phase transition from regular solid-like structure to very disordered gaseous state. The phase diagram obtained under this condition are plotted in $\kappa_m - \Gamma_m$ *plane A relation between critical magnetic field and size of the particles has been established numerically. The results are very important and useful for the study of Coulomb crystals in magnetized plasma both in laboratory and astrophysical objects.*

7.1 Introduction:

The knowledge of crystal formation of dust particles in magnetized dusty plasma has attracted the attention of plasma physicists due to its usefulness from the astrophysics point of view. It also provides a suitable platform for the study of physics of strongly coupled plasma. There may exist strong interaction between the highly charged dust particles. This leads to the formation of ordered structures of liquid and crystal. Research in dusty plasma is stimulated in last two decades due to this feature of dusty plasma. One important aspect of dust crystal is to understand the interaction mechanism among dust particles. In presence of magnetic field, the trajectories of plasma particles change so that the effective interaction among the grains get modified. To understand the phase transition in strongly coupled plasma in presence of magnetic field, it is necessary to include proper interaction potential.

Plasma crystals having two or more layers undergo a phase transition from an *ordered, vertically aligned, hexagonal structure via a liquid to an almost gas like state* when the plasma parameters attain certain values[118,130]. Schweigert et al.[209] have presented a nonlinear model of the non-equilibrium melting transition of the plasma crystal. Vaulina et al.[210] have proposed phenomenological criteria for various phase transitions in the Yukawa system of charged macro-particles in a complex plasma. Joyce et al.[211] have shown that two-stream instability is the explanation for the high kinetic temperature of the dust grains in low-pressure experiments and the collisional stabilization of the two stream instability is the trigger for condensation of the dust into a solid state.

In the last decade, several experiments have been performed in different laboratories throughout the world to study about the influence of magnetic field on dynamics of dust particles in plasma. The rotation of dusty plasma structure in presence of an external magnetic field is one of the most important results of such plasma. Sato and his colleagues have performed series of experiments on dynamics of dust particles in the presence of a vertical magnetic field[138,212,213]. Cheung et al.[214] have performed an experiment with dust clusters from 2 to 12 particles in a magnetic field upto 100 Gauss and have measured rotational parameters such as cluster radius, angular momentum and threshold magnetic field.

There have been many theoretical studies on attractive interaction among negatively charged dust particles. Fortov et al.[215] developed a theory for influence of an external magnetic field on the interaction of dust particles in a gas discharge plasma. They showed that the attractive force of dust particles in weak magnetic fields grows with the increasing field and tends to a constant in the limit of strong magnetic fields. Yaroshenko et al.[216] have elaborately discussed about various mutual dust-dust interactions in complex plasmas, including the forces due to induced magnetic and electric moments of the grains. Nambu and Nitta[217] have presented a detailed theory of the "Shukla-Nambu-Salimullah" (SNS) potential in a magnetized electron-ion plasma, which is anisotropic in comparison with the effective potential in unmagnetized plasma. Tsytovich et al.[218] have done elaborate study on interaction among dust grains in presence of magnetic field. Their investigation shows that the dust-dust interaction can be substantially increased by presence of an external magnetic field and that the distance of the first attraction well perpendicular to the magnetic filed is substantially smaller than that along the magnetic field.

Molecular dynamics simulation has been widely used for understanding the phenomena of Coulomb crystallization and phase transition in strongly coupled plasma. In almost all the simulations done to study plasma crystal in presence of magnetic field, Debye-Hückel potential is considered to be the interaction potential among the dust particles[137,141,205]. In a very recent work, it is pointed out that in presence of magnetic field, the interaction potential among the dust grains get modified and becomes anisotropic[219].

In this Chapter, dusty plasma is considered in the strongly coupled regime. Here, we again consider that in presence of magnetic field, dust grains interact with each other via modified Yukawa potential as developed by Shukla et al.[204] and becomes anisotropic. In equation of motion, the term $Q_d(\vec{v} \times \vec{B})$ arising due to force on dust particles in presence of the magnetic field has been included. The effect of magnetic field on phase transition of the system from crystalline to fluid state has been investigated. The relation between size of dust and critical magnetic field at the point of phase transition has been found out.

Section 7.2 of this chapter deals with the theoretical model and development of MD code that is used to study this problem. Section 7.3 deals with the results and numerical calculations along with discussions. The conclusions drawn from the study are included in section 7.4.

7.2 Theoretical Model and development of MD code:

Here, we consider a 3D dusty plasma system of identical, spherical particles of mass m_d and charge Q_d immersed in a neutralizing background plasma subjected to an external magnetic field $\vec{B_0}$ applied along z-direction. The motion of the plasma particles along z-direction is not affected by the magnetic field. Along this direction the inter-dust interaction may be considered to be of Debye-Hückel (Yukawa) type. The dynamics of the plasma particles in $x-y$ plane completely change in presence of the magnetic field. The system under consideration no longer remains isotropic. The magnetic field affects the motion of plasma particles and that leads to change in the shielding potential of dust grains. The inter-dust interaction may be considered to be of modified Debye-Hückel type[204], given by equation (6.2.1), of Chapter 6.

The equation of motion for the 'i'th dust particles may be written as

$$m_d \frac{d^2\vec{r_i}}{dt^2} = \vec{F_i}(t) \tag{7.2.1}$$

Were,

$$\vec{F}_i(t) = -\sum \nabla_i \phi(r_{ij}) + Q_d \vec{v}_i(t) \times \vec{B} \tag{7.2.2}$$

for i = 1, 2, 3, ..., N and $j \neq i$. Here, F_i is the force acting on the ith particle and Φ_{ij} is given by equation (6.2.1) of Chapter 6, in $x - y$ plane and by equation (3.3.2) of Chapter 3, along z-direction.

The presence of magnetic field affects the behaviour of strongly coupled plasma in a complicated manner. As mentioned earlier in Chapter 6, in magnetized strongly coupled plasma, the two characterizing parameters Γ and κ get modified to Γ_m and κ_m defined by equations (6.2.3) and (6.2.4) respectively, in the $x - y$ plane.

To perform the simulation, 686 particles for BCC crystal structure and 500 particles for FCC crystal structure are taken under periodic boundary conditions, in a 3D cubic simulation box of side L. These lattices are used as initial conditions. In this problem, the space, mass, time, velocity, energy and external magnetic field strength are normalized by λ_D, m_d, $\sqrt{(m_d\lambda_D^2) / (K_BT_d)}$,$\sqrt{(m_d/K_BT_d)}$, K_BT_d and $\sqrt{(m_d/4\pi\epsilon_0 a^3)}$. Of the several existing algorithms for solving equation (7.2.1) we use in our MD calculation the efficient Velocity Verlet algorithm, given by equation (3.2.3) of chapter 3. To simulate structural properties of the system, constant temperature MD is used. The conservation of energy and momentum is verified to check whether the simulation is self consistent, and can be used for new interaction models.

To characterize the structural order of the system, radial distribution function $g(r)$, given by equation (6.2.6), has been computed in $x - y$ plane. Phase diagram is obtained by plotting lattice correlation factor in $\Gamma_m - \kappa_m$ plane. The point of intersection of lines representing solid FCC-like, solid BCC-like and fluid states may be defined as the triple point of transition in magnetized plasma. The critical magnetic field then may be determined easily from the values of Γ_m or κ_m at the triple point. The knowledge of critical magnetic field and its size dependence may be very useful for designing future experiments in laboratory for production of Coulomb crystal in presence of magnetic field and for understanding the behaviour of Coulomb crystal in different astrophysical plasma.

7.3 Results and Discussions:

The effect of strong to ultra-strong magnetic fields on phase transition of dust crystal from solid to fluid state is studied by calculating Radial distribution function (RDF) using a MD code. Figures 7.1 - 7.3 show the RDF plots for the two different cases. The black line represents the variation of $g(r)$ with modified Yukawa potential as the interaction term among the grains taking into the account the effect of $Q_d(\vec{v}\times\vec{B})$ term on dynamics of dust particles. The red line on the other hand ignores the dynamics of dust particles. Although the presence of the term $Q_d(\vec{v} \times \vec{B})$ does not affect the pattern and overall behaviour of $g(r)$ plot, it helps in the crystallization process. In all the plots, it is seen that both height and sharpness of the peaks are more in presence of this term. With the increase in magnetic field, the Larmor radius of the grains becomes smaller. As a result, the particles are confined to the small Larmor orbits. This facilitates the formation of ordered structure of the dusty system.

For studying the phase transition of the dust crystal under the application of magnetic field, $g(r)$ has been plotted in Figures 7.4 - 7.6. Fig.7.4 shows the $g(r)$ plot across r/λ_D for particles of radius $2.0\mu m$ and magnetic field ranging from $0.2T$ to $3.0T$. With the increase in magnetic field, the sharpness of the peaks increases, indicating a more ordered arrangement of the particles. At 0.7T, the peak height has been found to be maximum. With the further increase in the field, the pattern shows a gradual transition to the fluid state. At $B = 3.0$T, the particles become completely disordered with flat $g(r)$ plot. Similar behaviour is seen from Fig.7.5 and Fig.7.6 for

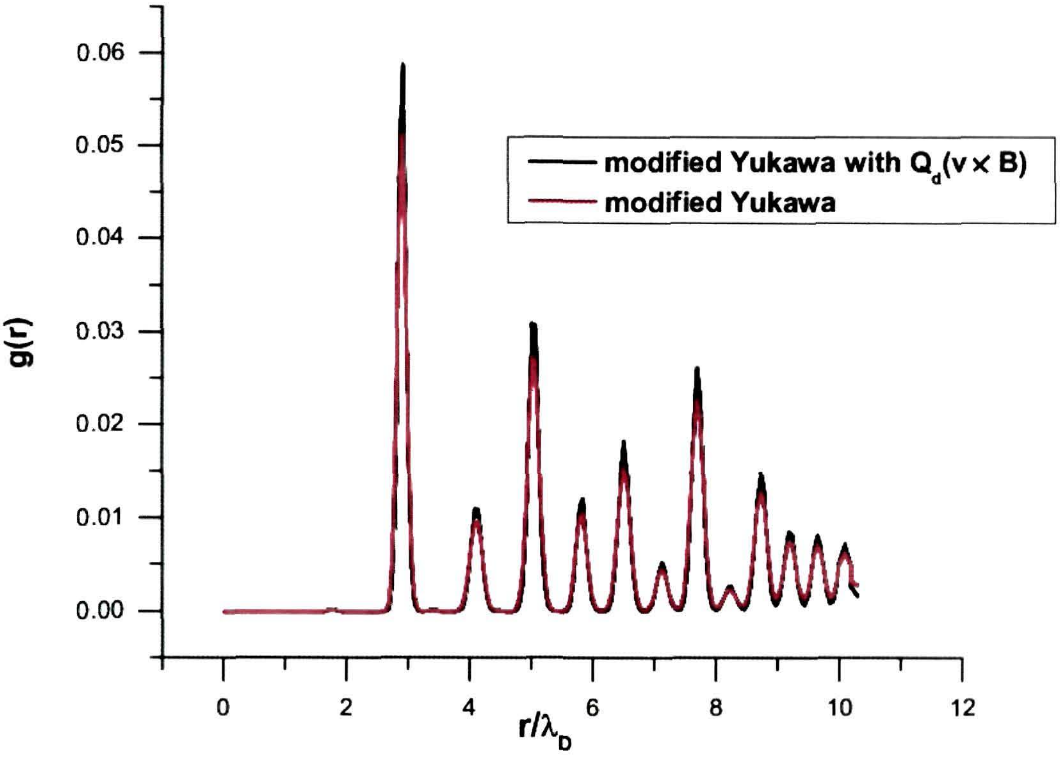

Figure 7.1: Plot of $g(r)$ vs. r/λ_d, for grain radius of 2 μm with magnetic field of 0.7 T.

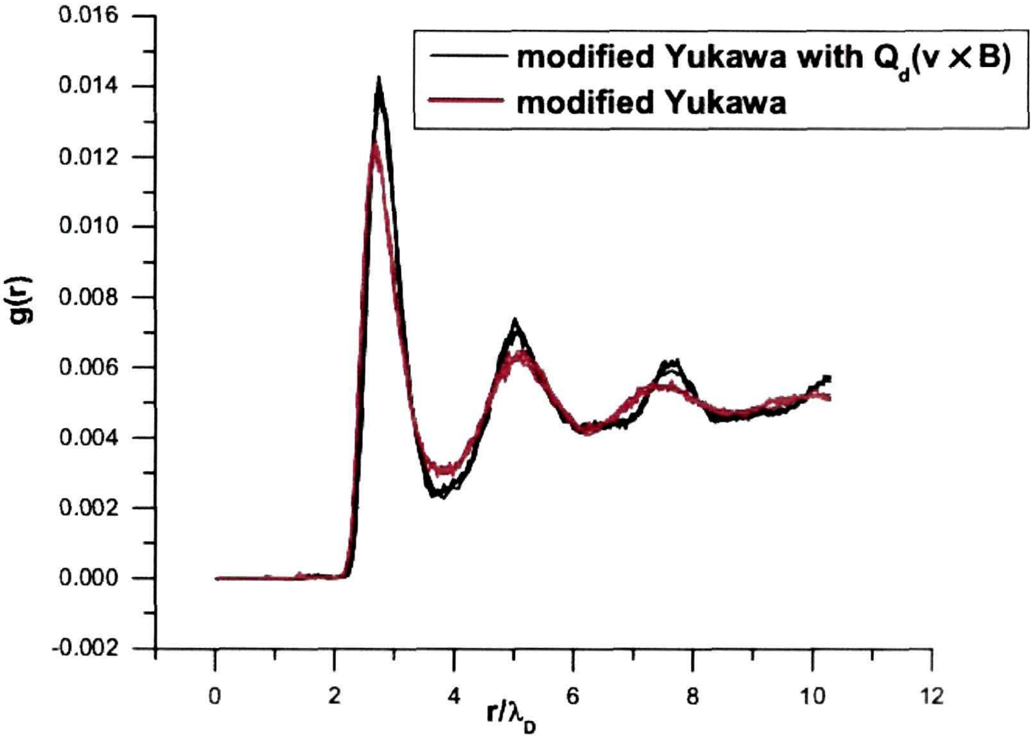

Figure 7.2: Plot of $g(r)$ vs. r/λ_d, for grain radius of 2 μm with magnetic field of 2.0 T.

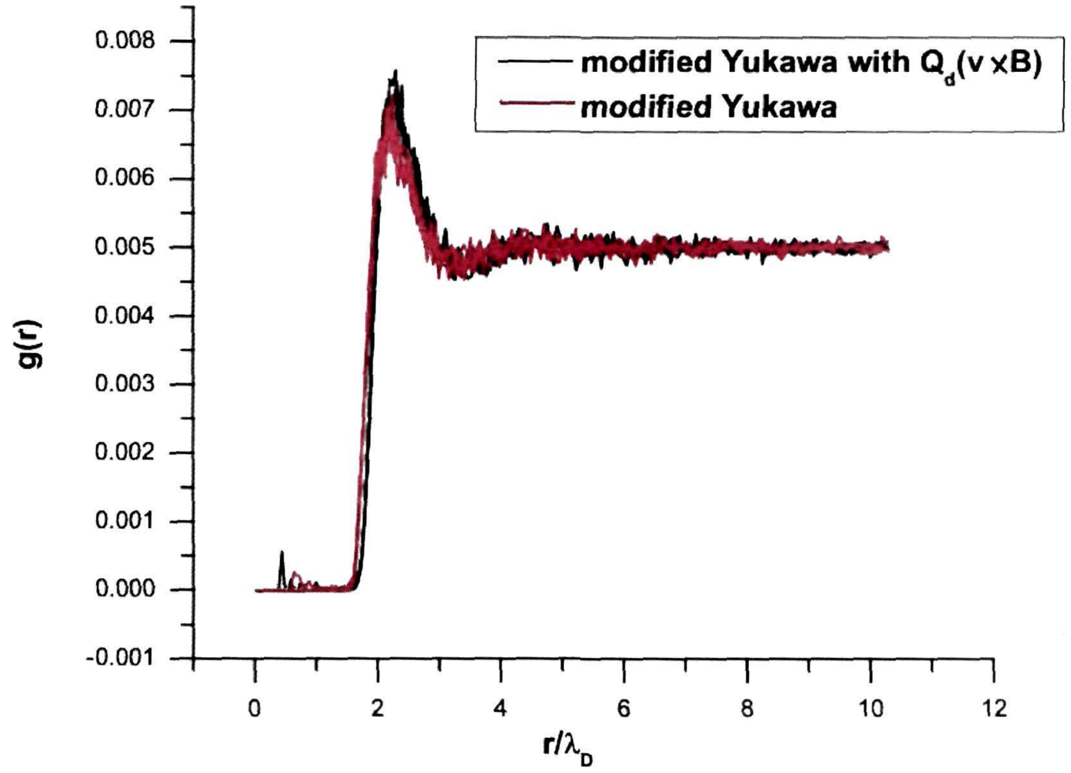

Figure 7.3: Plot of $g(r)$ vs. r/λ_d, for grain radius of 2 μm with magnetic field of 3.0 T.

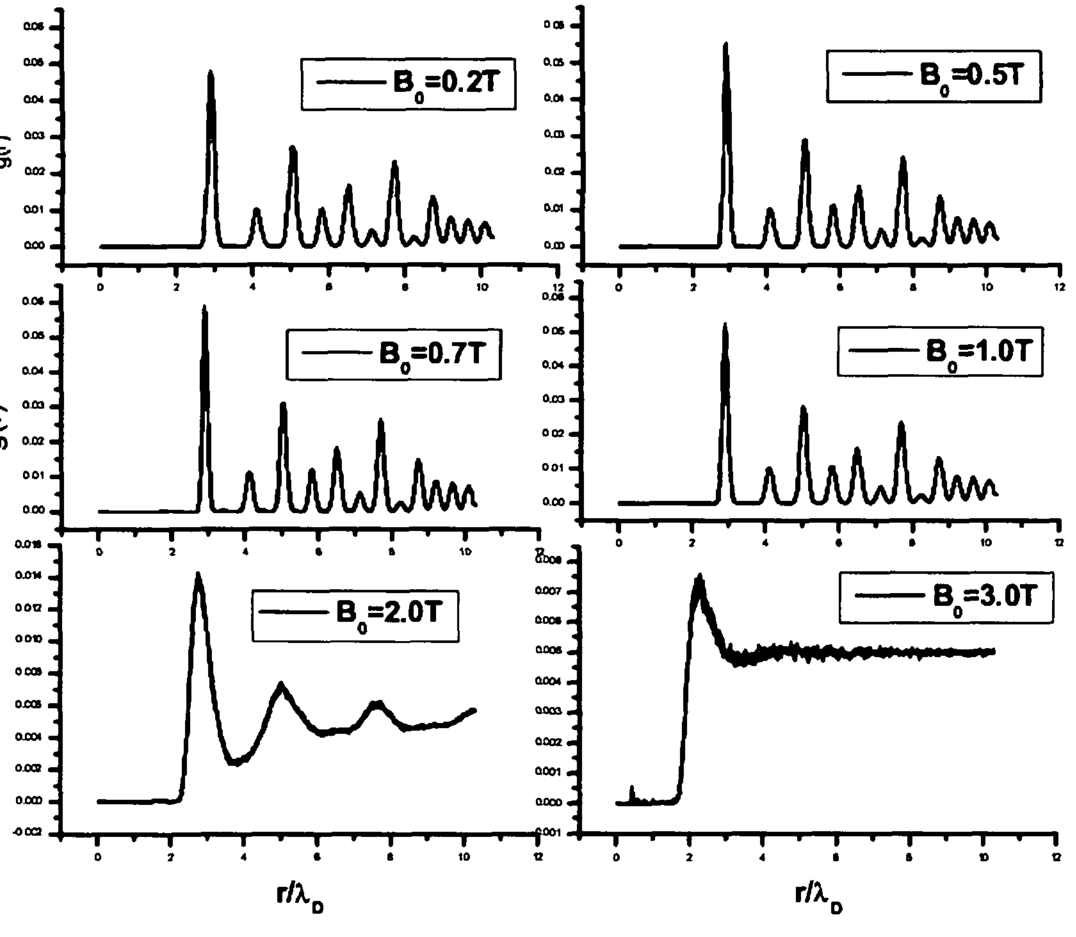

Figure 7.4: Plot of $g(r)$ vs. r/λ_d, for $B = 0.2, 0.5, 0.7, 1.0, 2.0$ and $3.0\ T$ respectively, taking grain radius $r_d = 2.0\ \mu m$.

dust grains with size 2.5 μm and 3.0 μm respectively.

In all the cases, sharpness and heights of RDF-peaks become maximum at $B =$ 0.7T. With the rise in magnetic field from 0.2T to 0.7T, the term $Q_d/(4\pi\epsilon_0 r_{ij} f)$ in equation (6.2.1) of chapter 6, is dominating. The interaction potential increases with the increasing values of magnetic field for this range. This results in gradual increase in the sharpness and height of g(r) plot. With further increase in magnetic field, the exponential term in the expression for modified Yukawa potential, viz. $exp(-r_{ij}/\rho_s)$ decreases very rapidly. For $B = 1.0T$ or more than that, the contribution due to the term $Q_d\vec{v_i}(t) \times \vec{B}$ becomes appreciable. This term tends to facilitate the formation of dust crystal. With the increase in magnetic field, the gyro-radius of dust decreases and as a result the particles are confined near the gyro-center. However even for strong magnetic field up to $5.0T$ that has been investigated here, the effect of the modified Yukawa term is more dominating than $Q_d\vec{v_i}(t) \times \vec{B}$ term. Hence, with the rise in magnetic field beyond $0.7T$, the peak height gradually decreases.

As the values of magnetic field are increased beyond $0.7T$, the crystalline and ordered state of the particles is gradually lost. Smaller the dimension of the particles, higher is the tendency to go to the fluid state. The particles with $2.0\mu m$ radius completely transits to gaseous state, whereas particles with $3.0\mu m$ radius attains fluid state at $B = 3.0T$.

More specific information about phase transition may be obtained from Fig.7.7 (a), (b), (c), (d), (e), (f) and (g). The phase diagrams plotted in Fig.7.7, may give more specific information about phase transition of our system. As has been mentioned earlier, in presence of magnetic field, the Coulomb coupling parameter and screening constant get modified to Γ_m and κ_m respectively. Triple points are obtained for dust particles with different radii ranging from $1.5\mu m$ to $4.7\mu m$ from the phase diagram. The magnetic field corresponding to the triple point may be defined as the critical magnetic field, that causes phase transition from crystalline to fluid state. It is seen

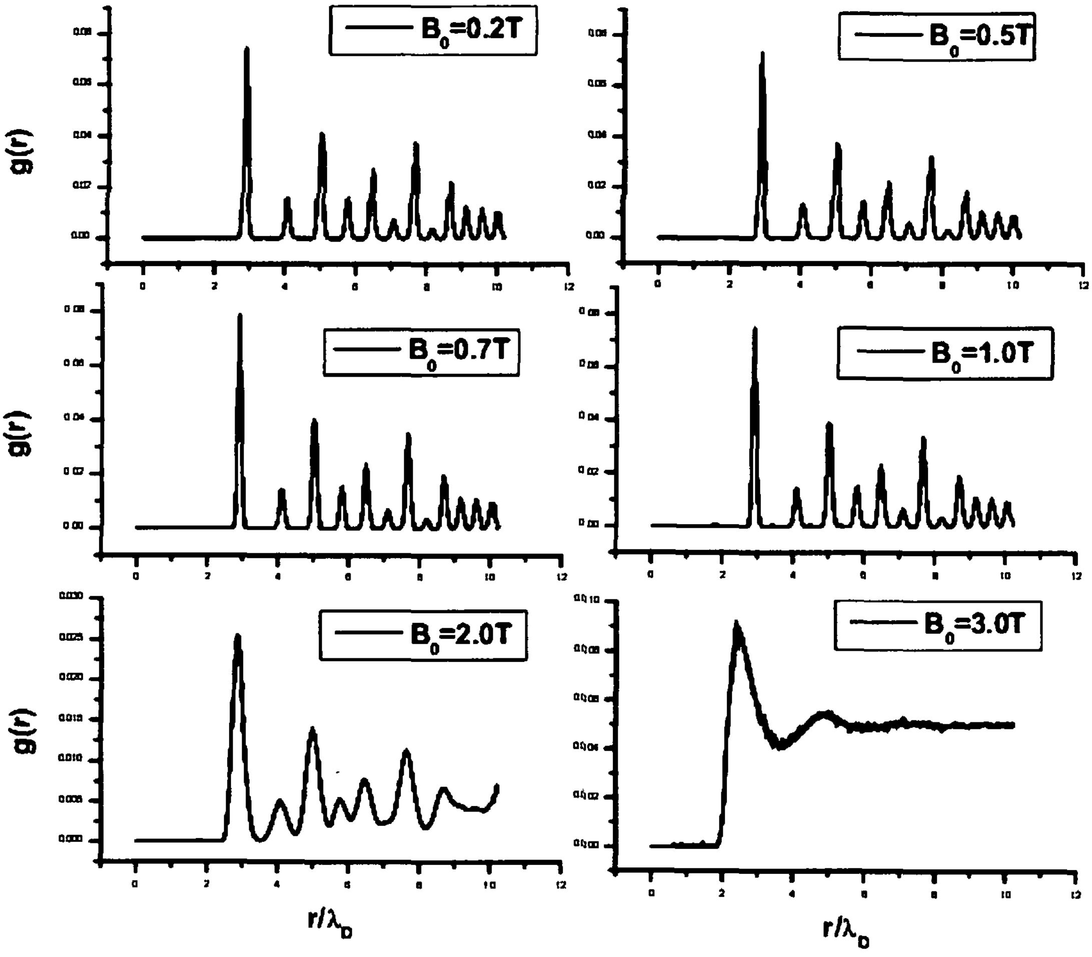

Figure 7.5: Plot of $g(r)$ vs. r/λ_d, for $B = 0.2, 0.5, 0.7, 1.0, 2.0$ and $3.0\ T$ respectively, taking grain radius $r_d = 2.5\ \mu m$.

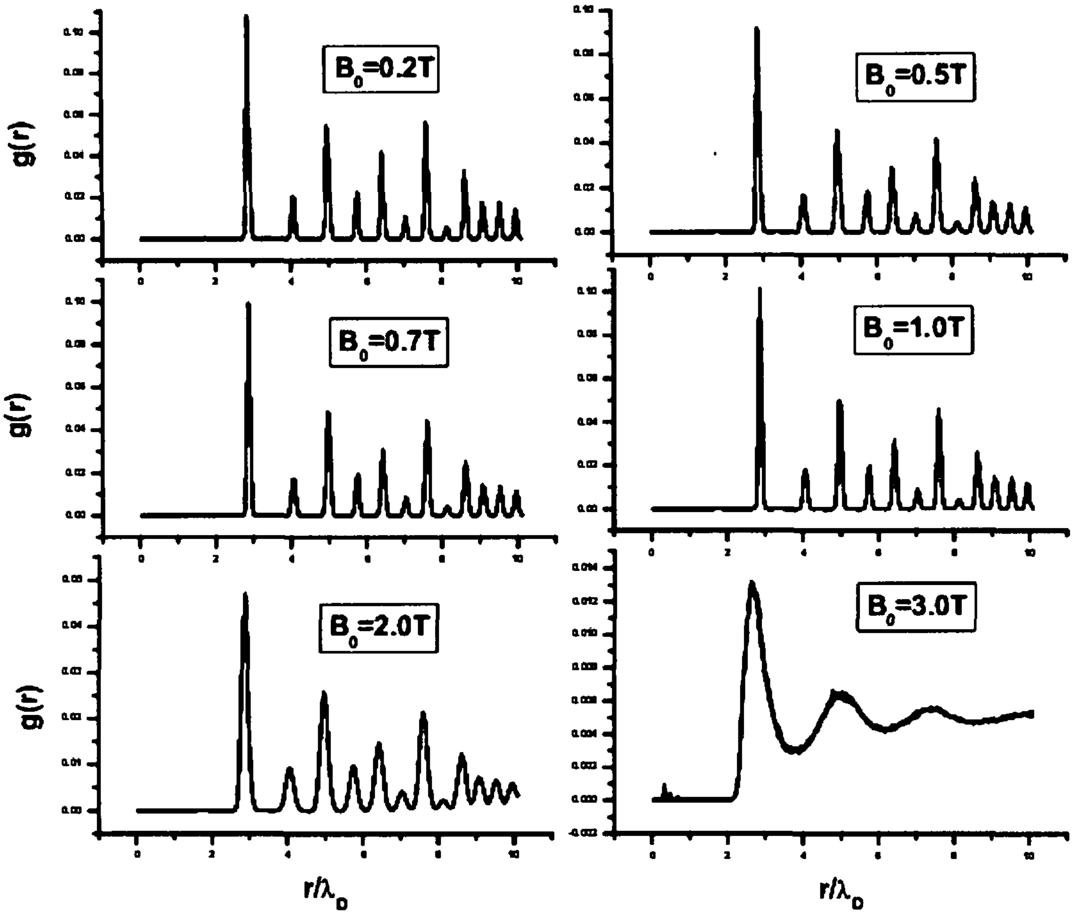

Figure 7.6: Plot of $g(r)$ vs. r/λ_d, for $B = 0.2$, 0.5, 0.7, 1.0, 2.0 and 3.0 T respectively, taking grain radius $r_d = 3.0\ \mu m$.

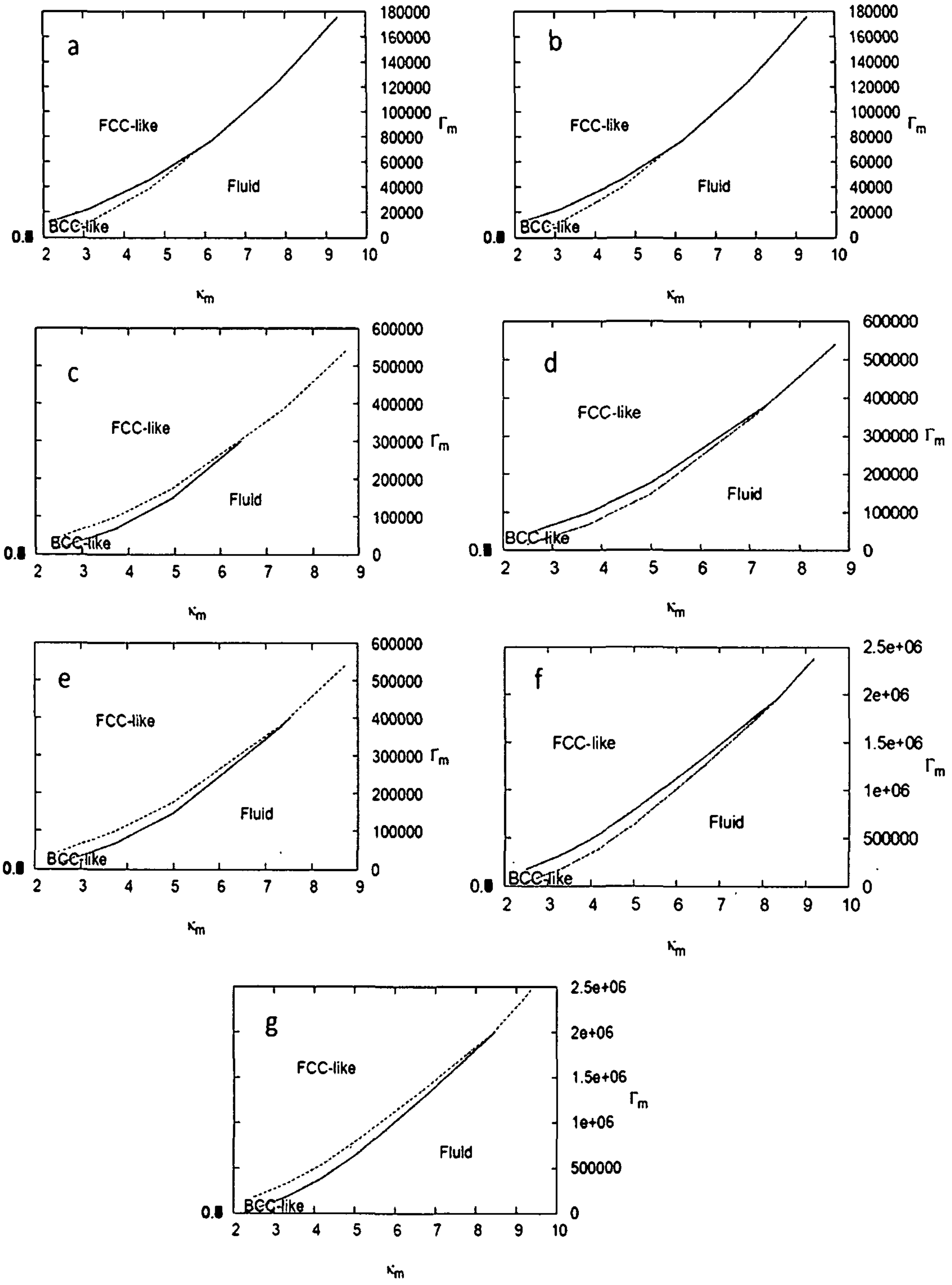

Fig.7.7: Phase diagrams in (κ_m, Γ_m) plane for grain size of (a) = 1.5 μm, (b) = 2.0 μm, (c) = 2.5 μm, (d) = 3.0 μm, (e) = 3.5 μm, (f) = 4.0 μm and (g) = 4.7 μm respectively.

Table 7.1: Values of Γ_m, κ_m, and B_c for different values of r_d

r_d in μm	Γ_m	κ_m	B_c in Tesla
1.5	7.1686×10^4	5.89	1.69
2.0	7.72645×10^4	6.16	1.985
2.5	3.02465×10^5	7.03	2.35
3.0	3.76414×10^5	7.32	2.94
3.5	4.02803×10^5	7.54	3.7
4.0	1.96351×10^6	8.38	5.02
4.7	2.00822×10^6	8.47	7.8

from the phase diagram of Fig.7.7 (a), that the critical magnetic field for dust particles of $1.5\mu m$ radius has been found to be 1.67 T with $T_d = 300K$, $n_d = 3.74 \times 10^{10} m^{-3}$, $n_i = 1 \times 10^{14} m^{-3}$. Below this magnetic field both FCC-like and BCC-like structures exist. The regular arrangement of the particles get distorted once the magnetic field is increased beyond $1.67T$ and the system makes phase transition to fluid state. We have further investigated the dependence of critical magnetic field on the grain size. This triple points for grain radius ranging from $r_d = 2.0\mu m - 4.7\mu m$ have been calculated from Fig.7.7 (b), (c), (d), (e), (f) and (g) respectively. The critical magnetic field B_c corresponding to triple points for seven different values of dust radii r_d are tabulated in Table.7.1.

The dependence of critical magnetic field on the grain size has also been investigated here. Fig.7.8 represents plot of critical magnetic field B_c across normalized value of dust radius. Using least square method, a relation may be obtained between critical magnetic field and dust radius as

$$B_c = 0.82402 + 0.31809 e^{(r_d/(1.57191\times10^{-6}))} \tag{7.3.1}$$

. It is seen that larger the dust grain, higher will be the critical magnetic field at the point of phase transition. The interaction potential increases with the charge

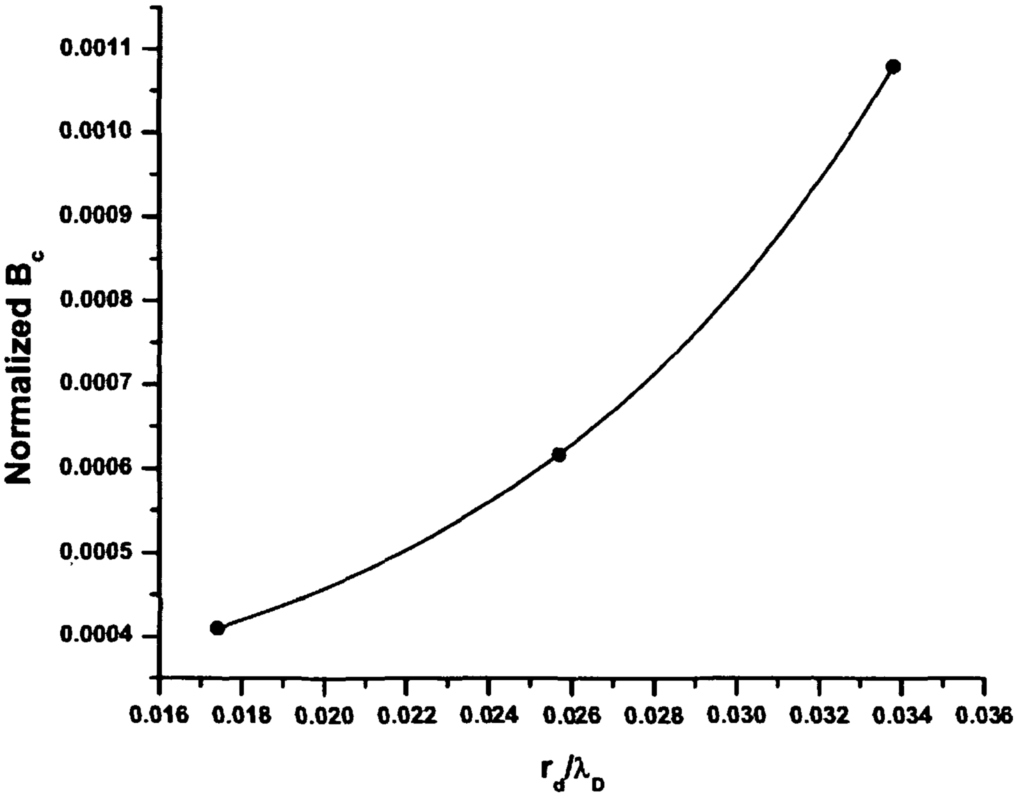

Figure 7.8: Plot of fitting of curve between critical magnetic field and grain radius.

on dust. In our simulation dust charge is taken as $Q_d = (4\pi\epsilon_0 r_d)4\frac{K_B T_e}{e}$, where r_d is the grain radius. Since dust charge is directly proportional to radius of the grains, the tendency to remain in crystalline state increases with the increase in size of the particles. Moreover, with the increase in charge, Larmor radius of dust particles becomes smaller. The particles as a result are more confined about their gyro-centers. In our study it is seen that with the increase in magnetic field beyond $0.7T$, the system gradually goes to disordered states. Larger is the radius of the grain relatively higher magnetic field is required to cause the transition. Hence the critical value of the magnetic field at which phase transition occurs shifts towards larger values for increasing grain radius. The particles with large size can maintain ordered, crystalline state even for higher values of magnetic field. Hence the critical magnetic field is proportional to the size of the dust particles.

7.4 Conclusions:

In this Chapter, a 3D MD code has been developed to study phase transition of strongly coupled magnetized plasma. We have emphasized in the fact that the interaction potential among dust particles in presence of magnetic field cannot be described by Debye-H$\ddot{u}$ckel potential. The magnetic field affects the motion of plasma particles and that leads to change in the shielding potential of dust grains. The term $Q_d\vec{v_i}(t) \times \vec{B}$ has been incorporated in the equation of motion in order to study its effect on crystal formation for large magnetic field. From our study it is seen that low magnetic field may facilitate formation of Coulomb crystal. However, for moderately strong magnetic field in the range $0.7T < B < 8.0T$, the effect becomes reverse for particles with size $2.0 - 3.0\mu m$. Karasev et al.[220] investigated the dust structure in conditions of dc glow discharge with an external magnetic field. They compared pair correlation function for their system with different values of magnetic field. Their results clearly show that dust structure is changing from almost hexatic to a gaseous disordered state with an increase of magnetic induction. The results of our simulation agree with their observation.

We have pointed out a procedure for determining critical magnetic field at the point of phase transition. The relation between critical magnetic field and size of the particles is clearly seen from the phase diagrams. Knowledge of this critical magnetic field may be very useful to perform experiments on Coulomb crystal in magnetized plasma. This simulation may be extended for ultra-strong magnetic field which would be suitable for explaining the observations obtained from some of the astrophysical objects like magnetars with extremely strong magnetic fields.

Chapter 8

Summary and Conclusions

Dusty plasmas has received considerable attention in astrophysical contents, as well as laboratory plasma devices and industrial processes. One of the novel properties of dusty plasma is related to the relatively large value of the charge and mass on the particles. Usually, the strongest force acting on dust particles in the vicinity of stars or planets is gravity or radiation pressure. However, the charged dust particles are also affected by electric and magnetic fields. There are many phenomena occurring in dusty plasma, which are still not explained in a convincing manner. The increased interest in dusty plasmas was due to two major discoveries in very different areas: one is the discovery by the Voyager 2 spacecraft in 1980 of the radial spokes in Saturns B ring and another is the discovery in the early 80s of the dust contamination problem in semiconductor plasma processing devices. More recently, the realization of the presence of dust particles in magnetic fusion plasmas, has led to interest to understand how these particles interact with plasmas. This is of particular concern for the design of the ITER device. Besides these, there are numerous other examples, where dusty plasma plays a key role.

The characteristics that make dusty plasma so important, is arising due to massive mass and fluctuating charge of dust grains. In addition, the dust particles may change the properties of the plasma itself and change the dispersion relation of various, usually low frequency, plasma waves and give rise to new type of instabilities. In chapter 2 of this thesis, the emphasis has been given on studying the damping of low-frequency drift mode which arises due to the dust particle density gradient in presence of a magnetic field in collisional dusty plasma. For this study dust charge fluctuation is also taken into consideration. The dynamics of the plasma is governed by the dust particles. The role of ion-neutral collision, changing frequency and dust density gradient on the damping rate of the instability is investigated for different values of physical parameters of interest. Both numerical and analytical techniques are used to study the problem. From our investigation it is observed that an increase in the dust particle inhomogeneity, results in decrease of the damping rate. The role of ion -neutral collision on the damping rate of drift wave is also investigated. The effect of dust charge fluctuation on the behaviour of low-frequency drift wave in such weakly ionized plasma is also studied.

The characteristic feature of dusty plasma is the strong interaction between dust particles, which can lead to the formation of ordered liquid-like and crystal-like structures. The investigation of the response of the dusty plasma to various external actions is of great interest. Such actions can be used to control the spatial position, and dynamics of dusty plasma structures. Moreover, the laboratory dusty plasma in the presence of external actions is a good experimental model for investigating the formation of dust and dusty plasma structures in space and various industrial and power facilities. The most intriguing aspect of dusty plasmas is that the particles can be directly imaged and their dynamical behavior recorded and studied visually. This is accomplished using laser light scattering and fast digital video cameras. This allows for the unprecedented ability to study the dynamics of the dusty plasma at the kinetic level. In Chapter 3 of this thesis, a detailed theory of crystal formation and phase transition of 3D complex plasma system have been discussed. The method of Molecular Dynamics (MD) simulation is used for this study. The MD simulation is an important and powerful tool in the study of large collections of atoms and molecules. This simulational method can be considered as one of the standard tool that can be employed in the study of structural properties and growth phenomena associated to dusty plasma. MD method follows the evolution of many-body system by tracking the trajectory of every particle in the system by numerically integrating its equation of motion including all the forces acting on the particle. For our study a self-consistent Molecular Dynamics simulation program is developed to investigate crystal formation and phase transition of dust grains in plasmas. Starting from any given initial phase-space distribution of dust grains, the dusts are allowed to evolve according to Newton's law of motion with a model Yukawa dust-dust interaction potential. The simulation is started under a constant-temperature constraint so that the system achieves equilibrium state. The conservation of energy and momentum is verified to check whether the simulation is self consistent and can be used for new interaction models. The structure of the complex system is investigated by calculating Radial Distribution Function (g(r)) for different values of temperature, density and size of dust grains. The results of our simulation show that as the temperature of dust T_d is reduced, the structure becomes highly ordered. The system attains an ordered solid state for dust density larger than $n_d = 1.78 \times 10^9 m^{-3}$ and disordered fluid state for n_d below that value for the range of values of parameters used in this study. It is also seen that even a slight change in the size of dust particles affects the structure to a large extent. The crystal formation becomes more probable with grains of relatively large size. The long-range order is studied from the plot of the strength of lattice correlation with time. The phase diagram for the system shows the existence of three phases, solid(FCC), solid(BCC) and fluid. The study may be helpful to identify accurately the parameters suitable for the formation of Coulomb crystal in a Yukawa dusty plasma system.

Besides the role of strong coupling among the dust grains for the formation of dust crystal, the effect of different mechanisms involving ion-mediated attractive forces are also found to play a key role. The effect of attractive Shadowing force on structure of 3D dust crystal using MD simulation has been investigated in Chapter 4. This force arises due to asymmetrical current flow to the grain. A comparative study has been made between Yukawa and the combined Yukawa-Shadowing potential by calculating pair-correlation function, for different values of Coulomb coupling parameter, screening constant and grain radius. In our discussion, we have concentrated mainly on effect of Shadowing force on phase transition of the dust crystal to liquid and gaseous states. From our study it is seen that the attractive Shadowing force predominates over Yukawa force for grains with large size and for large screening parameter. The investigation done here may confirm the role of Shadowing force in crystal formation suggested by the theorists and experimentalists.

In Chapter 5 of this thesis, an effort has been made to do a comparative study between the effect of coupled Yukawa-Shadowing potential and coupled Yukawa-Overlapping Debye Sphere (ODS) potential on 2D dust crystal formation by using MD simulation. The structural property of the system has been investigated by calculating Pair correlation function ($g(r)$) for different values of Γ, κ and dust number densities n_d. From the results discussed here it is found that Coulomb coupling parameter does not have significant effect on both ODS and Shadowing force. Both ODS and Shadowing potentials equally dominate for small values of screening parameter κ and large values of dust density. However, the attractive Shadowing force is more dominant for grains with large screening parameter and smaller values of dust density. The results for Yukawa-Shadowing and ODS potential are also compared with experimental results and a close agreement is obtained for attractive Shadowing force. The comparison of our simulation results with the experimental observation clearly reveal that Yukawa-Shadowing potential leads to better agreement with the real situation.

In Chapter 6, the investigation has been done on the formation of dust crystal and phase transition of a three-dimensional dusty plasma system in presence of external magnetic field by molecular dynamics (MD) simulation. It has been pointed out that due to the presence of the magnetic field, the interaction potential among the dust grains gets modified and no longer remains isotropic. The pair correlation function has been calculated for different values of magnetic field strength. The triple point is calculated from the phase diagram. The effect of the magnetic field on the crystalline behaviour and triple point is investigated from the simulational result. Higher value of magnetic field disturbs the organized structure of dust crystal. It is seen from our results that the triple point of the transition shifts towards higher value of coupling parameter and lower value of screening strength. The results of our simulation may find application in various space and laboratory plasma situations. Proper knowledge about the behaviour of dust particles in presence of magnetic field is relevant for fabrication of micro and nano-scale mechanical devices and various dynamical processes observed in planetary rings and space nebulae.

Chapter 7 of this thesis describes the study of critical magnetic field for phase transition from crystalline state to liquid state of strongly coupled magnetized plasma. Modified Yukawa potential is used as the interaction potential among the grains. Besides that, the effect on dust grains in presence of the magnetic field has been taken into account by incorporating the term $Q_d\left(\overrightarrow{v} \times \overrightarrow{B}\right)$ in the equation of motion for strong magnetic field. Our study reveals that low magnetic field ($< 1T$) may facilitate formation of Coulomb crystal. It is seen that for moderately strong magnetic field in the range $0.7T < B < 8.0T$, the effect becomes reverse for particles with size $1.5\mu m - 4.7\mu m$. The relation between critical magnetic field and size of the particles is clearly seen from the phase diagrams. It is seen that larger the dust grain, higher will be the critical magnetic field at the point of phase transition. The knowledge of critical magnetic field and its size-dependence may be very useful for designing future experiments in laboratory for production of Coulomb crystal in presence of magnetic field. In order to study the astrophysical observations like soft gamma repeaters (SGRs), anomalous X-ray pulsars, magnetars with extremely strong magnetic fields and different space phenomena, it is essential to understand formation of dust crystal in dusty plasma in presence of magnetic field.

Thus, in this thesis an effort has been made to understand low frequency phenomena like drift mode in presence of dust particles in a weakly ionized plasma. Besides that, physics of dust crystal formation has been extensively studied under various conditions using MD simulation technique. This study may be helpful for understanding astrophysical plasma related events as well as for designing dusty plasma experiments.

Bibliography

1. Shukla, P. K. A Survey of Dusty Plasma Physics. *Phys. Plasmas* **8**, 1791-1803 (2001).

2. Verheest, F. *Waves in dusty space plasmas* (Kluver Academic Publishers, Dordrecht, 2000).

3. Alfven, H. *On the origin of the solar system* (Calrendon Press, Oxford, U K. 1954).

4. Mauk, B. H., Keath, E. and Krimigis, S. The Voyager program at APL. *Johns Hopkins APL Tech. Dig.* **11**, 63-71 (1990).

5. Horanyi, M., Morfill, G. and Grun, E. Mechanism for the acceleration and ejection of dust grains from Jupiter's magnetosphere. *Nature* **363**, 144-146 (1993).

6. Verheest, F. Dusty plasmas in application to astrophysics. *Plasma Phys. Control. Fusion***41**, A445-A451 (1999).

7. Tagger, M., Henriksen, R., Sygnet, J. and Pellat, R. Spiral waves and instability in magnetized astrophysical disks. *Astrophys. J.* **353**, 654-657 (1990).

8. Smith, B. A. *et al.* A new look at the Saturn system: the Voyager 2 images. *Science* **215**, 504-537 (1982).

9. Hill, C. J. and Mendis, D. A. Charged dust in the outer planetary magnetospheres. *Moon and Planets* **23**, 53-71 (1980).

10. Goertz, C. K. and Morfill, G. A model for the formation of spokes in Saturn's

ring. *Icarus* **53**, 219-229 (1983).

11. Avinash, K. and Sen., A. A model for the fine structure of Saturn's rings. *Phys. Lett. A* **194** 241-5 (1994).

12. Snow, T. P. and McCall., B. J. Diffuse Atomic and Molecular Clouds. *Ann. Rev. Astron. Astrophys.* **44**, 367-414 (2006).

13. Angelis, U. de. The physics of dusty plasmas. *Physica Scripta* **45** 465-474 (1992).

14. Grun, E. *et al.* Interstellar dust in the heliosphere. *Astron. Astrophys.* **286**, 915-924 (1994).

15. Svedhem, H., Münzenmayer, R. and Iglseder, H., *In Physics, Chemistry, and Dynamics of Interplanetary Dust* (San Francisco: Astron. Soc. of Pac. Press, 1996).

16. Kortenkamp, S. J. and Dermott, S. F. Accretion of interplanetary dust particles by the Earth. *Icarus* **135**, 469-495 (1998).

17. Mendis, D. A. and Rosenbegr, M. Cosmic Dusty Plasma. *Annu. Rev. Astron.Astrophys.* **32**, 419-463 (1994).

18. Saito, T., Kozuka, Y., Saito, K. and Minami, S. *Dusty and Dirty Plasmas, Noise, and Chaos in Space and in the Laboratory* (Plenum Press, New York, 1994).

19. Shukla, P. K. and Mamun, A. A. *Introduction to Dusty Plasma Physics* (Institute of Physics Publishing Ltd., Bristol, 2002).

20. Besedina, Yu. N. and Popel, S. I. Synoptic-scale cyclonic vortices and possible transport of fine particles from the troposphere into the stratosphere. *Doklady Earth Sciences* **423A**, 1475-1478 (2008).

21. McNeil, W., Lai, S. and Murad, E. Differential ablation of cosmic dust and implications for the relative abundances of atmospheric metals. *J. Geophys. Res.* **103**, 10 899-10 911 (1998).

22. Popel, S. I. and Tsytovich, V. N. Shocks in Space Dusty Plasmas. *Astrophys. Space Sci.* **264**, 219-226 (1999).

23. Gavrilov, B. G. *et al.* Diamagnetic effect produced by the Fluxus-1 and -2 artificial plasma jet *Geophys. Res. Letters* **26**, 1549-1555 (1999).

24. Bernhardt, P. A., Ganguli, G., Kelley, M. C. and Swartz, E. Enhanced radar backscatter from space shuttle exhaust in the ionosphere. *J. Geophys. Res.* **100**, 23811-23818 (1995).

25. Havnes, O. *et al.* Meter-scale variations of the charge carried by mesospheric dust. *Planet. Space Sci.* **44**, 1191-1194 (1996).

26. Goree, J. Charging of Particles in a Plasma. *Plasma Sources Sci.* **3**, 400-406 (1994).

27. Allen, J. E. Probe Theory - the Orbital Motion Approach. *Physica Scripta* **45**, 497-503 (1992).

28. Merlino, Robert L. and Goree, John A. Dusty plasmas in the Laboratory. Industry and Space *Physics Today*, **57**, 32-38 (2004).

29. Goertz, C. K., Morfill, G. A model for the formation of spokes in Saturn's ring. *Icarus* **53**, 219-229 (1983).

30. Tsytovich V. N., Morfill, G. E., Vladimirov, S. V. and Thomas, H. *Elementary Physics of Complex Plasmas* (Springer, New York 2006).

31. Xu W, D'Angelo N. Merlino R.L. Dusty Plasmas : The Effect of Closely Packed Grains. *Geophys. Res.* **98**, 7843-7847 (1993).

32. Horanyi, M. and Goertz, C. K. Coagulation of Dust Particles in a Plasma. *Ap. J.* **361**, 155-161 (1990).

33. Safranov, V. S. *Evolution of the Protoplanetary Cloud and the Formation of the Earth and Planets (NASA-TT-F-677)* (Israel Program for Scientific Translations, 1972).

34. Northrop, T. G. and Birmingham, T. J. Plasma Drag on a Dust Grain due

to Coulomb Collisions. *Planet. Space Sci.* **38**, 319-326 (1990).

35. Chow, V. W. and Mendis, D. A., Rosenberg, M. Role of Grain Size and Particle Velocity Distribution in Secondary Electron Emission in Space Plasmas. *J. Geophys. Res.* **98**, 19065-19076 (1993).

36. Opik, E. J. Interplanetary dust and terrestrial accretion of meteoric matter. *Irish Astron. J.* **4**, 84-135 (1956).

37. Singer, S. F., Walker, E. H. Electrostatic dust transport on the lunar surface. *Icarus* **1**, 112-120 (1962).

38. Mendis, D. A., Hill, J. R., Houpis, H. L. F and Whipple, E. C. On the electrostatic charging of the cometary nucleus. *Astrophys. J.* **249**, 787-797 (1981).

39. Mitchell, C. J., Hornyi, M., Havnes, O. and Porco, C. C. Saturn's Spokes: Lost and Found. *Science* **311**, 1587-1589 (2006).

40. Talbot, L., Cheng, R. K., Schefer, R. W. and Willis, D. R. Thermophoresis of Particles in a Heated Boundary Layer. *J. Fluid Mech.* **101**, 737-758 (1980).

41. Vasilyak, L. M., Vetchinin, S. P., Polyakov, D. N. and Fortov, V. E. Formation of complex structures in dusty plasmas under temperature gradients. *JETP* **100**, 1029-1034 (2005).

42. Jellum, G. M., Daugherty, J. E., Graves, D. B. Particle thermophoresis in low pressure glow discharges. *J. Appl. Phys.* **69**, 6923-6934 (1991).

43. Cabarrocas, P. R., Stahel, P., Poissant, S. Hamma Y. *Proceedings of the 2nd World Conference and Exhibition on Photovoltaic Solar Energy Conversion* (European Commission, Vienna, 1998).

44. Fortov, V. E., Khrapak, A. G., Khrapak, S. A., Molotkov, V. I. and Petrov, O. F. Dusty Plasmas. *Phys. Usp.* **47**, 447-492 (2004).

45. Grün, E. and Landgraf, M., Fast Dust in the Heliosphere, *Space Sci. Rev.* **99**, 151-164 (2001).

46. Baines, M. J., Williams, I. P. and Asebiomo, A. S. Resistance to the motion of a small sphere moving through a gas. *Mon. Not. R. Astron. Soc.* **130**, 63-74 (1965).

47. Fortov, V. E. and Iakubov, I. T. *Physics of Nonideal Plasma* (World Scientific Publishing Co. Pte. Ltd., Singapore, 1990).

48. Shukla, P. K. Low-frequency Modes in Dusty Plasmas. *Phys. Scr.* **45**, 504-507 (1992).

49. Rao, N. N., Shukla, P. K. and Yu. M. Y. Dust-acoustic waves in dusty plasmas. *Planet Space sci.* **38**, 543-546 (1990).

50. Merlino, R. L., Barkan, A., Thomas, C. and D'Angelo, N. Experiments on waves and instabilities in dusty plasmas. *Plasma Phys. Control Fusion* **39**, A421-A429 (1997).

51. Melandsø, F. Lattice waves in dust plasma crystals. *Phys. Plasmas* 3, 3890-3901 (1996).

52. Morfill, G. E., Thomas H. M. and Zuzic, M. *Advances in Dusty Plasmas* (World Scientific, Singapore, 1997) pp. 99-142.

53. Homann, A., Melzer, A., Petrs, S. and Piel, L. Determination of the dust screening length by laser-excited lattice waves. *Phys. Rev. E* **56**, 7138-7141 (1997).

54. Shukla, P. K. and Silin, V. P. Dust Ion-Acoustic Wave. *Physica Scripta* **45**, 508-508 (1992).

55. Rosenberg, M. Ion- and dust-acoustic instabilities in dusty plasmas. *Planet. Space Sci.* **41**, 229-233 (1993).

56. Rao, N. N. DustCoulomb waves in dense dusty plasmas. *Phys. Plasmas* **6**, 4414-4417 (1999).

57. Barkan, A., Merlino, R. L. and DAngelo, N. Laboratory observation of the dust-acoustic wave mode. *Phys. Plasmas* **2**, 3563-3565 (1995).

58. Pieper, J. B. and Goree, J. Dispersion of Plasma Dust Acoustic Waves in the Strong-Coupling Regime. *Phys. Rev. Lett.* **77**, 3137-3140 (1996).

59. Thompson, C., Barkan, A., DAngelo, N. and Merlino, R. L. Dust acoustic waves in a direct current glow discharge. *Phys. Plasmas* **4**, 2331-2335 (1997).

60. DAngelo, N. Ion-acoustic waves in dusty plasmas. *Planet. Space Sci.* **42**, 507-511 (1994).

61. Barkan, A., DAngelo, N. and Merlino, R. L. Experiments on Ion-Acoustic waves in Dusty Plasmas. *Planet. Space Sci.* **44**, 239-242 (1996).

62. Melandsø, F., Aslaksen, T. K. and Havnes, O. A new damping effect for the Dust-Acoustic Wave. *Planet. Space Sci.* **41**, 321-325 (1993).

63. Melandsø, F., Aslaksen, T. K. and Havnes, O. A Kinetic Model for Dust Acoustic Waves Applied to Planetary Rings. *J. Geophys. Res.* **98**, 13315-13323 (1993).

64. Rao, N. N. Dust-Coulomb and Aust-Acoustic Aave propagation in dense Dusty Plasmas with high fugacity. *Phys. Plasmas* **6**, 795-807 (2000).

65. Shukla, P. K., Yu, M. Y., Bharuthram, R. Linear and Nonlinear Dust Drift Waves. *J. Geophys. Res.* **96**, 21,343-21,346 (1991).

66. Chu, J. H. and I., Lin Coulomb solids and low-frequency fluctuations in RF Dusty Plasmas. *J. Phys. D.* **27**, 296-300 (1994).

67. D'Angelo, N. Coulomb solids and low-frequency fluctuations in RF dusty plasmas. *J. Phys. D. Appl. Phys.* **28**, 1009-1010 (1995).

68. Praburam, G. and Goree, J. Experimental observation of very low-frequency macroscopic modes in a Dusty Plasma,. *Phys. Plasmas* **3**, 1212-1219 (1996).

69. Barkan, A., D'Angelo, N., and Merlino, R. L. Laboratory Experiment on Electrostatic Ion Cyclotron Waves in a Dusty Plasma. *Planetary Space Sci.* **43**, 905-908 (1995).

70. D'Angelo, N. Low-frequency electrostatic waves in Dusty Plasmas. *Planet.*

Space Sci. **38**, 1143-1146 (1990).

71. Chow, V. W. and Rosenberg, H. Electrostatic ion cyclotron instability in Dusty Plasmas. *Planet. Space Sci.*, **43**, 613-618 (1990).

72. Bharuthram, R. and Shukla, P. K. Large amplitude ion-acoustic solitons in a dusty plasma. *Planet. Space Sci.* **40**, 973-977 (1992).

73. Melandsø, F. and Shukla, P. K. Theory of dust-acoustic shocks. *Planetary Space Sci.* **43**, 635-648 (1995).

74. Popel, S. I. *et al.* Shock waves in charge-varying Dusty Plasmas and the effect of Electromagnetic Radiation. *Phys. Plasmas* **7**, 2410-2416 (2000).

75. Mamun, A. A. and Shukla, P. K. The Role of Dust Charge Fluctuations on Nonlinear Dust Ion-Acoustic Waves. *IEEE Trans. Plasma Sci.* **30**, 720-724 (2002).

76. Nakamura, Y., Bailung, H. and Shukla, P. K. Observation of ion-acoustic shocks in a dusty plasma. *Phys. Rev. Lett.* **83**, 16021605 (1999).

77 Verheest, F. Parallel solitary Alfvn waves in warm multi-species beam-plasma systems. Part 2. Anisotropic pressures. *J. Plasma Phys.* 47, 25-37 (1992).

78. Schamel, H., Das, Nilakshi, Rao, N. N. Electrostatic thermal modes in dusty plasmas. *Physics of Plasmas* **8**, 671-674 (2001).

79. Nunomura, S., Samsonov, D. and Goree, J. Transverse Waves in a Two-Dimensional Screened-Coulomb Crystal (Dusty Plasma). *Phys. Rev. Lett.* **84**, 5141-5144 (2000).

80. Pramanik, J., Prasad, G., Sen, A. and Kaw, P.K. Experimental Observations of Transverse Shear Waves in Strongly Coupled Dusty Plasmas. *Phys. Rev. Lett.* **88**, 175001 (2002).

81. Chen, Francis F. *Introduction to Plasma Physics and Controlled Fusion, Volume 1* (Plenum Press, New York, 1984).

82. Rosenberg, M. and Chow, V. W. Farley-Buneman instability in a dusty

plasma. *Planet. Space Sci.* **46**, 103-108 (1998).

83. Rosenberg, M. Effect of charged dust on Hall current instabilities in the E region. *IEEE Trans. Plasma Sci.* **29**, 261-266 (2001).

84. Pandey, B. P. and Lakhina, G. S. Jeans-Buneman instability in a dusty plasma. *Pramana* **50**, 191-204 (1998).

85. Havnes, O. On the motion and destruction of grains in Interstellar clouds. *Astron. Astrophys.* **90**, 106-112 (1980).

86. Havnes, O. A Streaming instability interaction between the Solar wind and Cometary Dust. *Astron. Astrophys.* **193**, 309-312 (1988).

87. Bharuthram, R., Saleem, H. and Shukla, P. K. Two-stream instabilities in unmagnetized dusty plasmas. *Phys. Scr.* **45**, 512-514 (1992).

88. Rosenberg, M. and Shukla, P. K. Iondust two-stream instability in a collisional magnetized dusty plasma. *J. Plasma Phys.* **70**, 317-322 (2004).

89. Merlino, R. L., Current driven Ion Acoustic Instability in a collisional Dusty Plasma, *IEEE Trans. Plasma Sci.* **25**, 60-65 (1997).

90. Annou, R. Current-driven dust Ion-Acoustic Instability in a collisional Dusty Plasma with a variable charge. *Phys. Plasmas* **5**, 2813 (1998).

91. Rosenberg, M. and Krall, N. A. High frequency Drift Instabilities in a Dusty Plasma. *Planetary Space Sci.* **42**, 889-894 (1994).

92. Rosenberg, M. and Krall, N. A. Modified twostream Instabilities in Dusty Space Plasmas. *Planet. Space Sci.* **43**, 619-624 (1995).

93. Kalman, G. J. and Rosenberg, M. Instabilities in strongly coupled plasmas. *J. Phys. A* **36**, 5963-5969 (2003).

94. Merlino, R. L., Barkan, A., Thompson, C. and D'Angelo, N. Laboratory Studies of Waves and Instabilities in Dusty Plasmas. *Phys. Plasmas* **5**, 1607-1614 (1998).

95. D'Angelo, N. Current-driven Electrostatic Dust-Cyclotron instability in a

collisional Plasma. *Planet. Space Sci.* **46**, 1671-1676 (1998).

96. Rosenberg, M. A note on the Electrostatic Dust Cyclotron Instability in a collisional Plasma with warm Dust. *Phys. Scr.* **82**, 035505,1-035505-6 (2010).

97. Rosenberg, M. On Ion-Dust Streaming Instability in a collisional magnetized Plasma with warm Dust. *J. Plasma Phys.*, 1-6, (2010).

98. D'Angelo, N and Song, B. The Kelvin-Helmholtz instability in a dusty plasmas. *Planet Space Sci* **38**, 1577-1579 (1990).

99. Bharuthram, R. and Shukla, P. K. Vortices in non-uniform dusty plasmas. *Planet. Space Sci.* **40**, 647-654 (1992).

100. Rawat, S. P. S. and Rao, N. N. Kelvin Helmholtz instability driven by sheared dust flow. *Planet. Space Sci.* **41**, 137-140 (1993).

101. Singh, S. V., Rao, N. N. and Bharuthram, R. The Kelvin-Helmholtz instability in the presence of dust charge fluctuations. *Phys. Plasmas* **5**, 2477-2479 (1998).

102. Luo, Q. Z., D'Angelo, N. and Merlino, R. L. The KelvinHelmholtz instability in a plasma with negatively Charged Dust. *Phys. Plasmas* **8**, 31-35 (2001).

103. D'Angelo, N. The Rayleigh-Taylor instabilities in Dusty Plasmas. *Planet. Space Sci.* **41**, 469-474 (1993).

104. Jana, M. R., Sen, A. and Kaw, P. K. Influence of grain charge fluctuation dynamics on collective modes in a Magnetized Dusty Plasma. *Phys. Scr.* **51**, 385-389 (1995).

105. Morfill, G. E. *et al.* From Fluid Flows to Crystallization: New Results from Complex Plasmas. *Physica Scripta* **T107**, 59-64 (2004).

106. Morfill, G. E. *et al.* Highly Resolved Fluid Flows: "Liquid Plasmas" at the Kinetic Level. *Phys. Rev. Lett.* **92**, 175004-1-175004-4 (2004).

107. Veeresha, B. M., Das, Amita and Sen, Abhijit RayleighTaylor instability

driven nonlinear vortices in Dusty Plasmas. *Phys. Plasmas* **12**, 044506-1-044506-2 (2005).

108. Sen, S., Fukuyama, A. and Honary, F. Rayleigh Taylor instability in a dusty plasma. *Journal of Atmospheric and Solar-Terrestrial Physics* **72**, 938-942, 2010.

109. Rosenberg, M. and Krall, N.A. Low frequency drift instabilities in a dusty plasma. *Phys. Plasmas* **3**, 644-649 (1996).

110. Rosenberg, M. and Shukla, P. K. Low-frequency Drift instabilities in a strongly magnetized collisional Dusty Plasma. *Plasma Phys. Control. Fusion* **46**, 1807-1814 (2004).

111. Rosenberg, M. and Shukla, P. K. Dust-acoustic-drift wave instability in a space dusty plasma. *J. GeoPhys. Research* **107**, 1492-1497 (2002).

112. D'Angelo, N. Ionization instability in dusty plasmas. *Phys. Plasmas* **4**, 3422-3426 (1997).

113. Shukla, P. K. and Morfill, G. Ionization instability of Dust-Acoustic waves in weakly ionized colloidal Plasmas. *Phys. Lett. A* **216**, 153-156 (1996).

114. D'Angelo, N. Dusty plasma Ionization Instability with ion drag. *Phys. Plasmas* **5**, 3155-3160 (1998).

115. Shukla, P. K., Mirza, A. M., Murtaza, G. and Faria, Jr. R. T. Drift-ballooning modes in the presence of charged dust impurities in a nonuniform rotating magnetoplasma. *Phys. Plasmas* **5**, 167-172 (1998).

116. Piel, A., Klindworth, M., Arp, O., Melzer, A. and Wolter, M. Obliquely Propagating Dust-Density Plasma Waves in the Presence of an Ion Beam. *Phys. Rev. Lett.* **97**, 205009-1-205009-4 (2006).

117. Morfill, G. E. and Thomas, H. Plasma Crystals. *J. Vac. Sci. Technol. A* **14**, 490-495 (1996).

118. Thomas, H. M. and Morfill, G. E. Melting dynamics of a plasma crystal.

Nature **379**, 806-809 (1996).

119. Ikezi, H. Coulomb Solid of Small Particles in Plasmas. *Phys. Fluids* **29**, 1764-1766 (1986).

120. Chu, J. H. and I, Lin Direct Observation of Coulomb Crystals and Liquids in Strongly Coupled RF Dusty Plasmas. *Phys. Rev. Lett.* **72**, 4009-4012 (1994).

121. Thomas, H. *et al.* Plasma Crystal: Coulomb Crystallization in a Dusty Plasma. *Phys. Rev. Lett.* **73**, 652-655 (1994).

122. Hayashi, Y. and Tachibana, K. Mie-Scattering Ellipsometry for Analysis of Particle Behaviors in Processing Plasmas. *Jpn. J. Appl. Phys.* **33**, L804-L478 (1994).

123. Melzer, A., Trottenberg, T. and Piel, A. Experimental Determination of the Charge on Dust Particles forming Coulomb Lattices. *Phys. Lett. A* **191**, 301-308 (1994).

124. I, Lin., Juan, W. T., Chiang, Chih-Hui and Chu, J. H. Microscopic Particle Motions in Strongly Coupled Dusty Plasmas. *Science* **272**, 1626-1628 (1996).

125. Fortov, V. E. *et al.* Crystallization of a dusty plasma in the positive column of a glow discharge. *JETP* **64**, 92-98 (1996).

126. Nunomura, S., Samsonov, D. and Goree, J. Instability of Dust Particles in a Coulomb Crystal due to Delayed Charging. *Phys. Rev. Lett.* **83**, 1970-1973 (1999).

127. Agarwal, A. K. and Prasad, G. Experimental Study of Coulomb crystal formation in Hollow Cathode discharge. *AIP Conf. Proc.* **649**, 261-264 (2002).

128 Quinn, R. A. *et al.* Structural analysis of a Coulomb lattice in a dusty plasma. *Phys. Rev. E* **53**, R2049R2052

129. Morfill, G. E., Thomas, H. M., Konopka, U. and Zuzic, M. The Plasma Condensation: Liquid and Crystalline Plasmas. *Phys. Plasmas* **6**, 1769-1780 (1999).

130. Melzer, A., Homman, A. and Piel, A. Experimental investigation of the melting transition of the plasma crystal. *Phys. Rev. E* **53**, 2757 (1996).

131. Zheng, X. H. and Earnshaw, J. C., Plasma-Dust Crystals and Brownian Motion, *Phys. Rev. Lett.* **75**, 4214-4217 (1995).

132. Hayashi, Y. and Takahashi, K. Structure Changes of Coulomb Crystal in a Carbon Fine-Particle Plasma. *Jpn. J. Appl. Phys.* **36**, 4976-4979 (1997).

133. Nefedov, A. P., Kharpak, A. G., Kharpak, S. A., Petrov, O. F. and Samarayan, A. A. Anomalously high kinetic energy of charged macroparticles in a plasma. *JETP* **85**, 272-275 (1997).

134. Hamaguchi, S., Farouki, R. T. and Dubin, D. H. E. Triple point of Yukawa systems. *Phys. Rev. E* **56**, 4671-4682 (1997).

135. Hammerberg, James E., Lemons, D. S., Murillo, Michael S. and Winske, Dan Molecular dynamics simulations of plasma crystal formation including wake effects. *IEEE Trans. Plasma Sci.* **29**, 247-255 (2001).

136. Khrapak, S. *et al.* Compressional waves in complex Dusty Plasmas under microgravity conditions. *Phys. Plasmas* **10**, 1-4 (2003).

137. Konopka, U. *et al.* Rigid and differential plasma crystal rotation induced by magnetic fields. *Phys. Rev. E* **61**, 1890 (2000).

138. Sato, N., Uchida, G., Kaneko, T., Shimizu, S. and Lizuka, S. Dynamics of fine particles in magnetized plasmas. *Phys. Plasmas* **8**, 1786-1790 (2001).

139. Uchida, G., Konopka, U. and Morfill, G. Wave Dispersion Relation of Two-Dimensional Plasma Crystals in a Magnetic Field. *Phys. Rev. Lett.* **93**,155002-1-155002-4 (2004)

140. Hou, L. J., Wang, Y. N. and Mišković, Z. L. Two-dimensional radio-frequency sheath dynamics over a nonflat electrode with perpendicular magnetic field. *Phys. Plasmas* **11**, 4456-4461 (2004).

141. Hou, L. J., Wang, Y. N. and Mišković, Z. L. Formation and rotation

of two-dimensional Coulomb crystals in magnetized complex plasma. *Phys. Plasmas* **12**, 042104-1-042104-9 (2005).

142. Law, D. A., Steel, W. H., Annaratone, B. M. and Allen, J. E. Probe-Induced Particle Circulation in a Plasma Crystal. *Phys. Rev. Lett* **80**, 4189-4192 (1998).

143. Arp, Oliver, Block, Dietmar, Piel, Alexander and Melzer, A. Dust Coulomb Balls: Three-Dimensional Plasma Crystals. *Phys. Rev. Lett.* **93**, 165004-1-165004-4 (2004)

144. Baiko, D. A. Coulomb crystals in the magnetic field. *Phys. Rev. E* **80**, 046405-1-046405-11 (2009).

145. Mohideen, U., Rahman, H. U., Smith, M. A., Rosenberg, M. and Mendis, D. A. Intergrain Coupling in Dusty-Plasma Coulomb Crystals. *Phys. Rev. Lett.* **81**, 349-352 (1998).

146. Lee, H. C. and Chen, D. Y. Phase diagram of crystals of dusty plasma. *Phys. Rev. E* **56**, 4596-4607 (1997).

147. Nambu, M., Vladimirov, S. V. and Shukla, P. K. Attractive forces between charged particulates in plasmas. *Phys. Lett. A* **230**, 40-42 (1995).

148. Shukla, P. K., and Rao, N. N. Coulomb crystallization in Colloidal Plasmas with streaming ions and dust grains. *Phys. Plasmas* **3**, 1770-1772 (1996).

149. Hou, L. J., Shukla, P. K. and Piel, A. Effect of Overlapping Debye Spheres on Structures of 2D Dusty Plasmas. *Phys. Lett. A* **373**, 458-461 (2009).

150. Baruah, Swati and Das, Nilakshi A comparative study between effects of Shadowing potential and ODS on Coulomb crystal formation. *J. Plasma Phys.*, doi:10.1017/S0022377810000723 (2010) .

151. Kaw, Predhiman and Singh, R. Collisional Instabilities in a Dusty Plasma with Recombination and Ion-Drag Effects. *Phys. Rev. Lett.*79, 423-426 (1997).

152. Ivlev, A. V., Samsonov, D., Goree, J., Morfill, G. and Fortov, V. E. Acoustic modes in a collisional dusty plasma. *Phys Plasmas* **6**, 741-750 (1999).

153. Shukla, P. K. and Mamun, A. A. Solitons, shocks and vortices in dusty plasmas. *New J. Phys.* **5**, 17.1-17.37 (2003).

154. Benkadda, S. and Tsytovich, V. N. Modulational instability in dusty plasmas. *Phys. Plasmas* **2**, 2970-2974 (1995).

155. Benkadda, S., Gabbai, P, Tsytovich, V. N and Verga, A. Nonlinearities and instabilities of dissipative drift waves in dusty plasmas. *Phy. Rev. E* **53**, 2717-2725 (1996).

156. Shukla, P. K. and Rosenberg, M. Drift wave excitation in a collisional dusty magnetoplasma with multi-ion species. *J. Plasma Phys.* **75**, 153158 (2009).

157. Alder, B. J. and Wainwright, T. E. Studies in molecular dynamics. I. General methods. *J. Chem. Phys.* **31**, 459-466 (1959).

158. Frankel, Daan and Smit, Berend *Understanding Molecular Simulation from Algorithms to Applications* (Academic Press, USA, 1996).

159. McCammon, J., Andrew, Gelin, Bruce R. and Karplus, Martin Dynamics of folded proteins. *Nature* **267**, 585-590 (1977).

160. Vladimirov, S. V., Maiorov, S. A., Yu, M. Y. and L. Stenflo Mechanical model for the plasma maser effect. *Phys. Rev. E* **63**, 067401-1-067401-4 (2001).

161. Perez, D. and Lewis, L. J. Ablation of solids under femtosecond laser pulses. *Phys. Rev. Lett.* **89**, 255504-1-255504-4 (2002).

162. Breu, A. P. J., Ensner, H. M., Kruelle, C. A. and Rehberg, I. Reversing the Brazil-Nut Effect: Competition between Percolation and Condensation. *Phys. Rev. Lett.* **90**, 014302-1-014302-3 (2003).

163. Rapaport, D. C. *The art of Molecular Dynamics Simulation* (Cambridge University Press, USA, 1995).

164 Warrier, Manoj Molecular Dynamics Simulations. http://www.ipr.res.in/ manoj/ (2007).

165. Zuzic, M., Thomas, H. and Morfill, G. E. Wave propagation and damping

in plasma crystals. *J. Vac. Sci. Technol. A*, **14**, 496-500 (1996).

166. Thomas, H. and Morfill, G. E. Solid/liquid/gaseous phase transitions in plasma crystals. *J. Vac. Sci. Technol. A*, **14**, 501-505, (1996).

167. Tsytovich, V. N., Khodataev, Y. K. and Bingham, R. Formation of a Dust Molecule in Plasmas as a first step to Supper-Chemistry, Comments Plasma. *Commun. Plasma Phys. Control. Fusion*, **17**, 249-264, (1996).

168. Ignatov, A. M. Lesage gravity in dusty plasmas. *Plasma Phys. Rep.* **22**, 585 - 589 (1996).

169. Khodataev, Ya. K., Bingham, R., Tarakanov, V. P. and Tsytovich, V. N. Mechanisms for the interaction of dust particles in plasmas. *Plasma Phys. Reports* **22**, 932-942 (1996).

170. Samsonov, D., Ivlev, A. V., Morfill, G. E. and Goree, J. Long-range attractive and repulsive forces in a two-dimensional Complex (Dusty) Plasma. *Phys. Rev. E* **63**, 025401-1 - 025401-4 (2001).

171. Nambu, M. and Akama, H. Attractive potential between resonant electrons. *Phys. Fluids* **28**, 2300-2301 (1985).

172. Nambu, M. and Salimullah, M. Three-dimensional wake potential in a flowing magnetized plasma. *Phys. Lett. A* **286**, 418-422 (2001).

173. Vladimirov, S. V. and Nambu, M. Attraction of charged particulates in plasmas with finite flows. *Phys. Rev. E* **52** R2172-R2174 (1995).

174. Takahashi, K., Oishi, T., Shimomai, K., Hayashi, Y. and Nishino, S. Analyses of attractive forces between particles in Coulomb crystal of dusty plasmas by optical manipulations. Phys. Rev. E. 58, 7805-7811 (1998).

175. Vlamidimirov, S. V. and Ishihara, O. On plasma crystal formation. *Phys. Plasmas* **3**, 444-446 (1996).

176. Ishihara, O. and Vlamidimirov, S. V. Wake potential of a Dust grain in a Plasma with ion flow. *Phys. Plasmas* **4**, 69-74 (1997).

177. Nasim, M. H., Mirza, A. M., Murtaza, G. and Shukla, P. K. Wake-field excitations in a multi-component Dusty Plasma. *Physica Scripta* **T89**, 191-194 (2001).

178. Ali, S., Nasim, M. H. and Murtaza, G. Attractive wake field formation due to an array of dipolar projectiles in a multi-component dusty plasma. *Phys. Plasmas* **10**, 941-947 (2003).

179. Bingham, R. and Tsytovich, V. N. New mechanism of dust growth and gravitation-like instabilities in astrophysical plasmas. *Astrophys. Astron.* **376**, L43-L47 (2001).

180. Bingham, R., Tsytovich, V. N. and Resendes, D. P. *Dust Plasma Interaction in Space* (New York: Nova Science, 2002).

181. Shukla, P. K. Interaction potentials in a plasma with streaming ions and non-spherical dust rods. *Phys. Lett. A* **289**, 89-92 (2001).

182. Shukla, P. K. Dipole-oscillons generating wWakefields in a Dusty Plasma. *Phys. Plasmas* **8**, 5043-5044 (2001).

183. Lapenta, G. Dipole Moments on Dust Particles Immersed in Anisotropic Plasmas. *Phys. Rev. Lett.* **75**, 4409-4412 (1995).

184. Lapenta, G. Simulation of Charging and shielding of Dust particles in drifting Plasmas. *Phys. Plasmas* **6**, 1442-1447 (1999).

185. Resendes, D. P. Dipolar interaction in a colloidal plasma. *Phys. Rev. E* **61**, 793-800 (2000).

186. Tskhakaya, D. D. and P. K. Shukla Dipole-dipole interactions between dust grains in plasmas. *JETP* **98**, 53-61 (2004).

187. Blum, J. *et al.* Growth and Form of Planetary Seedlings: Results from a Microgravity Aggregation Experiment. *Phys. Rev. Lett.* **85**, 2426-2429 (2000).

188. Lampe, M., Joyce, G., Ganguli, G. and Gavrishchaka Interactions between dust grains in a dusty plasma. *Phys. Plasmas* **7**, 3851-3861 (2000).

189. Totsuji, H., Kishimoto, T., Totsuji, C. and Tsuruta, K. Yukawa Mixtures with and without Gravity. *Physica Scripta* **T89**, 117-121 (2001).

190. Pieper J B, Goree J and Quinn R A Three-dimensional structure in a crystallized dusty plasma. *Phys. Rev. E* **54**, 5636-5640 (1996).

191. Sato, N., Uchida, G., Ozaki, R. and Lizuka, S. *Phys of Dusty Plasmas* (American Institute of Physics, New York, 1997).

192. Totsuji, H., Kishimoto, T., Inoue, Y., Totsuji, C. and Nara, S. Yukawa Sytem (Dusty Plasma) in One-Dimensional External Fields. *Phys. Lett. A* **221**, 215-219 (1996).

193. Resendes, D. P., Mendonca, J. T. and Shukla, P. K. Formation of dusty plasma molecules. *Phys. Lett. A* **239**, 181-186 (1998).

194. Shukla, P. K. and Eliasson, B. Colloquium: Fundamentals of dust-plasma interactions. *Rev. Mod. Phys.* **81**, 25-44 (2009).

195. Melzer, A., Schweigert, V. A. and Piel, A. Transition from Attractive to Repulsive Forces between Dust Molecules in a Plasma Sheath. *Phys. Rev. Lett.* **83**, 3194-3197 (1999).

196. Konopka, U., Morfill, G. E. and Ratke, L. Measurement of the Interaction Potential of Microspheres in the Sheath of a rf Discharge. *Phys. Rev. Lett.* **84**, 891-894 (2000).

197. Ramazanov, T. S. *et al.* Effective interaction potential of dust particles in a plasma from experimental pair correlation functions. *J. Plasma Physics* **76**, 57-66 (2010).

198. Tsytovich, V. N. New physical concept of the formation of dust crystals. *JETP Lett.* **81**, 448-451 (2005).

199. Ishihara, O. and Sato, Noriyoshi Attractive force on like charges in a complex plasma. *Phys. Plasmas* **12**, 070705-070705-3 (2005).

200. Tsytovich, V. N. *et al.* From plasma crystals and helical structures towards

inorganic living matter. *New J. Phys.* **9**, 263-1-263-11 (2007).

201. Winget, D. E. The Physics of Crystallization From Globular Cluster White Dwarf Stars in NGC 6397 *et al. Astrophys. J.* **693**, L6-L10 (2009).

202. Baiko, D. A., Kaminker, A. D., Potekhin, A. Y. and Yakovlev, D. G. Ion Structure Factors and Electron Transport in Dense Coulomb Plasmas. *Phys. Rev. Lett.* **81**, 5556-5559 (1998).

203. Chugunov, A. I. and Yakovlev, D. G. Shear Viscosity and Oscillations of Neutron Star Crusts. *Astron. Rep.* **49**, 724-738 (2005).

204. Shukla, P. K. and Mendonca, J. T. Dust Quasiatom in a Magnetoplasma. *Physica Scripta* **T113**, 82-83 (2004).

205. Liu, Sonbfen, Wang, Xin, Hu, Beilai, Wang, Long and Liu, Yanhong The structure of a two-dimensional magnetic Dusty Plasma. *J. Phys. A : Math. Gen.* **38**, 3057-3063 (2005).

206. Kaw, P. K., Nishikawa, K. and Sato, N. Rotation in collisional strongly coupled dusty plasmas in a magnetic field. *Phys. Plasmas* **9**, 387-390 (2002).

207. Krasheninnikov, S. I., Shevchenko, V. I. and Shukla, P. K. Spinning of a charged dust particle in a magnetized plasma. *Phy. Lett. A* **361**, 133-135 (2007).

208. Dzlieva, E. S., Ivanov, A. Yu., Karasev, V. Yu. and Éǐkhval'd, A. I. On the possibility of Phase transitions in Dusty Plasma structures in a glow discharge under the action of a magnetic field. *Optics and Spectroscopy* **101**, 816-821 (2006).

209. Schweigert, V. A., Schweigert, I. V., Melzer, A., Homann, A. and Piel, A. Plasma Crystal Melting: A Nonequilibrium Phase Transition. *Phys. Rev. Lett.* **80**, 5345-5348 (1998).

210. Vaulina, O. S., Vladimirov, S. V., Petrov, O. F. and Fortov, V. E. Criteria of Phase Transitions in a Complex Plasma. *Phys. Rev. Lett.* **88**, 245002-1 - 245002-4 (2002).

211. Joyce, Glenn, Lampe, Martin and Ganguli, Gurudas Instability-Triggered Phase Transition to a Dusty-Plasma Condensate. *Phys. Rev. Lett.* **88**, 095006-1 - 095006-4 (2002).

212. Sato, N., Uchida, G., Kamimura, T. and Lizuka, S. *In Physics of Dusty Plasmas* (American Institute of Physics, New York, 1998).

213. Sato, N., Uchida, G., Ozaki, R. and Kamimura, T. *In Frontiers in Dusty Plasmas* (Elsevier Sciience, New York, 2000).

214. Cheung, Felix, Samarian, Alx and James, Brian The rotation of planar-2 to planar-12 dust clusters in an axial magnetic field. *New J. Phys.* **5**, 75.1 - 75.15 (2003).

215. Fortov, V. E., Nefedov, A. P. and Lakhno, V. D. Dusty molecules in a magnetic fields. *Phys. Lett. A* **250**, 149-151 (1998).

216. Yaroshenko, V. V., Morfill, G. E., Samsonov, D. and Vladimirov, S. V. Mutual interactions of magnetized particles in complex plasmas. *New. J. Phys.* **5**, 18.1-18.8 (2003).

217. Nambu, M. and Nitta, H. On the Shukla-Nambu-Salimullah potential in Magnetized Plasma. *Phys. Lett. A* **300**, 82-85 (2002).

218. Tsytovich, V. N. and Koller, J. Collective Dust-Dust Attraction in Strong Magnetic Field. *Contrib. Plasma Phys.* **44**, 317-326 (2004).

219. Baruah, Swati and Das, Nilakshi The effect of magnetic field on the structure of Coulomb Crystal in Dusty Plasma. *Phys. Plasmas.* **17**, 073702-1-073702-5 (2010).

220. Karasev, V. Yu., Dzlieva, E. S., Ivanov, A. Yu. and Eikhvald, A. I. Rotational motion of Dusty structures in glow discharge in Longitudinal magnetic field. *Phys. Rev. E* **74**, 066403-1 - 066403-12 (2006).

Appendix A

Appendix

The governing equations for dust particles are

$$m_d n_d \left(\frac{\partial \vec{v}_d}{\partial t} + \vec{v_d}.\nabla \vec{v_d} \right) = n_d Q_d \left(\vec{E} + \vec{v_d} \times \vec{B_0} \right) - \nabla \vec{p}_d - \left(\vec{v}_d - \vec{v}_n \right) m_d n_d \nu_{dn} \tag{A.0.1}$$

$$\frac{\partial n_d}{\partial t} + \nabla \left(n_d \vec{v_d} \right) = 0 \tag{A.0.2}$$

where, $m_d, n_d, \vec{v_d}$ are the mass, density and velocity of dust particles, p_d is the dust pressure, whereas ν_{dn} is the collision frequency of dust particles with the neutrals of mass m_n, density n_n and velocity v_n.

Dust-neutral collision frequency is taken as

$$\nu_{dn} = (4\pi/3)\, r_d^2 v_n n_n \left(m_n/m_d \right) \tag{A.0.3}$$

Diamagnetic drift is

$$\vec{v}_{dD} = -\frac{1}{B_0} \frac{T_d}{Q_{d0} n_{d0}} \frac{\partial n_{d0}}{\partial x} \hat{y}$$

Governing equations for ions

$$m_i n_i \left(\frac{\partial \vec{v}_i}{\partial t} + \vec{v_i}.\nabla \vec{v_i} \right) = n_i e \left(\vec{E} + \vec{v_i} \times \vec{B_0} \right) - \left(\vec{v}_i - \vec{v}_n \right) m_i n_i \nu_{in} \tag{A.0.4}$$

where, ion-neutral collision frequency is

$$\nu_{in} = n_n \sigma_{in} c_i \tag{A.0.5}$$

while σ_{in} is the ion-neutral collisional cross-section, and

$$c_i^2 = \frac{K_B T_i}{m_i}$$

and n_n is the neutral density.

Continuity equation for ion is

$$\frac{\partial n_i}{\partial t} + \nabla\left(n_i \vec{v_i}\right) = 0 \qquad (A.0.6)$$

Governing equations for electrons

$$m_e n_e \left(\frac{\partial \vec{v}_e}{\partial t} + \vec{v_e}.\nabla \vec{v_e}\right) = -n_e e\left(\vec{E} + \vec{v_e} \times \vec{B_0}\right) - \vec{\nabla} p_e \qquad (A.0.7)$$

$$\frac{\partial n_e}{\partial t} + \nabla\left(n_e \vec{v_e}\right) = 0 \qquad (A.0.8)$$

Governing equations for neutrals

$$m_n n_n \left(\frac{\partial \vec{v}_n}{\partial t} + \vec{v_n}.\nabla \vec{v_n}\right) = -\left(\vec{v}_n - \vec{v}_d\right) m_n n_n \nu_{dn} - \left(\vec{v}_n - \vec{v}_i\right) m_i n_i \nu_{in} \qquad (A.0.9)$$

$$\frac{\partial n_n}{\partial t} + \nabla\left(n_n \vec{v_n}\right) = 0 \qquad (A.0.10)$$

Charging equations

$$I_i = +\pi r_d^2 e \sqrt{\frac{8T_i}{\pi m_i}} n_i \left[1 - \frac{e(\Phi_{f0} - \Phi)}{K_B T_i}\right] \qquad (A.0.11)$$

$$I_e = -\pi r_d^2 e \sqrt{\frac{8T_e}{\pi m_e}} n_e exp\left(\frac{e(\Phi_{f0} - \Phi)}{K_B T_e}\right) \qquad (A.0.12)$$

$$\frac{dQ_d}{dt} = I_e + I_i \qquad (A.0.13)$$

where, Φ_{f0} is floating potential, Φ is plasma surface potential.

After linearization, perturbed quantities are substituted into linearized Poisson's equation

$$\nabla^2\Phi_1 = 4\pi[en_{e1} + Q_{d0}n_{d1} + Q_{d1}n_{d0} - en_{i1}] \tag{A.0.14}$$

The perturbed dust number density can be expressed as :

$$n_{d1} = \left(Q_{D2}E_{1y} + Q_{D3}E_{1z} + Q_{D4}Q_{d1}\right)/Q_{D1} \tag{A.0.15}$$

Where,

$$Q_{D1} = (\omega - in'_{d0}B_{d1x} + n_{d0}k_yB_{dy} + n_{d0}k_zB_{dz})$$

$$Q_{D2} = in'_{d0}G_{d2x}(\omega) - \frac{n_{d0}k_yC_{dy}}{A_{dy}}$$

$$Q_{D3} = in'_{d0}D_{d1x} - \frac{n_{d0}k_yD_{dy}}{A_{dy}} - n_{d0}k_zD_{dz}$$

$$Q_{D4} = -\frac{in'_{d0}E_{0x}G_{d1x}}{m_d} + \frac{n_{d0}k_yE_{0x}}{m_dA_{dy}}$$

Where,

$$B_{d1x} = \frac{1}{A_{dx}(\omega)}\left[B_{dx} + \frac{B_{dy}(\omega)}{A_{dy}(\omega)}Y_{dx}(\omega) + Z_{dx}(\omega)B_{dz}(\omega)\right]$$

$$B_{dx} = -\frac{Q_{d0}E_{0x}}{m_dn_{d0}} - i\frac{k_y\omega_{cd}T_d}{\omega'_dm_dn_{d0}} - \frac{\omega_{cd}}{\omega'_d}\frac{\nu_{dn}}{n_{d0}}(v_{d0y} - v_{n0y})$$

$$B_{dy} = \frac{ik_yT_d}{m_dn_{d0}} + \frac{\nu_{dn}}{n_{d0}}(v_{d0y} - v_{n0y}) + \frac{(\omega_{cd} - \nu_{dn}p_{nx})}{A_{dx}(\omega)}\left(B_{dx}(\omega) + Z_{dx}B_{dz}(\omega)\right)$$

$$B_{dz} = \frac{ik_zT_d(\nu_{dn} + ik_yv_{n0y})}{m_dn_{d0}\left[\nu_{dn}^2 - (\nu_{dn} + ik_yv_{doy})(\nu_{dn} + ik_yv_{n0y})\right]}$$

$$A_{dx} = \frac{1}{\omega'_d}\left(\omega'^2_d + \left(\omega_{cd}^2 - \nu_{dn}\omega_{cd}p_{nx}\right) - \omega'_d\nu_{dn}r_{nx}\right)$$

$$A_{dy} = -\omega'_d - \frac{\omega_{cd} - \nu_{dn}p_{nx}}{A_{dx}}Y_{dx} + \nu_{dn}p_{ny}$$

$$Y_{dx} = \omega_{cd}p_{ny}\frac{\nu_{dn}}{\omega'_d} + \nu_{dn}r_{ny}$$

$$Z_{dx} = \frac{\omega_{cd}\nu_{dn}}{\omega'_d}p_{nz} + \nu_{dn}r_{nz}$$

$$\omega'_d = \nu_{dn} + ik_yv_{d0y}$$

$$p_{nx} = -\frac{A_1 D_n}{ik_y v_{n0y} + A_{n1}} - D_{ny}$$

$$p_{ny} = -\frac{B_n A_1}{ik_y v_{n0y} + A_{n1}} + B_{ny}$$

$$p_{nz} = -\frac{A_1 B'_{nz}}{ik_y v_{n0y} + A_{n1}}$$

$$r_{nx} = -\frac{A_2 D_n}{ik_y v_{n0y} + A_3} + D_{nx}$$

$$r_{ny} = -\frac{A_2 B_n}{ik_y v_{n0y} + A_3} + B_{nx}$$

$$r_{nz} = -\frac{A_2 B'_{nz} B_{nz}}{ik_y v_{n0y} + A_3}$$

$$A_1 = (\nu_{dn} v_{d0y} - \nu_1 v_{n0y}) \left[X_n X_{n1} \left(\nu_{in}^2 + \omega_{ci}^2 \right)^2 - \omega_{ci}^2 \nu_{in}^4 \right]$$

$$A_2 = \frac{\nu_{in}^2 \omega_{ci} (\nu_{d0} v_{d0y} - \nu_1 v_{n0y})}{X_n X_{n1} n_{n0} (\nu_{in}^2 + \omega_{ci}^2)}$$

$$A_3 = \frac{A_{n1}}{X_n^2 X_{n1} n_{n0} (\nu_{in}^2 + \omega_{ci}^2)^2}$$

$$X_n = \nu_{dn} + ik_y v_{noy} + \frac{\nu_{in} \omega_{ci}^2}{(\nu_{in}^2 + \omega_{ci}^2)}$$

$$X_{n1} = \nu_1 + ik_y v_{n0y} - \frac{\nu_{in}^3}{(\nu_{in}^2 + \omega_{ci}^2)} + \frac{\nu_{in}^4 \omega_{ci}^2}{X_n (\nu_{in}^2 + \omega_{ci}^2)^2}$$

$$B_{nx} = \frac{\nu_{dn}}{X_n X_{n1}} \frac{\nu_1^2 \omega_{ci}^2}{(\nu_{in}^2 + \omega_{ci}^2)}$$

$$B_{ny} = \frac{\nu_{dn}}{X_n} \left[1 - \frac{\nu_1^2 \nu_{in}^2 \omega_{ci}^3}{X_n X_{n1} (\nu_{in}^2 + \omega_{ci}^2)^2} \right]$$

$$B_n = n'_{n0} B_{nx} + i n_{n0} k_y B_{ny}$$

$$B_{nz} = \frac{\nu_{dn}}{\nu_{dn} + ik_y v_{n0y}}$$

$$B'_{nz} = ik_z n_{n0} B_{nz}$$

$$\nu_1 = \nu_{dn} + \nu_{in}$$

$$A_{n1} = (\nu_{d0} v_{d0y} - \nu_1 v_{n0y}) \nu_{in}^2 \left[\left(1 + \frac{\omega_{ci}^2}{\nu_{in}^2} \right) X_n \left(n'_{n0} \omega_{ci} + ik_y n_{n0} X_{n1} \left(1 + \frac{\omega_{ci}^2}{\nu_{in}^2} \right) \right) - ik_y n_{n0} \omega_{ci}^2 \nu_{in}^2 \right]$$

$$D_n = \frac{\nu_{dn}}{X_n}\left(n'_{n0} - \frac{\imath n_0 k_y \nu_{in}^2 \omega_{ci}}{X_n(\nu_{in}^2 + \omega_{ci}^2)}\right)$$

$$D_{nx} = \frac{\nu_{dn}}{X_n}$$

$$D_{ny} = -\frac{\nu_{dn}\nu_{in}^2\omega_{ci}}{X_n^2(\nu_{in}^2 + \omega_{ci}^2)}$$

$$G_{d2x} = \frac{1}{A_{dx}(\omega)}\left[C_{dx}(\omega) + Y_{dx}\frac{C_{dy}(\omega)}{A_{dy}(\omega)}\right]$$

$$C_{dx}(\omega) = -\frac{\omega_{cd}Q_{d0}}{\omega'_d m_d} + \frac{e\nu_{dn}\omega_{cd}}{m_i\omega'_d}\left[C_{ny} - \frac{C_{nxy}A_1}{\imath k_y v_{n0y} + A_{n1}}\right] + \frac{e\nu_{dn}}{m_i}\left[C_{nx} - \frac{A_2 C_{nxy}}{\imath k_y v_{n0y} + A_3}\right]$$

$$C_{dy}(\omega) = \frac{Q_{d0}}{m_d} - \nu_{dn}\frac{e}{m_i}q_{ny} + \frac{(\omega_{cd} - \nu_{dn}p_{nx})}{A_{dx}}C_{dx}(\omega)$$

$$G_{d1x} = \frac{\left[1 + \frac{Y_{dx}}{A_{dy}}\right]}{A_{dx}}$$

$$D_{d1x} = \frac{1}{A_{dx}}\left[D_{dx} + Y_{dx}\frac{D_{dy}}{A_{dy}} + Z_{dx}D_{dz}\right]$$

$$D_{dx} = \frac{e}{m_i}\nu_{dn}S_{nz} + \frac{\omega_{cd}\nu_{dn}e}{m_i\omega'_d}q_{nz}$$

$$D_{dz} = \frac{\frac{Q_{d0}}{m_d}\left(\nu_{dn} + \imath k_y v_{n0y}\right) - \frac{e}{m_i}\nu_{dn}}{\nu_{dn}^2 - \left(\nu_{dn} + \imath k_y v_{d0y}\right)\left(\nu_{dn} + \imath k_y v_{d0y}\right)}$$

$$D_{dy} = \frac{(w_{cd} - \nu_{dn}p_{nx})}{A_{dx}}\left(Z_{dx}D_{dz} + D_{dx}\right) - \frac{\nu_{dn}}{em_i}q_{nz} - \nu_{dn}p_{nz}D_{dz}$$

$$Z_{dx} = \nu_{dn}r_{nz} + \frac{\nu_{dn}\omega_{cd}}{\omega'_d}p_{nz}$$

$$C_{nx} = \frac{\nu_{in}\omega_{ci}}{X_{n1}\left(\nu_{in}^2 + \omega_{ci}^2\right)}\left[1 + \frac{\nu_{in}^3}{X_n\left(\nu_{in}^2 + \omega_{ci}^2\right)}\right]$$

$$C_{ny} = \frac{\nu_{in}^2}{X_n\left(\nu_{in}^2 + \omega_{ci}^2\right)}\left[1 - \frac{\nu_{in}\omega_{ci}^2}{X_{n1}\left(\nu_{in}^2 + \omega_{ci}^2\right)}\left(1 + \frac{\nu_{in}^3}{X_n(\nu_{in}^2 + \omega_{ci}^2)}\right)\right]$$

$$C_{nxy} = n'_{n0}C_{nx} + \imath k_y n_{n0} C_{ny}$$

$$n'_{n0} = \tfrac{dn_{n0}}{dx}$$

$$
\begin{aligned}
q_{ny} &= -\frac{A_1 C_{nxy}}{\imath k_y v_{n0y} + A_{n1}} + C_{ny} \\
q_{nz} &= -\frac{A_1 C'_{nz}}{\imath k_y v_{n0y} + A_{n1}} \\
S_{nz} &= -\frac{A_2}{\imath \omega_n + A_3}\left[C'_{nz} + C_{nz} B'_{nz}\right] \\
C_{nz} &= \frac{1}{\nu_{dn} + \imath k_y v_{n0y}} \\
C'_{nz} &= \imath k_z n_{n0} \frac{e E_{1z}}{m_\imath (\nu_{dn} + \imath k_y v_{n0y})} \\
\omega_{c\imath} &= \frac{e B_0}{m_\imath} \\
\omega_{cd} &= \frac{Q_{d0} B_0}{m_d}
\end{aligned}
$$

Perturbed dust charge is given as

$$
Q_{d1} = \frac{1}{X}\left[A\left(1 + a_a Q_{d0}\right) n_{e1}\right] - \frac{B}{X}\left(1 - b_b Q_{d0}\right) n_{\imath 1} \tag{A.0.16}
$$

$$
\begin{aligned}
X &= \imath\omega - A a_a n_{e0} - B b_b n_{\imath 0} \\
A &= \pi r_d^2 e \left(\frac{8 T_e}{\pi m_e}\right)^{1/2} \\
B &= \pi r_d^2 e \left(\frac{8 T_\imath}{\pi m_\imath}\right)^{1/2} \\
a_a &= \frac{e}{c T_e} \\
b_b &= \frac{e}{c T_\imath}
\end{aligned}
$$

And

$$
n'_{d0} = \tfrac{\partial n_{d0}}{\partial x}
$$

The perturbed electric field is

$$
E_1 = E_{1y}\hat{y} + E_{1z}\hat{z} = \left(-\imath k_y \hat{y} - \imath k_z \hat{z}\right)\Phi_1
$$

The expression of perturbed electron number density is as follows:

$$n_{e1} = \frac{1}{A_{e1}}\left[C_{e1}E_{1y} + D_{e1}E_{1z}\right] \tag{A.0.17}$$

Where,

$$A_{e1} = -\left[\imath\omega_{e0} + \frac{n'_{e0}}{A_{ex}}B_{ex} + \imath k_y n_{e0} B_{ey}\right] + \imath k_z n_{e0} B_{ez}$$

$$D_{e1} = -\imath k_z n_{e0} D_{ez}$$

$$C_{e1} = -\left[\frac{n'_{e0}C_{ex}}{A_{ex}} + \imath k_y n_{e0} C_{ey}\right]$$

$$A_{ex} = m_e^2 \Omega_e^2 \left(1 + k_y^2 b_e^2\right)$$

Here,

$$b_e^2 = \frac{v_{e0y}^2}{\Omega_e^2}$$

and

$$n'_{e0} = \frac{\partial n_{eo}}{\partial x}$$

where, $\Omega_e = \frac{eB_0}{m_e}$ is the electron cyclotron frequency.

$$B_{ex} = \frac{\imath\omega_{e0}m_e}{n_{e0}}\left[eE_{0x} - T_e/b_e\right]$$

$$B_{ey} = \frac{\imath\Omega_e B_{ex}}{\omega_{e0}A_{ex}} - \frac{k_y T_e}{\omega_{e0} m_e n_{e0}}$$

$$B_{ez} = -\frac{k_z T_e}{\omega_{e0} m_e n_{e0}}$$

$$C_{ex} = -e^2 B_0$$

$$C_{ey} = \frac{ie}{m_e \omega_{e0}} + \frac{\imath\Omega_e C_{ex}}{\omega_{e0} A_{ex}}$$

$$D_{ez} = \frac{\imath e}{m_e \omega_{e0}}$$

The expression of perturbed ion number density is as follows:

$$n_{\imath 1} = \frac{1}{\omega}\left[Q_{\imath 1} n_{d1} + Q_{\imath 2} E_{1y} + Q_{\imath 3} E_{1z} + Q_{\imath 4} Q_{d1}\right] \tag{A.0.18}$$

Where,

$$Q_{\imath 1} = k_y n_{\imath 0} B_{\imath y} + k_z n_{\imath 0} B_{\imath z}$$

$$Q_{\imath 2} = k_y n_{\imath 0} C_{\imath y}$$

$$Q_{\imath 3} = k_y n_{\imath 0} D_{\imath y} + k_z n_{\imath 0} D_{\imath z}$$

$$Q_{\imath 4} = k_y n_{\imath 0} G^1_{\imath y}$$

And

$$C_{\imath x} = \frac{e\omega_{c\imath}}{m_\imath\left(\omega_\imath^2 + \omega_{c\imath}^2\right)} + \frac{a_{\imath x}}{A_{dx}}\left[C_{dx} + Y_{dx}\frac{C_{dy}}{A_{dy}}\right] + \frac{a_{\imath y}C_{dy}}{A_{dy}} + \frac{\nu_{\imath n}e}{m_\imath\left(\omega_\imath^2 + \omega_{c\imath}^2\right)}\left(q_{ny}\omega_{c\imath} + S_{ny}\omega_\imath\right)$$

$$D_{\imath x} = \frac{a_{\imath x}}{A_{dx}}\left(D_{dx} + Y_{dx}\frac{D_{dy}}{A_{dy}} + D_{dz}Z_{dx}\right) + \frac{a_{\imath y}D_{dy}}{A_{dy}} + a_{\imath z}D_{dz} + \frac{e\nu_{\imath n}\left(q_{nz}\omega_{c\imath} + \omega_\imath S_{nz}\right)}{m_\imath\left(\omega_\imath^2 + \omega_{c\imath}^2\right)}$$

$$B_{\imath y} = -\frac{\omega_{c\imath}}{\omega_\imath}B_{\imath x} + \frac{\nu_{\imath n}P_{n1x}}{\omega_\imath}$$

$$C_{\imath y} = \frac{e}{m_\imath\omega_\imath} - \frac{\omega_{c\imath}}{\omega_\imath}C_{\imath x} + \frac{\nu_{\imath n}P_{n3x}}{\omega_\imath}$$

$$D_{\imath y} = -\frac{\omega_{c\imath}}{\omega_\imath}D_{\imath x} + \frac{\nu_{\imath n}P_{n4x}}{\omega_\imath}$$

$$G^1_{\imath y} = -\frac{\omega_{c\imath}}{\omega_\imath}G^1_{\imath x}\frac{E_{0x}}{m_d} + \frac{\nu_{\imath n}}{\omega_\imath}P_{n2x}$$

$$B_{\imath z} = \frac{\nu_{\imath n}}{\omega_\imath}B_{nz}B_{dz}$$

$$D_{\imath z} = \frac{e}{\omega_\imath m_\imath} + \frac{\nu_{\imath n}}{\omega_\imath}D_{dz} + \frac{\nu_{\imath n}}{\omega_\imath}C_{nz}\frac{e}{m_\imath}$$

Assumption: $\omega_\imath = \nu_{\imath n} - \imath\omega \simeq \nu_{\imath n}$ for $\omega << \nu_{\imath n}$

$$B_{\imath x} = \frac{a_{\imath x}}{A_{dx}}\left[B_{dx} + Y_{dx}\frac{B_{dy}}{A_{dy}} + Z_{dx}B_{dz}\right] + \frac{a_{\imath y}B_{dy}}{A_{dy}} + a_{\imath z}B_{dz}$$

$$a_{\imath x} = \frac{\nu_{\imath n}\omega_{c\imath}p_{nx}}{\omega_\imath^2 + \omega_{c\imath}^2} + \frac{\nu_{\imath n}\omega_\imath r_{nx}}{\omega_\imath^2 + \omega_{c\imath}^2}$$

$$a_{\imath y} = \frac{\nu_{\imath n}\left(\omega_{c\imath}p_{nx} + \omega_\imath r_{ny}\right)}{\omega_\imath^2 + \omega_{c\imath}^2}$$

$$a_{iz} = \frac{\nu_{in}\left(\omega_{ci}p_{nz} + \omega_i r_{nz}\right)}{\omega_i^2 + \omega_{ci}^2}$$

$$G_{ix}^1 = -\left(1 + \frac{Y_{dx}}{A_{dy}}\right) - \frac{a_{iy}}{A_{dy}}$$

$$P_{n1x} = p_{nx}\frac{B_{dx}}{A_{dx}} + \frac{B_{dy}}{A_{dy}}\left(Y_{dx}\frac{p_{nx}}{A_{dx}} + p_{ny}\right) + B_{dz}\left(\frac{Z_{dx}}{A_{dx}} + p_{nz}\right)$$

$$P_{n2x} = -\frac{E_{0x}}{m_d}\frac{p_{nx}}{A_{dx}} - \frac{E_{0x}}{m_d A_{dy}}\left(Y_{dx}\frac{p_{nx}}{A_{dx}} + p_{ny}\right)$$

$$P_{n3x} = \frac{C_{dx}}{A_{dx}}p_{nx} + \frac{C_{dy}}{A_{dy}}\left[\frac{Y_{dx}}{A_{dx}}p_{nx} + p_{ny}\right] + \frac{e}{m_i}q_{ny}$$

$$P_{n4x} = \frac{D_{dx}}{A_{dx}}p_{nx} + \frac{D_{dy}}{A_{dy}}\left[Y_{dx}\frac{p_{nx}}{A_{dx}} + p_{ny}\right] + D_{dz}\left[p_{ns} + \frac{Z_{dx}}{A_{dx}}\right] + \frac{e}{m_i}q_{nz}$$

$$S_{ny} = -\frac{A_2 C_{nxy}}{ik_y v_{n0y} + A_3} + C_{nx}$$

Substituting n_{i1} and n_{e1} in equation (A.0.16) and doing some calculations, Q_{d1} can be expressed as

$$Q_{d1} = (\alpha_y E_{1y} + \alpha_z E_{1z})/\alpha_d \tag{A.0.19}$$

where

$$\alpha_y = \frac{A\left(1 + a_a Q_{d0}\right)}{(i\omega - B_1)A_{e1}}C_{e1} - \frac{B\left(1 - b_b Q_{d0}\right)}{(i\omega - B_1)\,\omega}Q_{i2} - \frac{B\left(1 - b_b Q_{d0}\right)}{(i\omega - B_1)\left(\omega - Q_1\right)}Q_{i1}Q_{D2}$$

$$\alpha_z = \frac{A\left(1 + a_a Q_{d0}\right)}{(i\omega - B_1)\,A_{e1}}D_{e1} - \frac{B\left(1 - b_b Q_{d0}\right)}{(i\omega - B_1)\,\omega}Q_{i3} - \frac{B\left(1 - b_b Q_{d0}\right)Q_{i1}Q_{D3}}{(i\omega - B_1)\left(\omega - Q_1\right)}$$

$$\alpha_d = 1 + \frac{B\left(1 - b_b Q_{d0}\right)}{(i\omega - B_1)\,\omega}Q_{i4} + \frac{B\left(1 - b_b Q_{d0}\right)Q_{i1}Q_{D4}}{(i\omega - B_1)\left(\omega - Q_1\right)}$$

$$B_1 = A a_a n_{e0} + B b_b n_{i0}$$

$$Q_1 = i n'_{d0} B_{d1x} - n_{d0} k_y B_{dy} - n_{d0} k_z B_{dz}$$

After substituting Q_{d1}, equation (A.0.15) can be rewritten as

$$n_{d1} = \frac{1}{(\omega - Q_1)}\left[Q_{dy}E_{1y} + Q_{dz}E_{1z}\right] \tag{A.0.20}$$

where

$$Q_{dy} = Q_{D2} + \frac{\alpha_y Q_{D4}}{\alpha_d}$$

$$Q_{dz} = Q_{D3} + \frac{Q_{D4}\alpha_z}{\alpha_d}$$

Substituting Q_{d1} in equation (A.0.18), n_{i1} becomes,

$$n_{i1} = Q_{iy}E_{1y} + Q_{iz}E_{1z} \tag{A.0.21}$$

where

$$Q_{iy} = \frac{Q_{dy}}{\omega\left(\omega - Q_1\right)}\left(Q_{i1} + Q_{i4}\right) + \frac{Q_{i2}}{\omega}$$

$$Q_{iz} = \frac{Q_{dz}}{\omega\left(\omega - Q_1\right)}\left(Q_{i1} + Q_{i4}\right) + \frac{Q_{i3}}{\omega}$$

Then, substituting equations (A.0.17), (A.0.19), (A.0.20) and (A.0.21) in Poisson's equation (A.0.14) we get the dispersion relation as,

$$1 + \chi_e + \chi_d + \chi_i = 0 \tag{A.0.22}$$

Here,

$$\chi_e = -\frac{4\pi i e}{k^2 A_{e1}}\left(k_y C_{e1} + k_{z1} D_{e1}\right)$$

$$\chi_d = -\frac{4\pi i}{k^2}\left[\frac{Q_{d0}}{\left(\omega - Q_1\right)}\left(k_y Q_{dy} + k_z Q_{dz} + n_{d0}\left(\frac{k_y \alpha_y}{\alpha_d} + \frac{k_z \alpha_z}{\alpha_d}\right)\right)\right]$$

$$\chi_i = \frac{4\pi i e}{k^2}\left(k_y Q_{iy} + k_z Q_{iz}\right)$$

Equation (A.0.22) can be written as

$$C_1\omega^5 + C_2\omega^4 + C_3\omega^3 + C_4\omega^2 + C_5\omega + C_6 = 0 \tag{A.0.23}$$

Where,

$$C_1 = iR_1$$

$$C_2 = -R_1B_1 - 2iQ_1R_1 - iR_2 - iQ_{d0}R_3 - p_4 n_{d0}$$

$$
\begin{aligned}
C_3 = & R_1\left(B_1Q_1+d_4+d_5\right)+Q_1R_1\left(B_1+iQ_1\right)+R_2\left(B_1+iQ_1\right)+Q_{d0}R_3\left(B_1+\imath Q_1\right)\\
&+i\left(Q_1R_2+R_3R_4\right)-p_4\left(-n_{d0}Q_1+Q_{d0}Q_{D4}\right)+n_{d0}\left(p_4Q_1+p_5+p_6\right)
\end{aligned}
$$

$$
\begin{aligned}
C_4 = & R_1d_4Q_1-\left(Q_1R_1+R_2+Q_{d0}R_3\right)\left(B_1Q_1+d_4+d_5\right)-\left(Q_1R_2+R_3R_4\right)\left(B_1+iQ_1\right)\\
&+p_4R_4d_4+\left(p_4Q_1+p_5+p_6\right)\left(Q_{d0}Q_{D4}-n_{d0}Q_1\right)-n_{d0}p_5Q_1
\end{aligned}
$$

$$
\begin{aligned}
C_5 = & d_4Q_1\left(Q_1R_1+R_2+Q_{d0}R_3\right)+\left(Q_1R_2+R_3R_4\right)\left(B_1Q_1+d_4+d_5\right)\\
&-R_4d_4\left(p_4Q_1+p_5+p_6\right)-p_5Q_1\left(Q_{d0}Q_{D4}-n_{d0}Q_1\right)
\end{aligned}
$$

$$
C_6=\left(Q_1R_2+R_3R_4\right)\left(-d_4Q_1\right)+R_4d_4p_5Q_1
$$

While,

$$
R_1=1-\frac{4\pi i}{k^2}\frac{e}{A_{e1}}\left(k_yC_{e1}+k_zD_{e1}\right)
$$

$$
R_2=-\frac{4\pi\imath e}{k^2}\left(k_yQ_{\imath 2}+k_zQ_{\imath 3}\right)
$$

$$
R_3=\frac{4\pi\imath}{k^2}\left(k_yQ_{D2}+k_zQ_{D3}\right)
$$

$$
p_4=\frac{k_yp_1}{A_{e1}}+\frac{k_zd_1}{A_{e1}}
$$

$$
p_1=A\left(1+a_aQ_{d0}\right)C_{e1}
$$

$$
d_1=A\left(1+aQ_{d0}\right)D_{e1}
$$

$$
d_4=B\left(1-b_bQ_{d0}\right)Q_{\imath 4}
$$

$$
d_5=B\left(1-b_bQ_{d0}\right)Q_{\imath 1}Q_{d4}
$$

$$
R_4=e\left(Q_{\imath 1}+Q_{\imath 4}\right)
$$

$$
p_5=\frac{k_yp_2}{A_{e1}}+\frac{k_zd_3}{A_{e1}}
$$

$$
p_6=\frac{k_yp_3}{A_{e1}}+\frac{k_zd_3}{A_{e1}}
$$

$$
p_2=B\left(1-b_bQ_{d0}\right)Q_{\imath 2}A_{e1}
$$

$$
p_3=B\left(1-b_bQ_{d0}\right)Q_{\imath 1}Q_{d2}A_{e1}
$$

$$
d_3=B\left(1-b_bQ_{d0}\right)Q_{\imath 1}Q_{d3}A_{e1}
$$

List of Publications :

Papers published / accepted for publication / under review :

1. "The effect of magnetic field on the structure of Coulomb Crystal in Dusty Plasma", Swati Baruah and Nilakshi Das *Phys. Plasmas.* **17**, 073702-1 (2010).
2. "A comparative study between effects of Shadowing potential and ODS on Coulomb crystal formation", Swati Baruah and Nilakshi Das *J. Plasma Phys.* doi:10.1017/S0022377810000723 (2010).
3. "Electrostatic drift instability in collisional dusty plasma", Swati Baruah and Nilakshi Das *J. Assam Sc. Soc.* **50**, 2 (2010).
4. "The effect of dust parameters on Coulomb crystal formation using MD simulation", Swati Baruaha, Nilakshi Dasb, and Manoj Warrier *J. Assam Sci. Soc.* (Accepted).

List of Presentations :

Papers presented in seminars / conferences :

1. “A study of low frequency drift instability in dusty plasma”, - Swati Baruah and Nilakshi Das ‘21st National Symposium on Plasma science and Technology (Plasma-2006)’, Malaviya National Institute of Technology, Jaipur, Dec-2006.

2. ”A Study on ionization instability in Dusty Plasma”, Swati Baruh ’22nd National Symposium On Plasma Science and Technology (Plasma-2007)’, Institute for Plasma Research, Gandhinagar, Ahmedabad, Dec-2007.

3. “Molecular Dynamics Simulation of Phase Transition in Complex Plasma”, Swati Baruah, Nilakshi Das and Manoj Warrier ’24th National Symposium On Plasma Science and Technology (Plasma-2009)’, National Institute of Technology, Hamirpur (H P), Dec-2009.

4. “Role of attractive force on dust crystal formation”, Swati Baruah and Nilakshi Das ’25th National Symposium on Plasma Science and Technology (Plasma 2010)’, Institute of Advanced Study in Science and Technology Guwahati, Assam, Dec-2010.

5. “Coulomb crystallization of Magnetized Dusty Plasma”, Swati Baruah and Nilakshi Das ’25th National Symposium on Plasma Science and Technology (Plasma 2010)’, Institute of Advanced Study in Science and Technology Guwahati, Assam, Dec-2010.